Electrocatalytic Reduction of Dioxygen at Chemically Modified Electrodes

Thesis by

Ching-Long Ni

In Partial Fulfillment of the Requirements

for the Degree of

Doctor of Philosophy

California Institute of Technology

Pasadena, California

1987

(Submitted October 28, 1986)

Acknowledgment

It is a true pleasure to acknowledge my advisor, Professor Fred Anson, for the patient guidance that he has given me over the past years. Much of the work contained in this Thesis resulted directly from his ideas and suggestions.

To Professor Sunney Chan, I owe great thanks for his support before my joining the Anson group. He has always been a source of inspiration for me.

I am deeply grateful to the past and present members of the Anson group, especially Rich Durand, Dan Buttry, Hsue-Yang Liu, Yu-Min Tsou, Tom Guarr, Mark Bowers, and Steve Gipson, for innumerable suggestions and kind support.

I would like to thank the California Institute of Technology for financial support during my tenure.

On the day before my 26th birthday, I dedicate this Thesis to my parents and grandparents for their love, concern, and support in each part of my life.

ABSTRACT

The kinetics of the reduction of O_2 by $Ru(NH_3)_6^{+2}$ as catalyzed by cobalt(II) tetrakis(4-N-methylpyridyl)porphyrin are described both in homogeneous solution and when the reactants are confined to Nafion coatings on graphite electrodes. The catalytic mechanism is determined and the factors that can control the total reduction currents at Nafion-coated electrodes are specified. A kinetic zone diagram for analyzing the behavior of catalyst-mediator-substrate systems at polymer coated electrodes is presented and utilized in identifying the current-limiting processes. Good agreement is demonstrated between calculated and measured reduction currents at rotating disk electrodes. The experimental conditions that will yield the optimum performance of coated electrodes are discussed, and a relationship is derived for the optimal coating thickness.

The relation between the reduction potentials of adsorbed and unadsorbed cobalt(III) tetrakis(4-N-methylpyridyl)porphyrin and those where it catalyzes the electroreduction of dioxygen is described. There is an unusally large change in the formal potential of the Co(III) couple upon the adsorption of the porphyrin on the graphite electrode surface. The mechanism in which the (inevitably) adsorbed porphyrin catalyzes the reduction of O_2 is in accord with a general mechanistic scheme proposed for most monomeric cobalt porphyrins.

Four new dimeric metalloporphyrins (prepared in the laboratory of Professor C. K. Chang) have the two porphyrin rings linked by an anthracene bridge attached to *meso* positions. The electrocatalytic behavior of the diporphyrins towards the reduction of O_2 at graphite electrodes has been examined for the following combination of metal centers: Co-Cu, Co-Fe, Fe-Fe, Fe-H_2. The Co-Cu diporphyrin catalyzes the reduction of O_2 to H_2O_2 but no further. The other three catalysts all exhibit mixed reduction pathways leading to both H_2O_2 and H_2O. However, the pathways that lead to H_2O do not involve H_2O_2 as an intermediate. A possible mechanistic scheme is offered to account for the observed behavior.

Table of Contents

CHAPTER I
INTRODUCTION

One of the most important electrochemical reactions is the reduction of dioxygen. This reaction takes place at the cathode of a fuel cell. A fuel cell is an electrochemical device in which a reductant (*e.g.*, H_2, N_2H_4, CH_3OH) is oxidized at the anode, while an oxidant (practically O_2) is reduced at the cathode(1). A fuel cell converts the free energy change occurring from the overall chemical reaction directly to electrical energy, and its efficiency is not limited by Carnot's theorem. It has the potential to become the best large-volume energy converter for electric vehicles(2). Major advantages of fuel cells, in addition to their high efficiencies, include low noise, low pollution, and low maintenance (no moving parts).

The electrolytes for fuel cells are preferably acidic, otherwise the carbon dioxide from air and anode oxidation products would accumulate in the form of carbonate (3). The thermodynamic constraints on the possible pathways of dioxygen reduction in 1M acid are the following (4):
direct four-electron reduction pathway

$$O_2 + 4H^+ + 4e^- = 2H_2O \quad (E_0 = 1.23V)$$

peroxide pathway

$$O_2 + 2H^+ + 2e^- = H_2O_2 \quad (E_o = 0.68V)$$

followed by

$$H_2O_2 + 2H^+ + 2e^- = 2H_2O \quad (E_o = 1.77V)$$

or

$$2H_2O_2 = 2H_2O + O_2$$

(these potentials are given versus the standard hydrogen electrode).

The direct four-electron reduction pathway can proceed at the reversible thermodynamic potential of +1.23V which is 0.55V more positive than the potential where the peroxide pathway can be initiated. This consideration makes the four-electron reduction of O_2 to H_2O a highly desirable process at the cathode of a fuel cell. However, the two-electron reduction of O_2 to H_2O_2 is still a kinetically challenging process as it also involves bond-breaking and bond-forming steps.

The reduction of dioxygen is as important to fuel cells as it is to life. Some enzymatic routes (5) appear to have more success than the electrocatalytic one. The main complexity of the dioxygen reduction reaction at electrodes arises from its proceeding through high-energy intermediates that cause sluggish kinetics. To date, platinum is the most effective catalyst for an acidic oxygen cathode. The economic incentive for replacing Pt with inexpensive electrode materials (*e.g.*, graphite) is enormous. Because of the slow kinetics and large overvoltages associated with the O_2 reduction at electrodes such as graphite, it is necessary to modify the electrode surfaces to develop efficient electrocatalytic systems.

To control the rates and selectivity of redox processes which occur at the electrode surfaces, electrochemists have been involved in the synthesis and characterization of chemical microstructures on electrodes (6, 7). Generally, modified electrodes can be prepared by several different techniques: (a) chemisorption of electrochemically reactive molecules to the electrode surfaces; (b) covalent attachment of molecules of interest to the electrode surfaces; (c) coating of polymers which are either electroactive themselves or have incorporated sites. Applications in which the modification of electrode properties would be advantageous include electrocatalysis, electrochromic display devices, inhibition of photoanodic corrosion at semiconductors and others (8).

The electrocatalytic behavior of many different types of non-noble-metal compounds towards the reduction of O_2 at carbon electrodes has been examined

(9, 10). Among these are metalloporphyrins which have been confined to electrode surfaces in various forms. Attachments to carbon electrodes can be made via chemisorption (3), direct covalent bonding to the functionalities of the electrodes (11), or covalent linkage to polymer coatings on the electrodes (12).

Mechanisms of the electrocatalytic reduction of dioxygen by metalloporphyrins, particularly cobalt (13, 14) and iron (15, 16) porphyrins, have been an attractive area of research. In general, the monomeric cobalt porphyrins catalyze the reduction of O_2 to H_2O_2 but no further while monomeric iron porphyrins are more successful in carrying out the full reduction of O_2 to H_2O with H_2O_2 as an intermediate. The direct four-electron reduction of dioxygen at fairly positive potentials (> 0.5 V vs. NHE) has only been observed for dimeric porphyrins (3. 17) and a recently reported monomeric Ir porphyrin (18).

The stability of adsorbed porphyrins on graphite electrodes poses a problem in the potential application of these catalysts partly due to some undesirable desorption processes in aqueous media. Buttry and Anson have used Nafion, a perfluorinated, sulfonate-based ion-exchange polymer, to bind cobalt tetraphenylporphyrin (CoTPP) and found that the stability of the catalyst was remarkably improved (19). Since the catalyst is highly immobilized, it is necessary to provide an electron mediator (*e.g.*, $Ru(NH_3)_6^{3+/2+}$) to shuttle electrons between the electrode and the porphyrin molecules.

A water-soluble porphyrin, cobalt tetrakis(4-N-methylpyridyl)porphyrin (CoTMPyP), is miscible with Nafion in isopropanol, and functioning electrode coatings can be fashioned from premixed solutions of soluble Nafion and porphyrin catalysts. This allows easy variation of porphyrin concentrations in Nafion coatings, which is important in the kinetic analysis. Chapter II (20) describes the kinetics of the reduction of O_2 by $Ru(NH_3)_6^{2+}$ as catalyzed by Co(II)TMPyP both in homogeneous solution and when the reactants are confined to Nafion coatings on graphite electrodes. The catalytic mechanism is

delineated and the factors which can control the total reduction currents at Nafion-coated electrodes are specified. A kinetic zone diagram for analyzing the behavior of catalyst-mediator-substrate systems at polymer-coated electrodes is presented and utilized in identifying the current-limiting processes. Good agreement is demonstrated between calculated and measured reduction currents at rotating disk electrodes. The experimental conditions that will yield the optimum performance of coated electrodes are discussed. This represents the first example in which the optimal coating thickness for electrocatalysis at redox polymer electrodes is defined in a quantitative way.

Chapter III (21) describes the relation between the reduction potentials of adsorbed and unadsorbed Co(III)TMPyP and those where it catalyzes the electroreduction of dioxygen. The two well-separated responses for the adsorbed and unadsorbed porphyrin can be revealed by the combination of cyclic and rotating disk voltammetry. There is an unusually large shift in the formal potentials of the Co(III/II) couple upon the adsorption of the porphyrin on the graphite electrode surface. The mechanism in which the adsorbed porphyrin catalyzes the reduction of O_2 is in accord with a general mechanistic scheme proposed for other monomeric cobalt porphyrins.

In Chapter IV (22) the electrocatalytic behavior of four anthracene-linked dimeric metalloporphyrins towards the reduction of O_2 at graphite electrodes is described for the following combination of metal centers: Co-Cu, Co-Fe, Fe-Fe, Fe-H_2. The Co-Cu diporphyrin catalyzes the reduction of O_2 to H_2O_2 but no further. The other three catalysts all exhibit mixed reduction pathways leading to both H_2O_2 and H_2O. However, the pathways that lead to H_2O do not involve H_2O_2 as an intermediate. A possible mechanistic scheme is offered to account for the observed behavior.

The kinetic behavior at polymer modified electrodes can often be described by second-order non-linear "master differential equations" (23). A computer

program which was used to solve the equation governing the kinetics in Nafion-coated electrodes as described in Chapter II is included in Appendix I.

Mercury electrodes have been widely used in the practice of electroanalytical chemistry (24). The surface of mercury electrodes is highly uniform and reproducible if the mercury is clean. A pulse polarographic study of $[Ru^{III}(edta)]_2$ was undertaken to learn more about the edta complexes of transition metals and to gain some "hands-on" experience on mercury electrodes. The dimeric edta complex of ruthenium(III) generated by the one-electron reduction of dimeric $[Ru^{III1/2}(edta)]_2$ at mercury electrodes dissociates into the well characterized, monomeric $Ru^{III}(edta)OH_2$ complex at a rate that increases with the proton concentration. The kinetic measurement of the dissociation reaction using normal and reverse pulse polarography is described in Appendix II. At high pH's, it is possible to record the visible absorption spectrum of $[Ru^{III}(edta)]_2$.

References and Notes

1. Bockris, J.O'M.; Srinivasan, S., "Fuel cells - Their Electrochemistry", McGraw-Hill, New York (1969).
2. United Technologies Corp. Final Report to LANL, P.O. 4-L61-3862V-1.
3. Collman, J.P.; Anson, F.C.; Bencosme, S.; Chony, A.; Collins, T.; Denisevich, P.; Evitt, E.; Geiger, T.; Ibers, J.; Jameson, G.; Konai, Y.; Koval, C.; Meier, K.; Oakley, R.; Pettman, R.; Schmittou, E.; Sessler, T., in "Organic Synthesis, Today and Tomorrow," Trost, B.M.; Hutchison, C.R.,eds., Pergamon Press, New York, p. 29 (1981).
4. Latimer, W.M., "Oxidation Potentials," Prentice-Hall, New York (1952).
5. Greenwood, C.; Gibson, Q.H., J. Biol. Chem., 242(1967)1782.
6. Murray, R.W., in "Electroanalytical Chemistry," Vol. 13, Bard, A.J., Ed., Dekker, NY, 1984, p.191.
7. Albery, W.J.; Hillman, A.R., Annual Reports C, Royal Society of London, 377(1981).
8. Faulkner, L.R.; Chemical and Engineering News, February 27, 1984, p.28.
9. Ross, P.N.,Jr.; Wagner, F.T., Final Report to Los Alamos National Laboratory (contract No. CRI-7090 W-1), March 1982.
10. Yeager, E., Electrochim. Acta., 29(1984)1527.
11. Lennox, J.C.; Murray, R.W.; J. Electroanal. Chem., 78(1977)395.
12. Bettelheim, A.; Chan, R.J.H.; Kuwana, T., J. Electroanal. Chem., 110(1980)93.
13. Durand, R.R.,Jr.; Anson, F.C., J. Electroanal. Chem., 134(1982)273.
14. Chan, R.J.; Su, Y.O.; Kuwana, T., Inorg. Chem., 24(1985)3777.
15. Shigehara, K.; Anson, F.C., J. Phys. Chem., 86(1982)2776.
16. Forshey, P.A.; Kuwana, T.; Kobayashi, N.; Osa, T., Adv. Chem. Ser., No.201(1982)601.
17. Liu, H.-Y.; Abdulmuhdi, I.; Chang, C.K.; Anson, F.C., J. Phys. Chem., 89(1985)665.

18. Collman, J.P.; Kim. K., preprint.

19. Buttry, D.A.; Anson, F.C., J. Am. Chem. Soc., 106(1984)59.

20. Anson, F.C.; Ni, C.-L.; Saveant, J.-M., J. Am. Chem. Soc., 107(1985)3442.

21. Ni, C.-L.; Anson, F.C., Inorg. Chem., 24(1985)4754.

22. Ni, C.-L.; Abdulmuhdi, I.; Chang, C.K.; Anson, F.C., J. Phys. Chem., submitted.

23. Andrieux, C.P.; Saveant, J.-M., J. Electroanal. Chem., 171(1984)65.

24. Lingane, J.J., "Electroanalytical Chemistry," 2nd ed., Wiley-Interscience, New York, 1958, Chapter 17.

25. Ni, C.-L.; Anson, F.C.; Osteryoung, J.G., J. Electroanal. Chem., 202(1986)101.

CHAPTER II

ELECTROCATALYSIS AT REDOX POLYMER ELECTRODES WITH SEPARATION OF THE CATALYTIC AND CHARGE PROPAGATION ROLES. DIOXYGEN REDUCTION CATALYZED BY COBALT(II) TETRAKIS(4-N-METHYLPYRIDYL)-PORPHYRIN

Introduction

Nafion coatings on electrodes offer unusually stable environments for attaching reactants to electrode surfaces (1,2). The attributes of such coatings were exploited by Buttry and Anson in their recent study of the catalysis of the electroreduction of dioxygen by cobalt tetraphenylporphyrin incorporated in Nafion coatings on graphite electrodes (2d). It was necessary to incorporate a mediator redox couple such as $Ru(NH_3)_6^{3+/2+}$ into the Nafion coating along with the cobalt porphyrin catalyst in order to carry electrons from the electrode surface to the essentially immobile catalyst sites. The resulting three-component coating (Nafion, catalyst, redox mediator) provided an effective means for the electroreduction of dioxygen, albeit at a potential determined by the formal potential of the redox mediator (2d). Three-component coatings allow the catalytic and charge propagation roles to be assigned to separate reactants that can be selected so as to maximize the overall rate of reaction of the substrate. It was therefore of interest to analyze the kinetics of dioxygen reduction by such a three-component electrode coating to understand how best to optimize experimental conditions in order to achieve high catalytic efficiency. This chapter is devoted to a kinetic analysis of a system in which cobalt(II) tetrakis(4-N-methylpyridyl) porphyrin was employed as the dioxygen reduction catalyst with $Ru(NH_3)_6^{3+/2+}$ as the redox mediator. The water solubility of the catalyst allowed the kinetics to be measured in homogeneous solution as well as with the catalyst and mediator incorporated in Nafion coatings on rotating graphite disk electrodes. In both cases, the reaction appears to follow a "preactivation" mechanism in which only a preformed dioxygen-catalyst adduct is able to accept electrons from the redox mediator at a high rate. The reaction scheme thus involves a combination of "chemical catalysis" (formation of the adduct) and "redox catalysis" (outer-sphere reduction of the adduct) in the sense defined and analyzed by Andrieux *et al.* (3). Such preactivation mechanisms seem likely to be among the most

frequently encountered in practical applications of electrodes coated with redox polymers. For example, the utilization of biological catalysts such as metalloenzymes as electrocatalysts is likely to involve both preactivation mechanisms and separate redox mediators to provide rapid charge propagation throughout electrode coatings. In this chapter, the kinetic behavior of this first example of a preactivation catalytic mechanism at a redox polymer electrode is described.

Experimental

Materials. $Ru(NH_3)_6Cl_3$ (Strem Chemical Co.) was purified according to the procedure of Pladziewicz *et al.* (4). Standard solutions of $Ru(NH_3)_6^{3+}$ were prepared by dissolving accurately weighed samples of $Ru(NH_3)_6Cl_3$ in 0.1 M lithium acetate-acetic acid buffer (pH 4.5). The resulting solution was deaerated with argon and reduced with zinc amalgam for 30 minutes to produce $Ru(NH_3)_6^{2+}$. Cobalt(II) was introduced into tetrakis(4-N-methylpyridyl)porphine p-toluenesulfonate (Mid-Century Chemical Co.) under an Ar atmosphere according to the published procedure (5) and the product precipitated by addition of excess NH_4PH_6. A gas mixture containing 2.1% O_2 in N_2 was obtained from Matheson.

Soluble Nafion (eq. wt. = 970) was available as a 5.2 wt% solution obtained some time ago from E. I. DuPont de Nemours and Co. Similar material is presently commercially available from C & G Processing, Rockland, DE. Basal-plane pyrolytic graphite (Union Carbide Co.) was cut and mounted on rotatable shafts to produce rotating disk electrodes as described in ref 6.

Apparatus and Procedures. Electrochemical measurements were conducted with appropriate combinations of PAR (EG & G Instrument Co.) instruments. Rotating disk electrodes were rotated with an ASR2 rotator and ASR controller from Pine Instrument Co. Absorption spectra were obtained with a Hewlett-Packard Model 8450A spectrophotometer and HP 7225A plotter.

Electrodes were coated with Nafion by transferring a few microliters of a

5.1 mM solution (prepared by diluting the 5.2 wt % stock solution with isopropanol) to a freshly cleaved electrode surface and allowing the solvent to evaporate. Coatings containing cobalt(II) tetrakis(4-N-methylpyridyl)porphyrin (CoTMPyP) were applied in a similar fashion by using the homogeneous solution prepared by mixing the Nafion stock solution in isopropanol with an equal volume of an aqueous solution of CoTMPyP. The resulting solution appeared homogeneous and no precipitate formed upon long standing. The absorption spectra of CoTMPyP dissolved in H_2O or in a 1:1 mixture of H_2O and isopropanol containing 0.5 wt% Nafion are almost identical. Both the spectrum of the Nafion-CoTMPyP mixture and the catalytic activity of coatings prepared from it remained constant for periods of several months.

$Ru(NH_3)_6^{3+}$ was incorporated into both types of coatings by soaking them in solutions of the complex. The quantity of CoTMPyP and $Ru(NH_3)_6^{3+}$ incorporated in the coatings was determined coulometrically as described in detail in the Results section.

Potentials were measured and are reported with respect to a saturated calomel reference electrode (SCE).

The rate of the reaction between O_2 and $Ru(NH_3)_6^{2+}$ was followed under pseudo-first-order conditions by means of a graphite rotating disk electrode. The electrode was rotated at 3600 rpm in an air-saturated solution which resulted in complete mixing of the solution within a few seconds. The electrode potential was maintained at 0.5 volt where the oxidation of $Ru(NH_3)_6^{2+}$ to $Ru(NH_3)_6^{3+}$ produced a limiting current proportional to the time-dependent concentration of $Ru(NH_3)_6^{2+}$. There were no significant contributions to the current from O_2, H_2O_2, or CoTMPyP at this potential and the kinetic runs were short enough to ensure that negligible quantities of $Ru(NH_3)_6^{2+}$ were consumed by the electrode reaction or by the H_2O_2 that was the product of the reduction of O_2. Kinetic runs were initiated by injecting an aliquot of $Ru(NH_3)_6^{2+}$ into

air-saturated reaction solution containing the rotating disk electrode and the desired concentration of CoTMPyP. Air from a gas dispersion tube was passed through the solutions throughout each run to ensure that the concentration of O_2 remained constant. The tube was positioned to ensure that the limiting currents were unaffected by the continuous flow of gas bubbles.

Results

Uncatalyzed Reduction of O_2 by $Ru(NH_3)_6^{2+}$. Curve 1 in Figure 2.1A traces the current for the oxidation of $Ru(NH_3)_6^{2+}$ at a rotating disk electrode in a solution saturated with air. The magnitude of the current produces a continuous measure of the concentration of $Ru(NH_3)_6^{2+}$ and the linear plot of log current vs. time in curve 1 of Figure 2.1B confirms that the rate of the uncatalyzed reduction of O_2 by $Ru(NH_3)_6^{2+}$ according to eqn. 2.0 is first-order in $Ru(NH_3)_6^{2+}$(7).

$$2H^+ + O_2 + 2Ru(NH_3)_6^{2+} \xrightarrow{k_0} H_2O_2 + 2Ru(NH_3)_6^{3+} \qquad (2.0)$$

The pseudo-first-order rate constant obtained from the slope of line 1 in Figure 2.1B is 4.4 x $10^{-2}s^{-1}$. Since reaction 2.0 is also known to be first-order in O_2 (7), this rate constant corresponds to a second-order constant of 79 $M^{-1}s^{-1}$ for an O_2 concentration of 0.28 mM in an air-saturated solution at 22°C(8). This value of k_0 is in reasonable argreement with the 63 $M^{-1}s^{-1}$ value reported by Stanbury *et al.* (7) indicating that the rotating disk procedure is a reliable method for following the kinetics of the reaction.

Catalyzed Reduction of O_2. Addition of small quantities of CoTMPyP ($\equiv$ CoP hereafter) to solutions of $Ru(NH_3)_6^{2+}$ and O_2 enhances the rate of reduction of O_2 significantly. Curves 2, 3 and 4 in Figure 2.1A show the effect of increasing quantities of the CoP catalyst. Curves 2-4 yield nonlinear plots of ln (current) vs. time (Figure 2.1B), indicating that the catalytic mechanism involves more than a simple preequilibrium between CoP and O_2 to form a

Figure 2.1.

(A) Current vs. time plots for the oxidation of $Ru(NH_3)_6^{2+}$ by O_2. Rotating disk electrode was held at +0.5 V(vs. SCE) and rotated at 3600 rpm. Initial concentration of $Ru(NH_3)_6^{2+}$: 500 μM. [CoP]= 0(1);5.0(2);9.7(3);19μM (4). Supporting electrolyte: $CH_3COOLi - CH_3COOH$, pH = 4.5, μ = 0.1 M.

(B) Corresponding plots of ln(current)vs. time. Curves 2,3 and 4 are not linear. See the text for details.

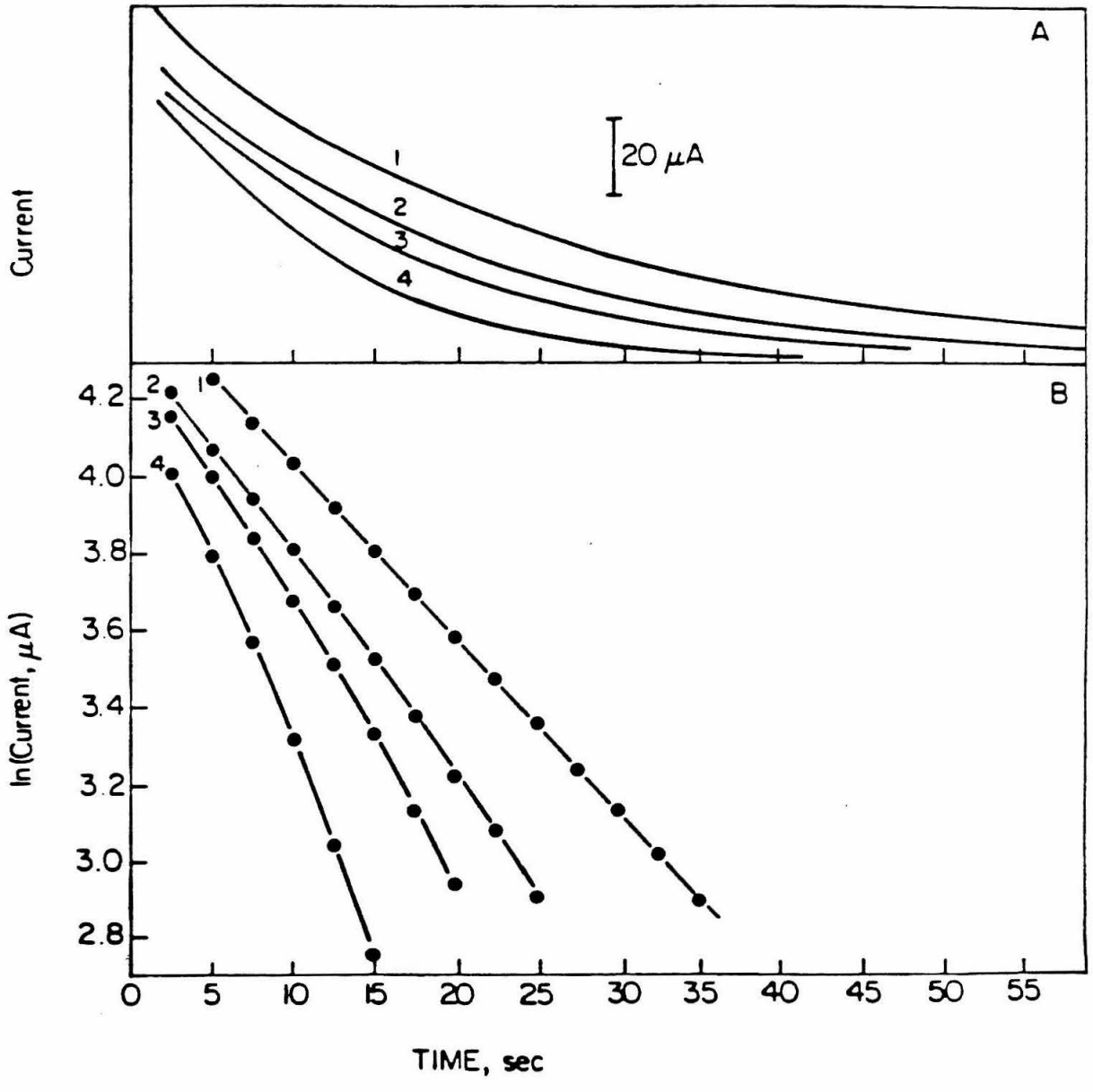
A
20 μA
1
2
3
4
Current
B
ln(Current, μA)
4.2
4.0
3.8
3.6
3.4
3.2
3.0
2.8
0
5
10
15
20
25
30
35
40
45
50
55
TIME, sec

more rapidly reduced adduct. (Separate experiments conducted in the absence of O_2 demonstrated that further reduction of the H_2O_2 produced in the primary reaction proceeds at a negligible rate both in the absence and the presence of CoP.)

The kinetics were therefore assumed to be controlled by the formation of a more reactive CoP-O_2 adduct whose concentration attained a small, steady-state value. The steps involved in the catalyzed reduction are believed to be those given in reactions 2.1 to 2.3 (9).

$$CoP + O_2 \underset{k_{-1}}{\overset{k_1}{<\!-\!-\!->}} PCoO_2 \tag{2.1}$$

$$PCoO_2 + Ru(NH_3)_6^{2+} \xrightarrow{k_2} [PCoO_2]^- + Ru(NH_3)_6^{3+} \tag{2.2}$$

$$[PCoO_2]^- + 2H^+ + Ru(NH_3)_6^{2+} \xrightarrow{fast} CoP + H_2O_2 + Ru(NH_3)_6^{3+} \tag{2.3}$$

The steady-state assumption for [$CoPO_2$] yields

$$[PCoO_2] = \frac{k_1[CoP][O_2]}{k_2[Ru^{II}] + k_{-1}} \quad , \tag{2.4}$$

where $Ru^{II} \equiv Ru(NH_3)_6^{2+}$. The rate of the catalyzed reduction of O_2 is then given by

$$-2\left(\frac{dO_2}{dt}\right)_{cat} = -\left(\frac{dRu^{II}}{dt}\right)_{cat} = \frac{2k_2k_1[CoP][O_2][Ru^{II}]}{k_2[Ru^{II}] + k_{-1}} \quad . \tag{2.5}$$

The overall, observed reduction rate is given by eqn. 2.6.

$$-2\left(\frac{dO_2}{dt}\right) = -\left(\frac{dRu^{II}}{dt}\right) = \frac{2k_2k_1[CoP][O_2][Ru^{II}]}{k_2[Ru^{II}] + k_{-1}} + 2k_0[O_2][Ru^{II}] \tag{2.6}$$

The second term on the rhs of eqn. 2.6 could be evaluated at every point of an experiment because k_0 and $[O_2]$ were known constants and $[Ru^{II}]$ was available from the magnitude of the oxidation current at the rotating disk electrode. Equation 2.6 was integrated numerically (10) to calculate values of $[Ru^{II}]$ vs. time for various values of the unknown rate constants.

Figure 2.2 compares plots of the calculated values of $[Ru^{II}]$ with the experimental data points for three kinetic runs. The values of $2k_1[Co^{II}][O_2]$ and $k_1/(2k_2k_1[Co^{II}][O_2])$ were varied to obtain the best agreement between the calculated curves and the data points. The best fit, shown in Figure 2.2, resulted for $k_1 = 3.6 \times 10^3 M^{-1}s^{-1}$ and $k_2/k_{-1} = 1.7 \times 10^3 M^{-1}$.

At concentrations of Ru^{II} where $k_2[Ru^{II}] << k_{-1}$, the formation of the CoP-O_2 adduct can be regarded as a rapid preequilibrium step and eqn. 2.6 can be integrated to give eqn. 2.7.

$$ln[Ru^{II}] = ln[Ru^{II}]_0 - k_{obs}t \quad , \tag{2.7}$$

where $[Ru^{II}]_0$ is the initial concentration of $Ru(NH_3)_6^{2+}$ and $k_{obs} = 2[O_2](((k_1k_2[CoP])/k_{-1}) + k_0)$. Figure 2.3A contains plots of ln (current) vs. t at low concentrations of Ru^{II} that exhibit the linearity expected from eqn. 2.7. The slopes of the lines and the known values of k_0 and $[O_2]$ were used to obtain values of $k_1k_2[CoP]$ that yielded the linear plots in Figure 2.3B, showing that the reaction rate is first-order with respect to the CoP catalyst. The slope and intercept of the line in Figure 2.3B correspond to $k_1k_2/k_{-1} = K_1k_2 = 1.3 \times 10^7 M^{-2}s^{-1}$ and $k_0 = 77 M^{-1}s^{-1}$, respectively. This value of K_1k_2 compares favorably with the value, $0.6 \times 10^7 M^{-2}s^{-1}$, obtained by fitting the curves in Figure 2.2, and the value of k_0 is close to the value measured independently.

At sufficiently high concentrations of $Ru(NH_3)_6^{2+}$ where $k_2[Ru^{II}] >> k_{-1}$, the rate of the CoP-catalyzed reduction of O_2 would be expected to reach a limiting value given by $k_1[CoP][O_2]$. We were not able to observe this condition

Figure 2.2. Comparison of calculated (curves) and experimental (points) values of $[Ru(NH_3)_6^{2+}]$ during its oxidation by O_2. The curves were generated by numerical intergration of equation 2.6 with the constants $k_1 = 3.6x10^3M^{-1}s^{-1}$ and $k_2/k_{-1} = 1.7x10^3M^{-1}$. The points were obtained from the corresponding curves of Figure 2.1A.

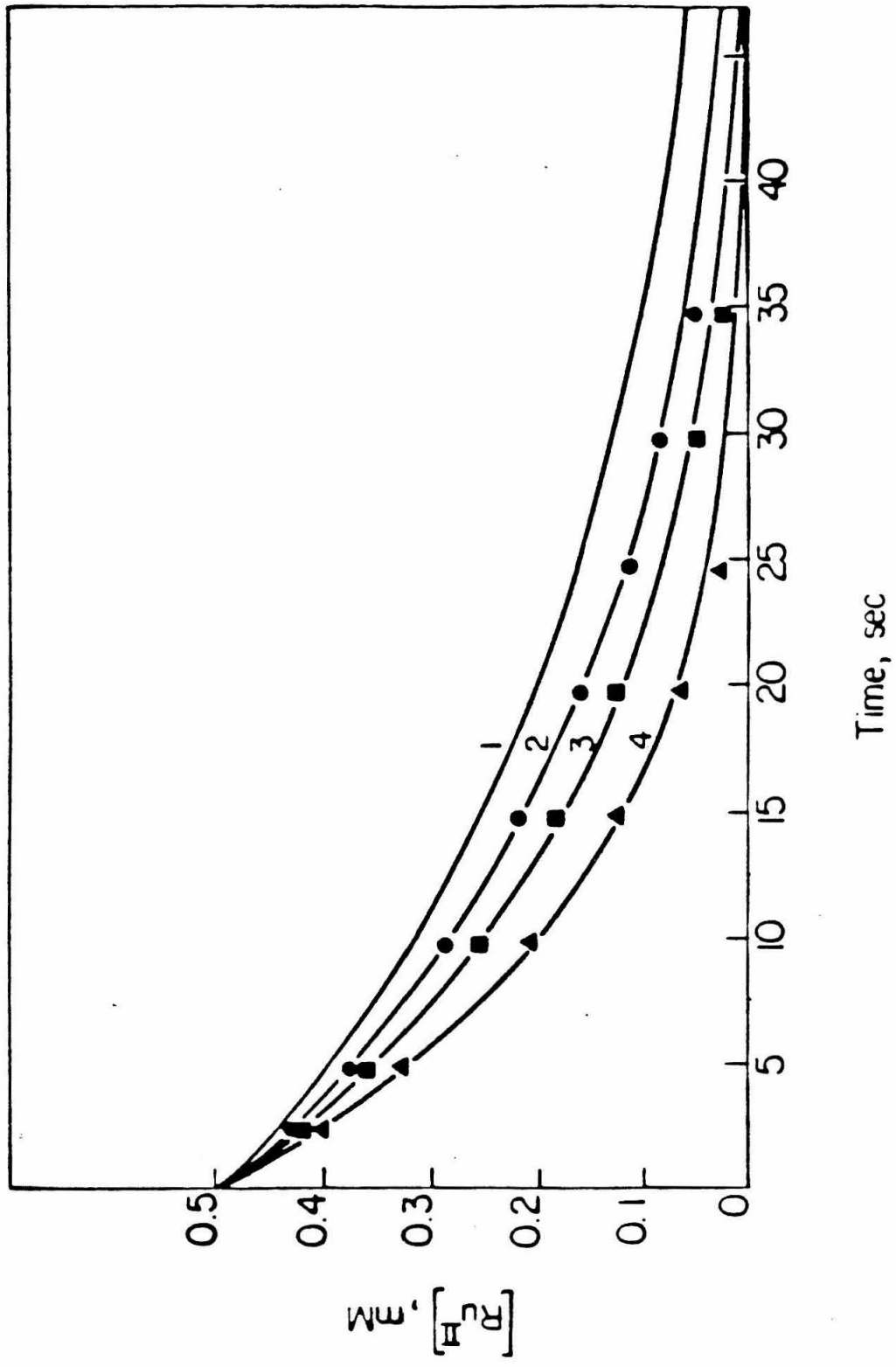
0.5
0.4
0.3
0.2
0.1
0
5
10
15
20
25
30
35
40
1
2
3
4
Time, sec

Figure 2.3.

(A) Kinetic plots of the oxidation of low concentrations of $Ru(NH_3)_6^{2+}$ by O_2. Initial $[Ru(NH_3)_6^{2+}] = 20\ \mu$ M. Other conditions as in Figure 2.2.

(B) Slopes of the lines in A vs. [CoP].

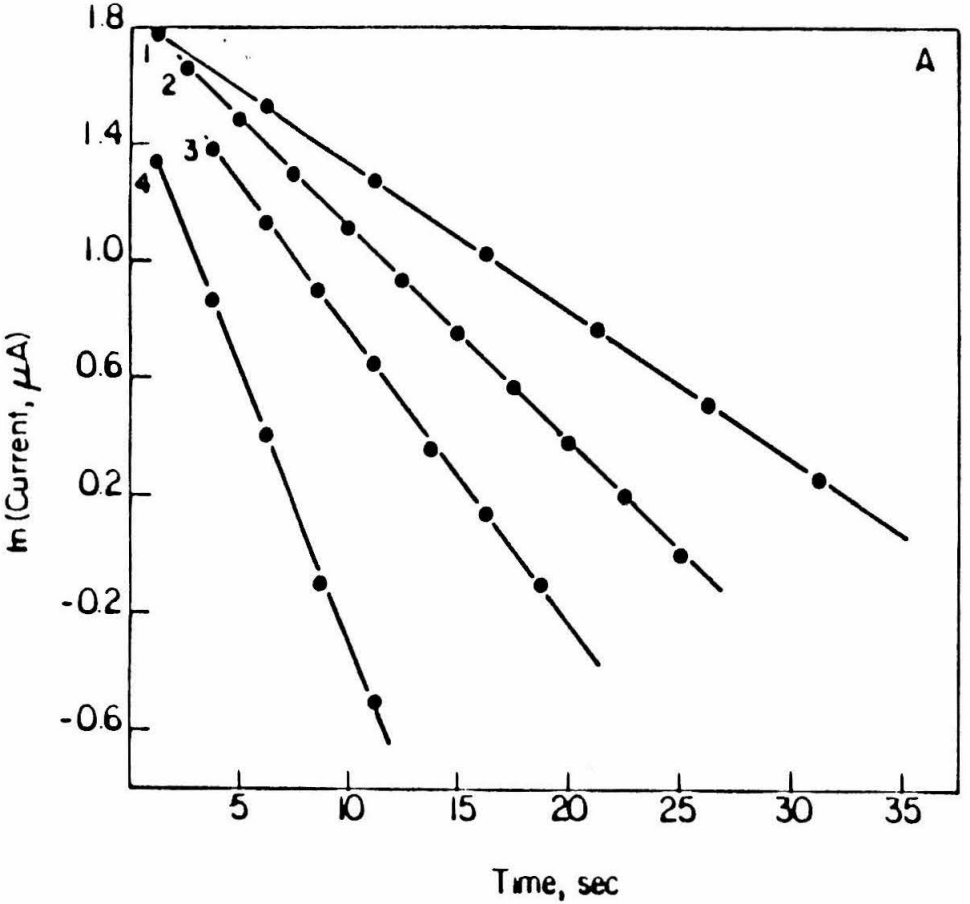
A
1
2
3
4
1.8
1.4
1.0
0.6
0.2
-0.2
-0.6
5
10
15
20
25
30
35
ln (Current, μA)
Time, sec

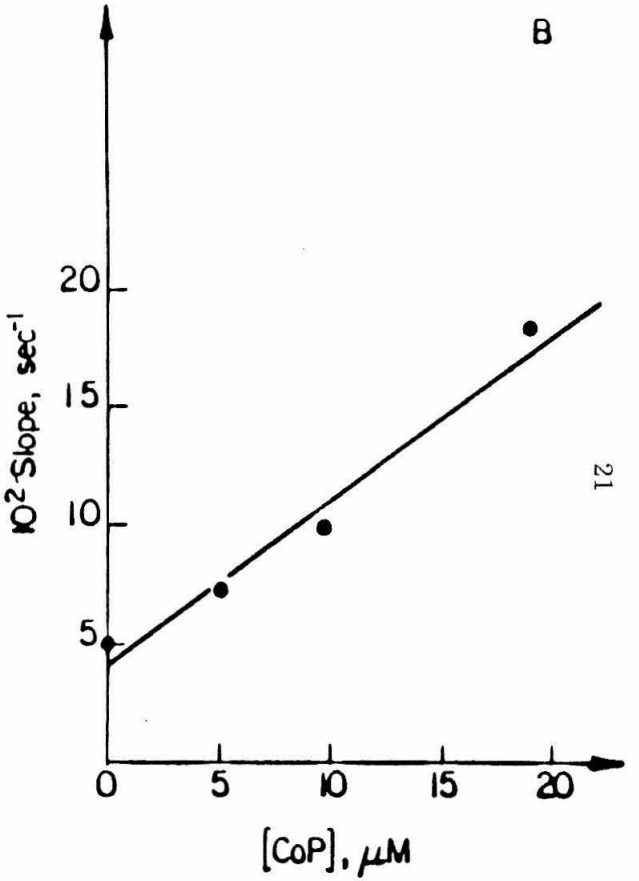
B
20
15
10
5
0
5
10
15
20
10^2 Slope, sec^{-1}
[CoP], μM

experimentally because the uncatalyzed reaction rate became dominant at the high concentrations of $Ru(NH_3)_6^{2+}$ necessary to reach the saturation rate of the catalyzed reaction pathway.

Voltammetry of CoP When Adsorbed on the Graphite Surface or Incorporated in Nafion Coatings. CoP is adsorbed on the surfaces of pyrolytic graphite electrodes strongly and irreversibly so that a voltammetric response remains when the electrodes are transferred to pure supporting electrolyte solutions. Curve A in Figure 2.4 shows the response obtained from ca. 3×10^{-11} mole cm^{-2} of CoP adsorbed on a graphite electrode. Adsorption of the porphyrin on the surface leads to a large increase in the background current, apparently because of an increase in the capacitive charging current. However, the responses arising from CoP and the quinone-hydroquinone functions on the graphite surface remain evident at 0.48 and 0.1 volt, respectively. The $Co^{III/II}$ response from adsorbed CoP appears at a considerably more positive value than the formal potential of the porphyrin in aqueous acid (0.17 volt) (11) showing that absorption on the graphite surface stabilizes $Co^{II}P$ much more than $Co^{III}P$, possibly as a result of axial coordination of unsaturated ligand groups present on the surface of the graphite. The adsorption behavior and its relation with the electrocatalysis of dioxygen reduction will be discussed in detail in Chapter III.

Curve B in Figure 2.4 resulted when the electrode was coated with a mixture of 1.5×10^{-7} mole cm^{-2} of Nafion and 3.7×10^{-9} mole cm^{-2} of CoP. There is essentially no faradaic response from the electrode coated with the CoP-Nafion mixture except for the background current associated with the graphite surface. (The reason for the absence of the quinone-hydroquinone waves in the dashed curve of Figure 2.4B is not clear.) The lack of response is the result of the very small diffusion coefficients of metalloporphyrins in Nafion coatings (2d) that prevent them from moving to the electrode surface to react at a significant

Figure 2.4. Cyclic voltammograms of CoP and a $Ru(NH_3)_6^{3+}$-CoP mixture at basal plane graphite electrodes.

(A) Bare graphite electrode on which ca. $3x10^{-11}$ mole cm^{-2} CoP had been adsorbed. The dashed line is the background response of the bare graphite electrode. Scan rate: 100 mV s^{-1}.

(B) Electrode coated with 1.5 x 10^{-7} mole cm^{-2} Nafion in which 3.7 x 10^{-9} mole cm^{-2} CoP was incorporated. The dashed line is the background response of the electrode coated only with 1.5 x 10^{-7} mole cm^{-2} Nafion. Scan rate: 100 mV s^{-1}.

(C) Cyclic voltammogram of $Ru(NH_3)_6^{3+}$ incorporated in a 1.5 x 10^{-7} mole cm^{-2} Nafion coating which also contained 2.5 x 10^{-9} mole cm^{-2} CoP. Scan rate: 5 mV s^{-1} . Supporting electrolyte: 0.1 M acetate buffer (pH 4.5) saturated with Ar. To record curve C, $2x10^{-8}$ M $Ru(NH_3)_6^{3+}$ was also present.

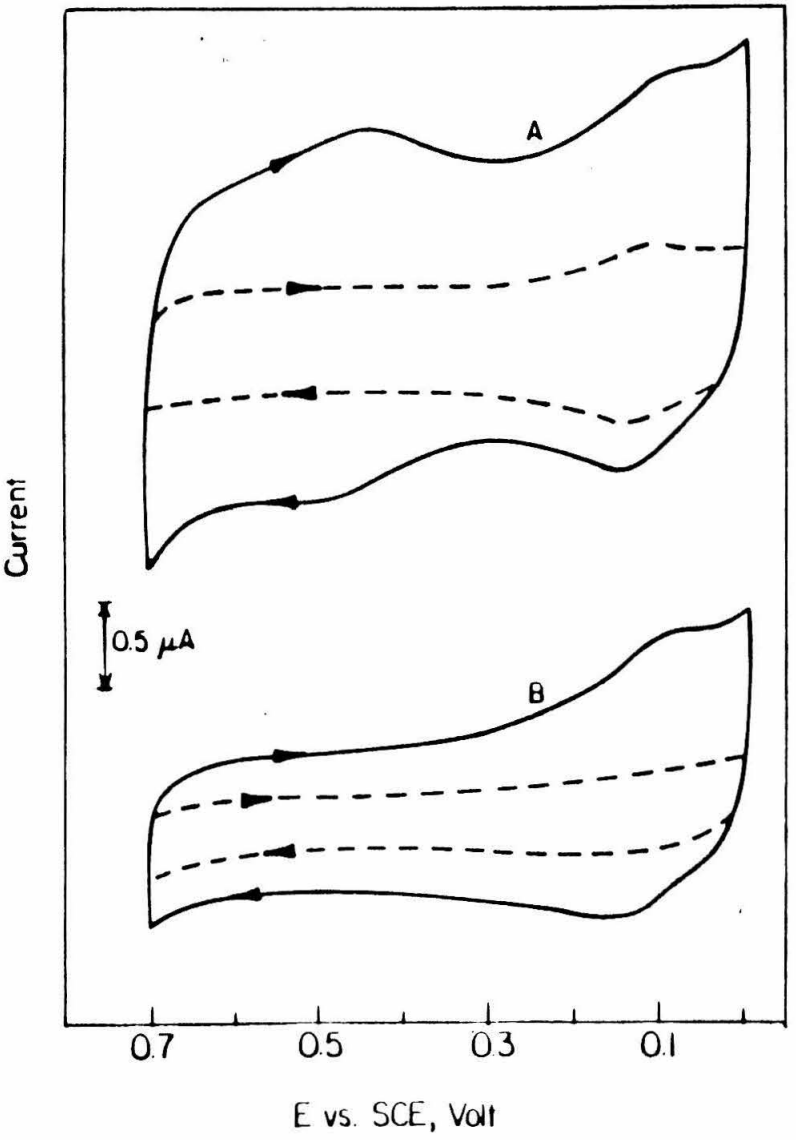
A
B
0.5 μA
Current
0.7
0.5
0.3
0.1
E vs. SCE, Volt

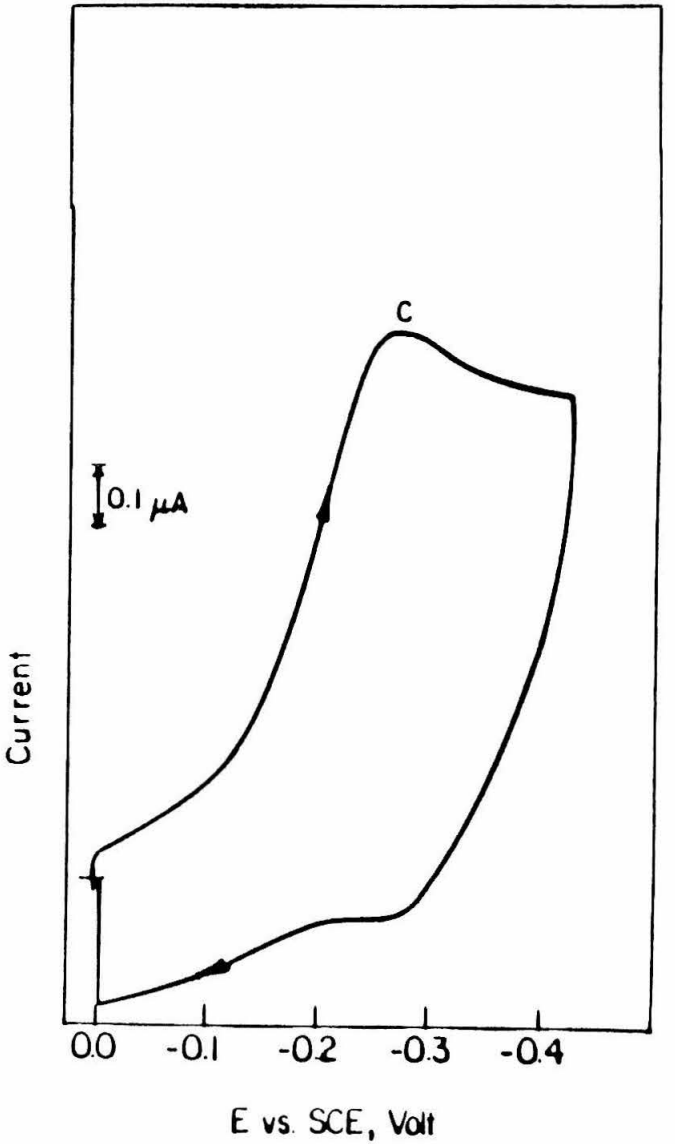
C
0.1 μA
Current
0.0
-0.1
-0.2
-0.3
-0.4
E vs. SCE, Volt

rate. The high cationic charge of CoP presumably makes its rate of diffusion through the polyanionic Nafion coating even smaller than that of uncharged porphyrins. To realize the catalytic activity of complexes that are immobilized in electronically insulating electrode coatings, it is convenient to introduce into the coating a rapidly diffusing redox couple that serves to shuttle electrons between the electrode and the catalyst sites (2d). The $Ru(NH_3)_6^{3+/2+}$ couple is suitable for this purpose, and Figure 2.4C shows the cyclic voltammetric response obtained when both $Ru(NH_3)_6^{3+}$ and $Co^{III}P$ are incorporated in a Nafion coating. (The $Co^{III}P$ was prepared by electrolysis of a solution of $Co^{II}P$ at 0.6V by using a graphite plate elctrode.) The cathodic peak at -0.27 volt involves the direct reduction of $Ru(NH_3)_6^{3+}$ at the electrode surface and the indirect reduction of $Co^{III}P$ by its reaction with $Ru(NH_3)_6^{2+}$. The anodic peak current is much smaller because only the oxidation of $Ru(NH_3)_6^{2+}$ contributes to it.

To measure the quantity of reducible $Co^{III}P$ present in the coating, a pair of coulometric experiments was performed: The potential of an electrode coating containing $Ru(NH_3)_6^{3+}$ and $Co^{III}P$ was swept slowly (2 mV s^{-1}) from 0 to -0.45 volt and maintained at this value until the current had decayed to background levels. The total cathodic charge that passed (for example, Figure 2.5A) corresponded to the sum of the electroactive $Co^{III}P$ and $Ru(NH_3)_6^{3+}$ present in the coating plus a very small contribution from the 2 x 10^{-7} M $Ru(NH_3)_6^{3+}$ that was added to the supporting electrolyte solution to suppress the loss of $Ru(NH_3)_6^{3+}$ from the coating. Next, the potential was maintained at 0 volt until all of the $Ru(NH_3)_6^{2+}$ that had been generated at -0.45 volt was reoxidized to $Ru(NH_3)_6^{3+}$ without reoxidation of any of the $Co^{II}P$. Finally, the initial coulometric measurement was repeated (for example, Figure 2.5B) to obtain a faradaic charge proportional to the total $Ru(NH_3)_6^{3+}$ in the coating. The difference between the two faradaic charges provided a measure of the

Figure 2.5. Coulometric responses of the electrode as in Figure 2.4C.

(A) The potential of an electrode coating containing $Ru(NH_3)_6^{+3}$ and $Co^{III}P$ is swept from 0 to -0.45V (scan rate: 2 mV s^{-1}).

(B) After all the $Ru(NH_3)_6^{2+}$ that has been generated in curve A is reoxidized to $Ru(NH_3)_6^{3+}$ (by holding the potential at 0 V), the potential of the same electrode is again swept from 0 to -0.45V.

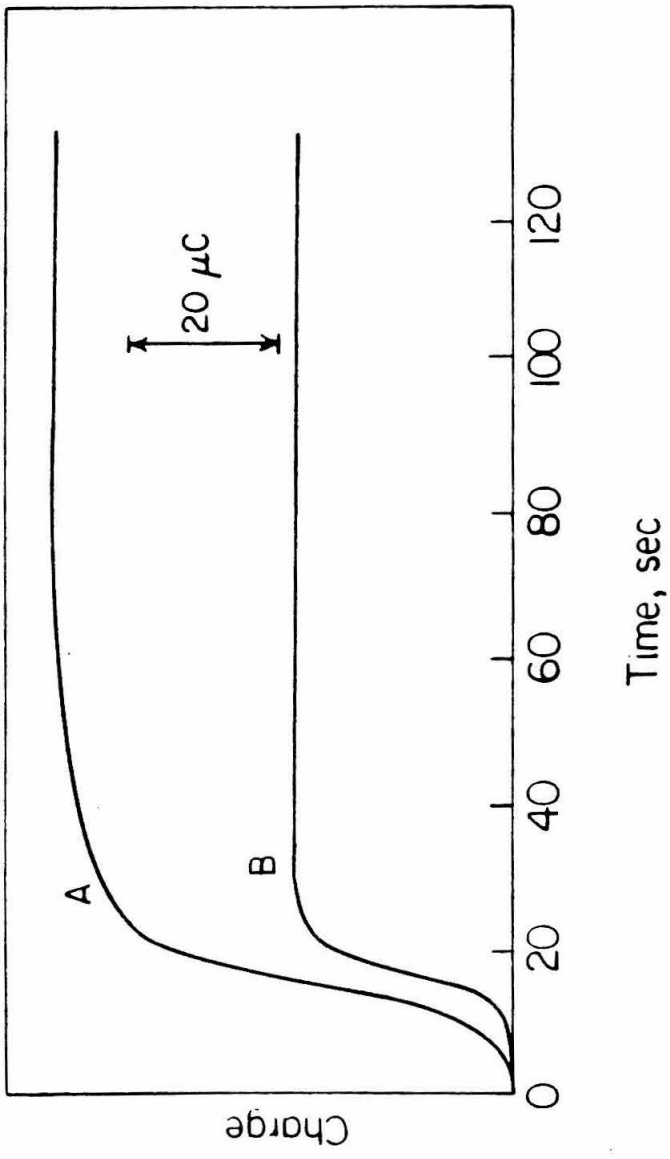
Charge
0
20
40
60
80
100
120
Time, sec
A
B
20 μC

quantity of the CoP within the coating that was accessible for reaction with the $Ru(NH_3)_6^{2+}$ redox mediator. Table 2.1 contains a set of measurements showing that about 80% of the CoP initially deposited on the electrode surface remains there and is available for reaction with $Ru(NH_3)_6^{2+}$. The missing CoP is not lost from the coating by dissolving in the solution because coatings deposited on transparent glass slides instead of graphite electrodes were shown by spectrophotometric measurements to retain all the CoP in the original coating even after long exposure to the supporting electrolyte solution. Similar electrochemical inaccessibility of reactants incorporated in Nafion coatings was also observed in a previous study in which $Ru(bpy)_2^{3+}$ (bpy = 2, 2'-bipyridine) was dissolved in the Nafion solution used to coat electrodes (le).

Reduction of O_2 at Coated Electrodes. To observe the catalyzed reduction of O_2 without contributions to the currents from the $Ru(NH_3)_6^{3+}$ incorporated in the electrode coating, steady-state measurements were made with rotating disk electrodes coated with the Nafion-CoP-$Ru(NH_3)_6^{3+}$ mixture. Figure 2.6A contains a set of current-potential curves for O_2 reduction at such electrodes in an air-saturated solution. The dashed curve shows the direct reduction of O_2 at the electrode surface that is obtained when no $Ru(NH_3)_6^{3+}$ is present in the coating. No clear current plateau appears in this case because the reduction of dioxygen merges with the background current for reduction of protons under these conditions. To avoid the slow loss of $Ru(NH_3)_6^{3+}$ from coatings in pure supporting electrolyte, 1 to 2 x 10^{-6} M $Ru(NH_3)_6^{3+}$ was usually added. This tactic was (surprisingly) effective in maintaining essentially constant levels of $Ru(NH_3)_6^{3+}$ in coatings over a wide range of values. Fortunately, the currents resulting from the reduction of such small concentrations of $Ru(NH_3)_6^{3+}$ were negligibly small compared to those for the reduction of O_2.

It is important to note that the curves in Figure 2.6A show increasing

Table 2.1: Coulometric Assay of $Co^{III}P$ in Nafion Coatings

Composition of Deposited Coating		Coulomertic Assay
$10^7\ \Gamma_{NF}$ [a]	$10^9\ \Gamma_{Co^{III}P}$ [b]	$10^9\ \Gamma_{Co^{III}P}$ [c]
mole cm^{-2}	mole cm^{-2}	mole cm^{-2}
1.5	2.5	1.9
1.5	3.7	3.0
0.9	1.5	1.1

a. Sulfonate groups in the aliquot of Nafion-$Co^{III}P$ solution used to coat the electrode.

b. Quantity of $Co^{III}P$ in the aliquot of Nafion-$Co^{III}P$ solution used to coat the electrode.

c. Quantity of $Co^{III}P$ in the coatings as measured coulometrically (see text).

Figure 2.6.

(A) Current-potential curves for the reduction of dioxygen at a rotating disk graphite electrode coated with Nafion in which 2.5 x 10^{-9} mole cm^{-2} CoP and 1.9 x 10^{-8} mole cm^{-2} $Ru(NH_3)_6^{3+}$ were incorporated. The dashed line is the response that resulted when the $Ru(NH_3)_6^{3+}$ was omitted. Supporting electrolyte: 0.1 M acetate buffer (pH 4.5) saturated with air. Scan rate: 2 mV s^{-1}.

(B) Levich plots of the limiting O_2 reduction current for curves such as those in part A vs. the (electrode rotation rate)$^{1/2}$. Coating compositions are as follows: curve, $10^9\Gamma_{Co}$(mole cm^{-2}), $10^8\Gamma_{Ru}$ (mole cm^{-2}); 1 and 4, 3, 1.8; 2 and 5, 1.9, 1.9; 3, 1.1, 1.2. The dashed lines are the calculated responses for the diffusin-convection limited, two-electron reduction of O_2. Other experimental conditions as in part A.

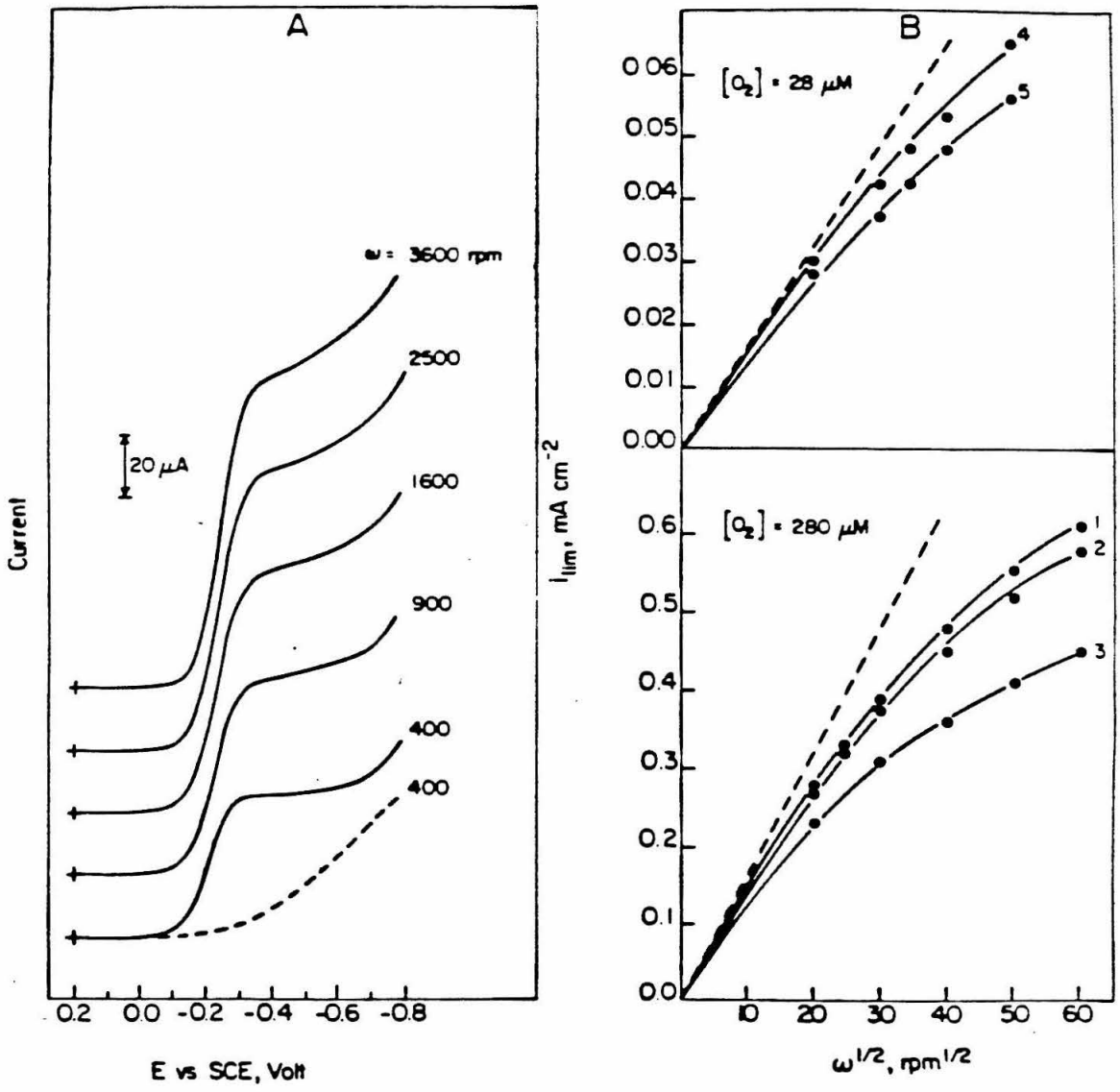
A
ω = 3600 rpm
2500
1600
900
400
400
20 μA
Current
0.2 0.0 -0.2 -0.4 -0.6 -0.8
E vs SCE, Volt
B
[O2] = 28 μM
4
5
0.06
0.05
0.04
0.03
0.02
0.01
0.00
[O2] = 280 μM
1
2
3
0.6
0.5
0.4
0.3
0.2
0.1
0.0
10 20 30 40 50 60
ω1/2, rpm1/2
Ilim, mA cm-2

contributions from the direct reduction of O_2 at the electrode as the electrode rotation rate increases. This is the behavior expected when the catalyzed reduction proceeds at too low a rate to consume all of the O_2 that is diffusing through the coating before it reaches the electrode surface. In such cases, a second, direct reduction wave appears that is useful diagnostically in assigning kinetic mechanisms at polymer-coated electrodes (12).

Levich plots (13) of the limiting currents vs. $\omega^{1/2}$ for curves such as those in Figure 2.6A are shown in Figure 2.6B for two concentrations of O_2 (estimated from the composition of the gas mixtures assuming Henry's law to apply). The measured currents fall below those calculated for the pure diffusion-convection-controlled reduction of O_2 to H_2O_2 (dashed lines in Figure 2.6B). Such behavior signals that the current is limited by a process other than the supply of O_2 reaching the surface of the coated electrode. The kinetics of the electron-transfer reactions proceeding within the coatings and the transport of O_2 and/or $Ru(NH_3)_6^{3+/2+}$ through the coating are all possible current-limiting processes.

At a fixed electrode rotation rate, ω, with a constant quantity of CoP in the coating, the magnitude of the limiting O_2 reduction currents depended on the quantity of $Ru(NH_3)_6^{3+}$ in the coatings as shown in Figure 2.7. With sufficient quantities of incorporated $Ru(NH_3)_6^{3+}$, the currents became independent of the amount of $Ru(NH_3)_6^{3+}$ present while remaining well below the calculated Levich currents for the two-electron reduction of O_2. Under these conditions, the rate of reaction 2.2 (proceeding within the coating) is so large that only reaction 2.1 needs to be considered as a possible current-limiting process. At the lower values of Γ_{Ru} where the measured currents become dependent on Γ_{Ru} (Figure 2.7), the kinetics of reaction 2.2 must also be considered.

Kinetic Analysis. In analyzing the interplay of the various kinetic and transport processes that determine the measured plateau currents at electrodes

Figure 2.7. Limiting O_2 reduction currents at an electrode coated with Nafion-CoP-$Ru(NH_3)_6^{3+}$ as a function of the quantity of $Ru(NH_3)_6^{3+}$ in the coating. Γ_{Co} = 3.7 x 10^{-9} mole cm^{-2}. Supporting electrolyte: 0.1 M acetate buffer (pH 4.5) saturated with air and also containing 2 x 10^{-6} M $Ru(NH_3)_6^{3+}$.

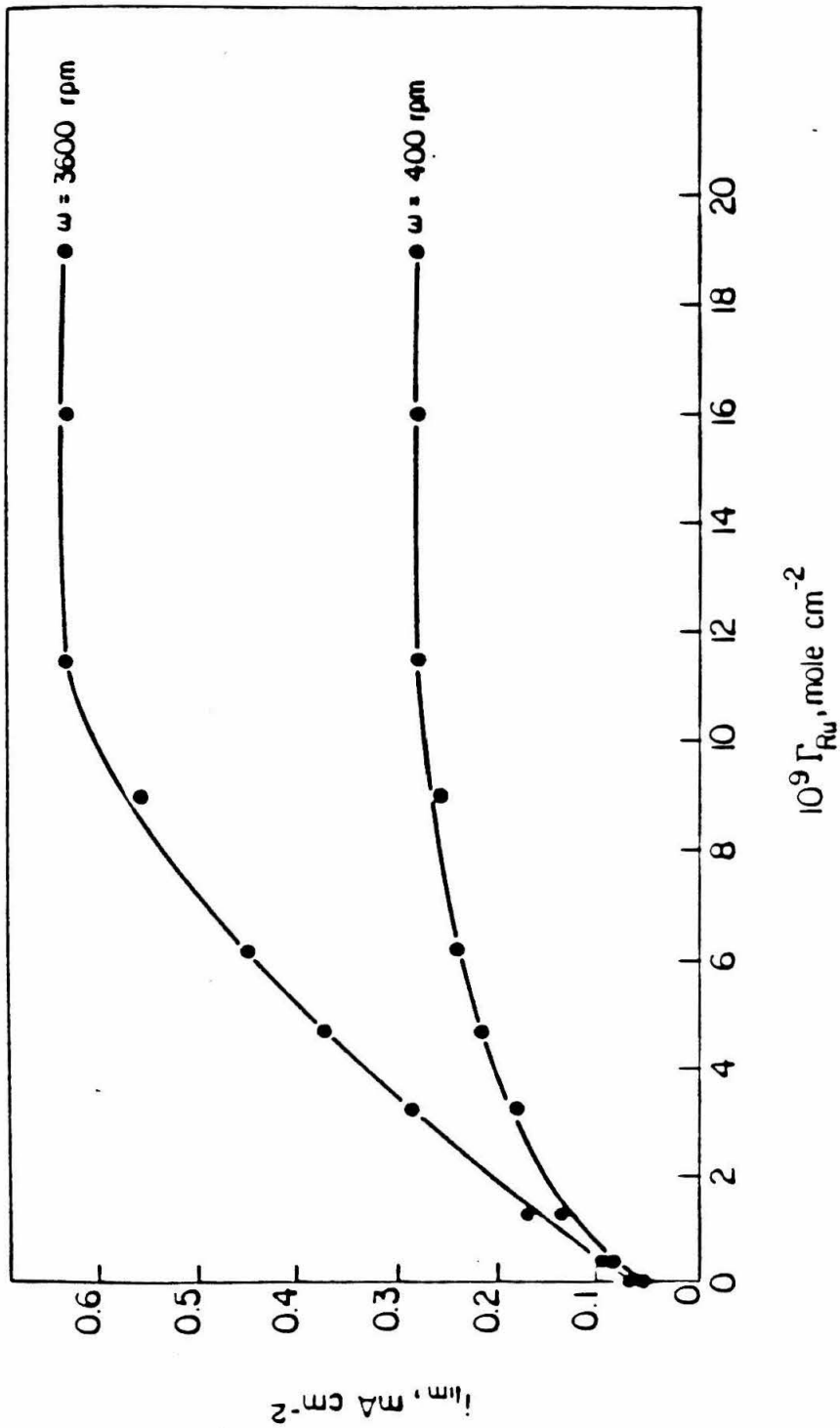
ω = 3600 rpm
ω = 400 rpm
i_{lim}, mA cm^{-2}
$10^9 \Gamma_{Rw}$, mole cm^{-2}
0
0.1
0.2
0.3
0.4
0.5
0.6
2
4
6
8
10
12
14
16
18
20

coated with redox polymers, it is instructive to utilize kinetic zone diagrams (14). Theoretical analyses and zone diagrams for CE mechanisms (*i.e.*, a slow chemical step preceding electron transfer) are available for cases involving homogeneous catalysis (15) as well as the catalysis of electrode processes proceeding at uncoated (14) and at polymer-coated electrodes (16). Zone diagrams presented previously for the case of rotating disk voltammetry (16) are not applicable to the present case because they were derived for simpler mechanisms in which the catalyst is also the reactant responsible for the transport of electrons between the electrode and the substrate. However, a recent treatment of "preactivation" mechanisms at redox polymer films was adaptable for use with the present system. Reaction 2.1 amounts to "preactivation" of the substrate (O_2) prior to its reduction in the same sense that the term is employed in reference 17 except that reaction 2.1 is a second- instead of a first-order reaction. However, it was possible to operate under pseudo-first-order conditions so that this difference presented no problem. The treatment of reference 17 also does not encompass the possibility of a parallel unactivated reaction pathway, *e.g.*, direct reduction of O_2 by $Ru(NH_3)_6^{2+}$. However, by operating under conditions where this pathway made negligible contributions to the measured currents, this possible complication was avoided. The relevant zone diagram for the mechanism embodied in reactions 2.1 to 2.3 under conditions where reaction 2.1 is rate-limiting (*e.g.*, at high concentrations of $Ru(NH_3)_6^{3+}$) is shown in Figure 2.8. The letters R, E, and S denote the various combinations of kinetic, electron-transport and substrate-transport processes, respectively, that can limit the measured currents (17).

To proceed with an analysis of our data on the basis of the diagram of Figure 2.8, it is necessary to evaluate three experimental parameters: i_s^*, i_E, and i_k^*. i_s, defined by eqn. 2.8, is the current density that measures the rate of

Figure 2.8. Kinetic zone diagram for a preactivation mechanism as adapted from reference 17 for application to the mechanism of reactions 2.1 to 2.3. The zones labeled ER1, R1, etc., specify the conditions where the various possible current-limiting processes become dominant (3). The vectorial diagram at the top gives the magnitude and direction of the movement within the diagram that results when the indicated experimental parameters are increased. The data points entered as small numbers in the diagram correspond to the experiment numbers in Table 2.3. Each point represents a different electrode rotation rate.

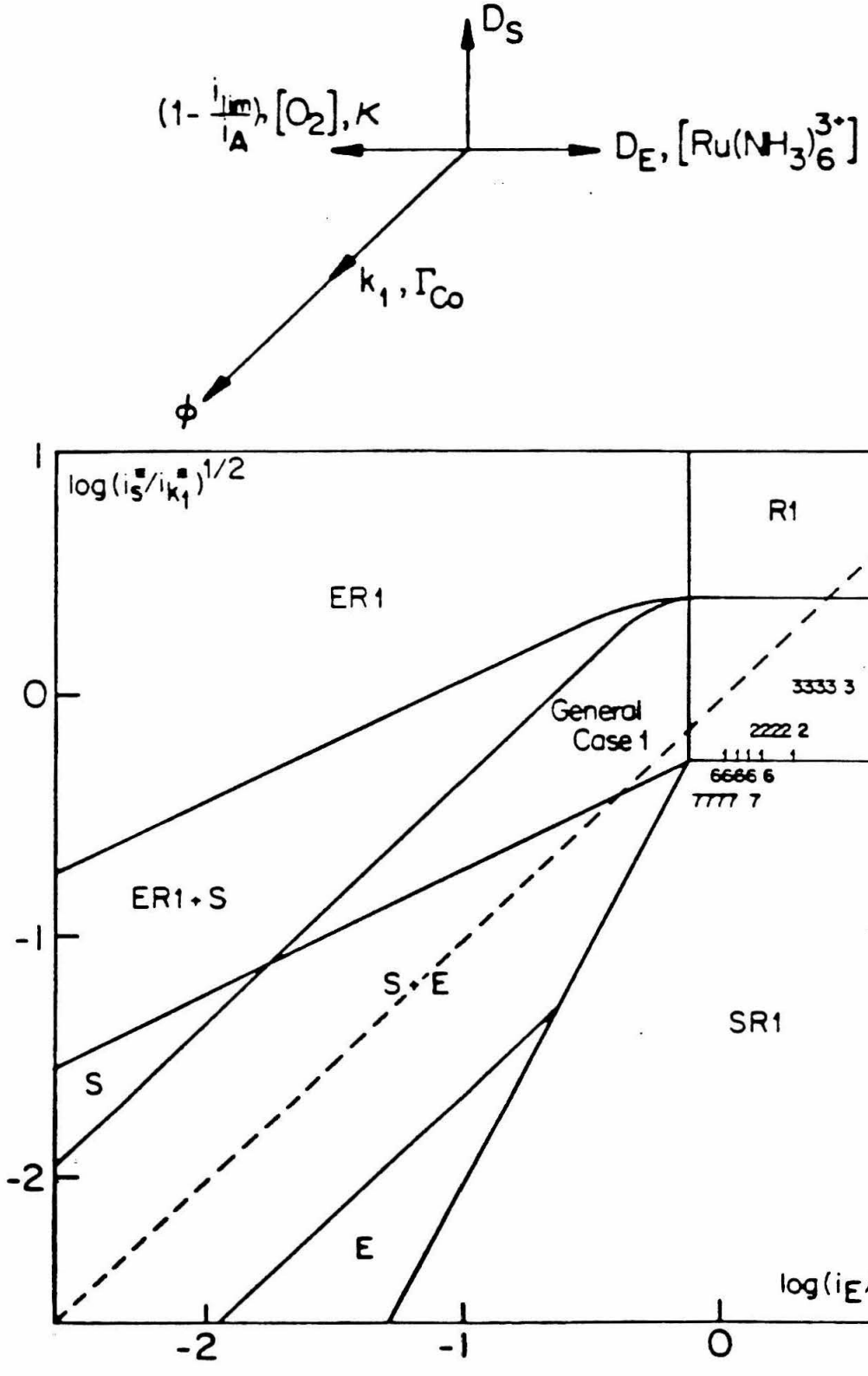
D_S
$(1-\frac{i_{lim}}{i_A})_h, [O_2], K$
$D_E, [Ru(NH_3)_6^{3+}]$
k_1, Γ_{Co}
ϕ
$\log(i_S^{\bullet}/i_{k_1}^{\bullet})^{1/2}$
R1
ER1
R1 + S
3333 3
General Case 1
2222 2
555 5
1111 1
444 4
6666 6
7777 7
ER1 + S
S + E
SR1
S
E
$\log(i_E/i_{k_1}^{\bullet})^{1/2}$
1
0
-1
-2
-2
-1
0
1

diffusion of the substrate, O_2, within the electrode coating (18)

$$i_s = \frac{2FC^b_{O_2}\kappa D_s}{\phi} \quad , \tag{2.8}$$

where F is Faraday's constant, $C^b_{O_2}$ is the bulk concentration of O_2, κ is the constant governing the partitioning of O_2 between the coating and the solution, D_s is the diffusion coefficient of O_2 within the coating, and ϕ is the thickness of the coating. i^*_s, defined by eqn. 2.9, measures the rate of O_2 diffusion through the coating normalized with respect to the varying concentration of O_2 at the coating/solution interface instead of $C^b_{O_2}$(16),

$$i^*_s = i_s\left(\frac{1 - i_{lim}}{i_A}\right), \tag{2.9}$$

where i_{lim} is the measured plateau current density and i_A is the electrode rotation rate-dependent Levich current density (13) corresponding to $C^b_{O_2}$.

To measure i_s, the graphite disk electrode was lightly plated with Pt before it was coated with pure Nafion. The reduction of O_2 to H_2O at the resulting electrode is limited by its rate of diffusion through the coating to reach the platinum catalyst sites on the underlying electrode (19). The intercepts of linear Koutecky-Levich plots (20) of the inverse limiting reduction currents vs. $\omega^{-1/2}$ were equated with $(2i_s)^{-1}$. The factor of 2 accounts for the fact that O_2 is reduced to H_2O at the platinum-plated electrode but only to H_2O_2 by CoP + $Ru(NH_3)^{2+}_6$. Some values of i_s obtained by this procedure are listed in Table 2.2. i^*_s was calculated from the measured i_{lim} values at each rotation rate and O_2 concentration by means of eqn. 2.9.

i_E is a measure of the rate at which electrons can be transported across the coating (18). i_E was evaluated from the slopes, S , of linear chronocoulometric charge-(time)$^{1/2}$ plots for the semiinfinite diffusion-limited reduction of the $Ru(NH_3)^{3+}_6$ incorporated in the coatings (21). Measurements were conducted after transfer of the coated electrodes to pure supporting electrolyte

Table 2.2: Evaluation of O_2 Penetration Currents, i_s, and $Ru(NH_3)_6^{3+/2+}$ Charge Propagation Currents, i_E, at Nafion-Coated Electrodes

$10^7\ \Gamma_{NF}$, [a]	$10^9\ \Gamma_{CoP}$, [b]	i_s, [c]
mole cm^{-2}	mole cm^{-2}	mA cm^{-2}
1.5	2.5	1.10
1.5	3.7	1.10
0.9	1.5	1.62

$10^7\ \Gamma_{NF}$, [a]	$10^8\ \Gamma_{Ru}$, [d]	i_E, [e]
mole cm^{-2}	mole cm^{-2}	mA cm^{-2}
1.5	1.9	1.6
1.5	1.8	1.5
0.9	1.2	2.8

a. Sulfonate groups in the Nafion used to coat the electrode.

b. Quantity of CoP present in the Nafion coatings.

c. Obtained from the intercepts of Koutecky-Levich plots for the reduction of O_2 at platinum-plated graphite electrodes coated with Nafion-CoP in the absence of $Ru(NH_3)_6^{3+}$ (see text).

d. Quantity of $Ru(NH_3)_6^{3+}$ incorporated in the Nafion coatings.

e. Obtained from equation 2.10.

solutions. Equation 2.10 relates the measured slopes and quantities of incorporated $Ru(NH_3)_6^{3+}$, Γ_{Ru} , to i_E.

$$i_E = \frac{\pi(S)^2}{4F\Gamma_{Ru}} \tag{2.10}$$

The measured values of i_E are given in Table 2.2.

$i^*_{k_1}$ is a kinetic current density defined by eqn. 2.11,

$$i^*_{k_1} = i_{k_1}\left(1 - \frac{i_{lim}}{i_A}\right) = 2k_1 F C^b_{O_2} \kappa \Gamma_{CoP}\left(1 - \frac{i_{lim}}{i_A}\right), \tag{2.11}$$

where i_{k_1} is the corresponding kinetic current density normalized with respect to the bulk concentration of O_2, $C^b_{O_2}(18)$, Γ_{CoP} is the quantity of cobalt porphyrin in the coating that participates in the catalyzed reduction of O_2, and the other terms have been previously defined. The procedures employed to evaluate i_{k_1} will be described below.

To identify the processes that control the magnitudes of the catalytic O_2 reduction currents and to locate the system on the zone diagram of Figure 2.7, it is useful to prepare Koutecky-Levich plots of i^{-1}_{lim} vs. $\omega^{-1/2}$ (7, 14) from the plateau currents of curves such as those shown in Figure 2.6. Figure 2.9 contains a set of Koutecky-Levich plots for two concentrations of O_2. The plots are linear and have slopes that match those calculated from the Levich equation(13, 22) for the reduction of O_2 to H_2O_2. In additon, the intercepts of the plots are inversely proportional to the concentration of O_2 in the solution and to the quantity of CoP within the coatings but are independent of the concentration of $Ru(NH_3)_6^{3+}$ in the coatings. The linearity and slopes of the Koutecky-Levich plots as well as their independence of the concentration of $Ru(NH_3)_6^{3+}$ indicate that the catalyst-coated electrode is not operating in any of the zones in Figure 2.8 that contain an E (17). That is, the currents are not limited by the rate of transport of electrons across the coating by the $Ru(NH_3)_6^{3+/2+}$ couple. The

Figure 2.9. Koutecky-Levich plots($1/i_{lim}$ vs. $\omega^{-1/2}$) of the data points from Figure 2.6B. The dashed lines have the same significance as in Figure 2.6B. The points shown as solid squares were calculated for conditions corresponding to curve 2 by numerical solution of the governing differential equation (see text).

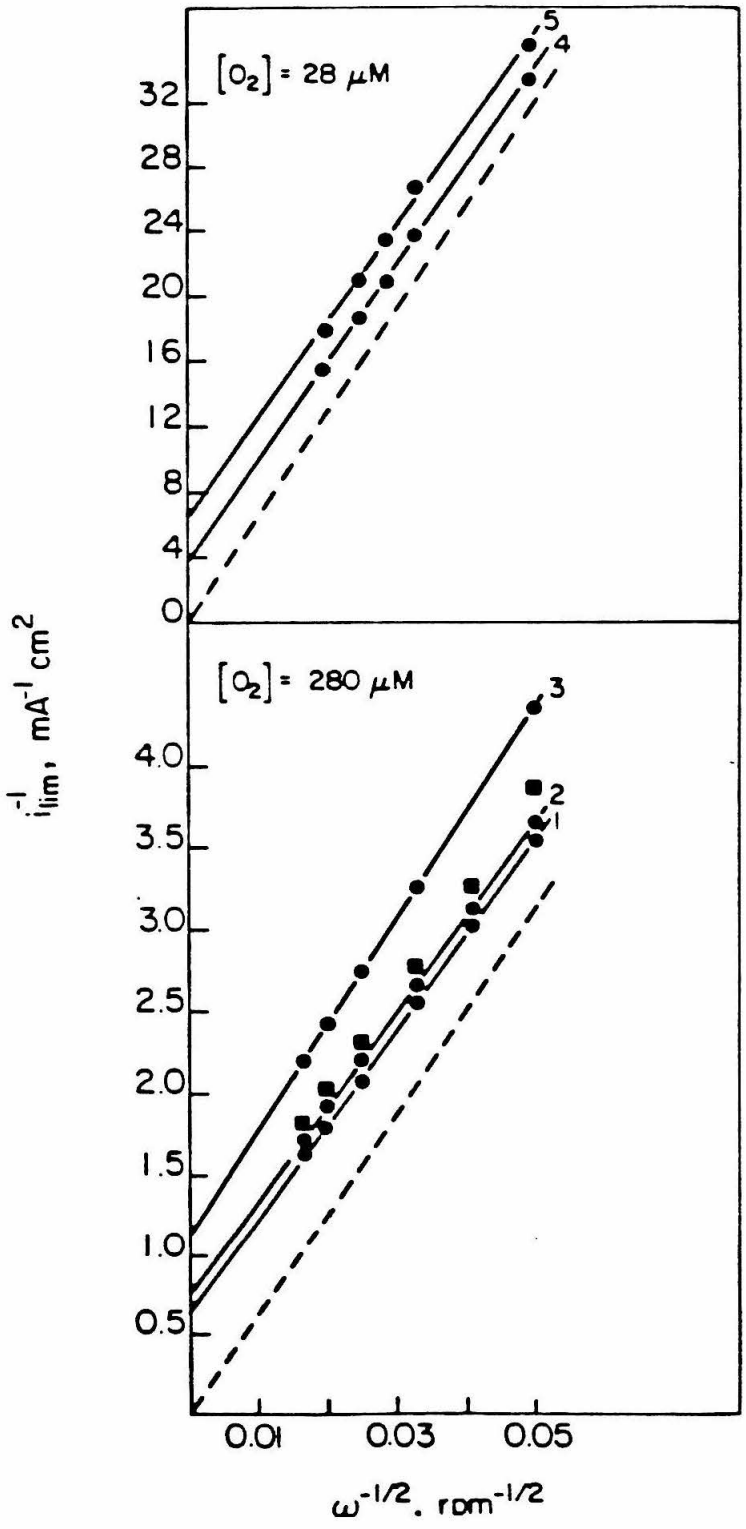
[O2] = 28 μM
[O2] = 280 μM
5
4
3
2
1
32
28
24
20
16
12
8
4
0
4.0
3.5
3.0
2.5
2.0
1.5
1.0
0.5
0.01
0.03
0.05
i_{lim}^{-1}, $mA^{-1}\,cm^2$
$\omega^{-1/2}$, $rpm^{-1/2}$

dependence of the Koutecky-Levich intercepts on the quantity of CoP in the coating indicates that the system is not operating within the zone labeled S (17). Thus, the Koutecky-Levich plots indicate that the portions of the diagram in Figure 2.8 that may be relevant for our experiments are those labeled "R1", "R1 + S", "SR1", and, possibly, "General Case". Since the R1 and SR1 situations are merely limiting versions of the more general R1 + S case (17), the kinetic behavior was first compared with the response expected of a system falling within the R1 + S domain. For such systems, an analytical expression for the plateau current, i_{lim} can be derived (17)

$$i_{lim} = (i^*_{k_1} i^*_s)^{1/2} tanh \left[(\frac{i^*_{k_1}}{i^*_s})^{1/2} \right], \qquad (2.12)$$

or, in view of the definitions of $i^*_{k_1}$ and i^*_s (eqns. 2.9 and 2.11),

$$(i_{lim})^{-1} = i_A^{-1} + \left\{ (i_{k_1} i_s)^{1/2} tanh \left[(\frac{i^*_{k_1}}{i_s})^{1/2} \right] \right\}^{-1}. \qquad (2.13)$$

Thus, the "film currents" (23), i_F, corresponding to the intercept of the Koutecky-Levich plots in Figure 2.8 should be given by equation 2.14

$$i_F = (i_{k_1} i_s)^{1/2} tanh \left[(\frac{i_{k_1}}{i_s})^{1/2} \right] \quad . \qquad (2.14)$$

Equation 2.14 and the values of i_s in Table 2.2 were used to evaluate i_{k_1}, and the product κk_1 was then calculated from eqn. 2.11. The resulting values, listed in Table 2.3, are fairly constant, but to be certain that the small variations in κk_1 did not result from the use of eqn. 2.14 instead of the equation corresponding to the "general case" in the zone diagram of Figure 2.8, the complete differential equation governing the behavior of the system (24) was solved numerically without approximations by using the values of i_{k_1} in Table 2.3. The complete computer program is included in Appendix I. The resulting calculated plateau currents agreed well with the experimental values. For example, the calculated

Table 2.3: Rate Constants for Reaction 2.1 Evaluated from Rotating Disk Data

Expt. No.	$10^7\ \Gamma_{NF}$, [a] mole cm $^{-2}$	$10^9\Gamma_{Co}$, [b] mole cm^{-2}	$[O_2]$, mM	i_{k_1}, [c] mA cm^{-2}	$10^{-4}\ \kappa k_1$, [d] $M^{-1}s^{-1}$	i_{k_1}, [e] mA cm^{-2}
1	1.5	3.0	0.28	2.75	1.7	3.56
2	1.5	1.9	0.28	2.05	2.0	2.26
3	0.9	1.1	0.28	1.09	1.8	1.33
4	1.5	3.0	0.028	0.69	4.3	0.35
5	1.5	1.9	0.028	0.27	2.6	0.23
6	1.8	3.6	0.28	2.81	1.5	4.12
7	2.1 [f]	4.2	0.28	3.20	1.4	5.03
					Avg. 2.2	

a. Sulfonate groups in the Nafion used to coat the electrode.

b. Quantity of CoP present in the Nafion coatings as measured coulometrically.

c. Calculated from equation 2.14.

d. Calculated from equation 2.11.

e. Self-consistent set of i_{k_1} values calculated from equation 2.11 using the average value of κk_1.

f. Increasing Γ_{Nf} by much larger factors, *e.g.*, to 15 x 10^{-7}mole cm^{-2}, produced smaller values of i_{k_1} than expected on the basis of the data for thinner coatings. This behavior was traced to a decrease in i_E with coating thickness greater than expected.

currents are plotted for comparison with the corresponding experimental values next to curve 2 of Figure 2.9.

The borders between the various regions of the zone diagram in Figure 2.8 are actually not as precisely defined as the thin lines on the figure might suggest because the distinction between two neighboring regions becomes somewhat arbitrary near their common boundary (17). It was therefore useful to locate the experimental data points within the diagram to confirm that they all lie within the R1 + S region. When the average value of κk_1 from Table 2.3 was used, a self-consistent set of $i^*_{k_1}$ values was calculated at each electrode rotation rate for the experiments summarized in Table 2.3. The resulting values of $i^*_{k_1}$ were combined with the corresponding values of i^*_s and i_E to locate each data point on the zone diagram in Figure 2.8. All of the data lie well within the R1 + S or SR1 region where the plateau currents are accurately described by equations 2.13 and 2.14. Thus, the use of these equations in analyzing the kinetic data obtained with sufficient $Ru(NH_3)_6^{3+}$ in the coatings is consistent with the location of the data points in the zone diagram. Physically, the location of the data points within the R1 + S and SR1 regions means that the plateau currents are limited by the forward rate of reaction 2.1. The reaction proceeds throughout the entire coating but with O_2 concentrations that decrease continuously between the coating/solution and electrode/coating interfaces.

The sets of data points move within the zone diagram as the experimental parameters are changed in accord with the vectorial display at the top of the diagram (as they must, of course, because of the way the values of $i^*_{k_1}$ were calculated). This feature of the zone diagram proved quite useful in designing experiments to check that the experimental system matched the kinetic model from which the zone diagram was derived (17).

Variation in the Concentration of $Ru(NH_3)_6^{3+}$. The experiments in Table 2.3 were all conducted in the presence of sufficient $Ru(NH_3)_6^{3+}$ to make

the measured currents independent of its concentration. If the concentration of $Ru(NH_3)_6^{3+}$ is decreased, one would expect to see an effect on the measured currents not only because i_E decreases but also because the rate of reaction 2.2 becomes comparable to that of reaction 2.1 as the ratio $(k_2\Gamma_{Ru})/(k_{-1}\phi) = (k_2[Ru(NH_3)_6^{3+}])/k_{-1}$ approaches unity. Table 2.4 summarizes rotating disk data obtained for three values of Γ_{Ru} and two rotation rates. As anticipated, the measured plateau currents decrease with Γ_{Ru}. Koutecky-Levich plots become nonlinear under these conditions (17), and it is necessary to solve the general governing differential equation numerically in order to compare the experimental currents with those calculated for a preactivation mechanism with partial control by the rate of reaction 2.2. (Note that the zone diagram of Figure 2.8 is also not applicable to plateau currents that exhibit a dependence on the concentration of $Ru(NH_3)_6^{3+}$. To display the behavior of such systems requires a three-dimensional zone diagram (17) that is beyond the intended scope of this work.) The numerical solution of the relevant differential equation (24) requires values of i_E, $i_s^*, i_{k_1}^*$, and $\sigma \equiv (k_2[Ru(NH_3)_6^{3+}])/k_{-1}$ in the coatings. The three characteristic current densities were available from independent measurements (Tables 2.2 and 2.3). In one set of calculations, k_2/k_{-1} was assumed to have the same value as was measured in the experiments in homogeneous solution, namely, $k_2/k_{-1} = 1.7 \times 10^3 M^{-1}$, and $[Ru(NH_3)_6^{3+}]$ was calculated from the measured values of Γ_{Ru} and an estimate of the coating thickness (0.3 μm for $\Gamma_{Nf} = 1.5 \times 10^{-7}$ mole cm^{-2} (2c)). The resulting values of σ (Table 2.1) were large enough to yield calculated plateau currents that were independent of Γ_{Ru} in disagreement with the experimental observations (Table 2.4). We believe that this apparent disagreement arises from the assumption that k_2/k_{-1} will have the same value in the Nafion coatings as in homogeneous solution. The value of k_1/k_{-1} must be small because we encountered no evidence for the formation of significant equilibrium concentrations of the $PCoO_2$ adduct. Since k_1 was

Table 2.4: Dependence of Plateau Currents for Catalyzed Reduction of O_2 on Γ_{Ru} at Constant Γ_{Co}[a]

$10^9\ \Gamma_{Ru}$	$[Ru(NH_3)_6^{3+}]$[b]	ω = 400 rpm			ω = 3600 rpm		
mole cm^{-2}	M	i_{lim},[c]	i_{calc},[d] mA cm^{-2}		i_{lim},[c]	i_{calc}, mA cm^{-2}	
		mA cm^{-2}	σ=1.7 x 10^3	σ =3.3	mA cm^{-2}	σ=1.7 x 10^3	σ=3.3
			$[Ru(NH_3)_6^{3+}]$	$[Ru(NH_3)_6^{3+}]$		$[Ru(NH_3)_6^{3+}]$	$[Ru(NH_3)_6^{3+}]$
18	0.6	0.28	0.27	0.26	0.63	0.64	0.57
9	0.3	0.25	0.27	0.25	0.56	0.64	0.50
4.6	0.15	0.22	0.27	0.25	0.38	0.63	0.40

a. $\Gamma_{Co} = 3.7\text{x}10^{-9}$mol cm^{-2} and$\Gamma_{Nf} = 1.5 \text{ x } 10^{-7}$ mol cm^{-2}.

b. Concentration of $Ru(NH_3)_6^{3+}$ in the coating, calculated as Γ_{Ru}/ϕ. For $\Gamma_{Nf} = 1.5\text{x}10^{-7}$mole cm^{-2}, $\phi = 3 \text{ x } 10^{-5}$ cm.

c. Measured plateau current for reduction of O_2.

d. Plateau current calculated by numerical solution of the governing differential equation for this case (24). For $\Gamma_{Ru} = 18\text{x}10^{-9}$ mole cm^{-2} the other parameters required were measured as $i_E = 1.5, i_s = 1.1$, and $i_k = 3.6$ mA cm^{-2}. For the other values of Γ_{Ru}, i_E was assumed to be proportional to Γ_{Ru}.

measured as $3.6\text{x}10^3\text{M}^{-1}\text{s}^{-1}$, it follows that k_{-1} must be larger than, say, 10^4s^{-1}. If k_{-1} were this large, k_2 measured as $1.7\text{x}10^3 k_{-1} M^{-1} s^{-1}$ in the kinetic experiments in homogeneous solution would be larger than $1.7\text{x}10^7\text{M}^{-1}\text{s}^{-1}$. This value exceeds the diffusion-limited rate constant, k_d, that can be estimated for $Ru(NH_3)_6^{3+}$ incorporated in Nafion from the Smoluchowski equation (25) and its diffusion coefficient as measured by $i_E, k_d \approx 4\text{x}10^5\text{M}^{-1}\text{s}^{-1}$ (2c). Thus, even if the reactivities of $Ru(NH_3)_6^{3+}$ and $PCoO_2$ remained the same in Nafion as in homogeneous solution, one would anticipate that k_2/k_{-1} should be considerably smaller with the reactants incorporated in Nafion. The fifth and last columns in Table 2.4 show the result of employing a smaller value of k_2/k_{-1} and, therefore, of σ, in caluculating the plateau currents. Much better agreement between the experimental and calculated currents results for a value of k_2/k_{-1} that is 500-fold smaller, which does not seem unreasonable in view of the arguments given above that the value of k_2, a second-order rate constant, is apt to be depressed much more than k_{-1}, a first-order rate constant, is apt to be enhanced by incorporation of the reactants in a Nafion coating. This lower value of k_2/k_{-1} can be used to obtain a (very approximate) estimate of the equilibrium constant, K_1, for the formation of the CoP-O_2 adduct in Nafion coatings: if k_2 is taken as $4 \text{ x } 10^5 M^{-1} s^{-1}$, *i.e.*, the diffusion-limited rate constant for $Ru(NH_3)_6^{3+}$ in Nafion as calculated from the Smoluchowski equation, and k_2/k_{-1} is set equal to $1/500 \text{ x } 1.7 \text{ x } 10^3 = 3.4\text{M}^{-1}$, *i.e.*, the value required to obtain the best agreement with the data in Table 2.4, $k_{-1} = 4\text{x}10^5/3.4 = 1.2\text{x}10^5\text{s}^{-1}$. Then $\kappa K_1 = \kappa k_1/k_{-1} = 2.2\text{x}10^4/1.2\text{x}10^5 = 0.2\text{M}^{-1}$. This rough estimate of κk_1 is consistent with the experimental fact that the binding of O_2 by CoP in Nafion is too weak to detect by spectral or electrochemical methods.

Discussion

The average value of κk_1 obtained from the rotating disk measurements, $2.2\text{x}10^4\text{M}^{-1}\text{s}^{-1}$ (Table 2.3), is about seven times larger than the value $k_1 =$

$3.1x10^3M^{-1}s^{-1}$ resulting from the kinetic measurements with homogeneous solutions of the reactants. It is possible that $\kappa > 1$ for O_2 at the Nafion-aqueous interface because of the well-known high solubility of O_2 in perfluorinated solvents (26). However, it would be surprising if O_2 were seven times more soluble in Nafion than in water. For example, a recent study has shown that O_2 is about three times more soluble in a hydrated Nafion membrane than in water (27). Thus, part of the difference between the measured values of κk_1 (within the Nafion coatings) and k_1 (in homogeneous solution) may reflect an increased reactivity of the CoP catalyst incorporated in Nafion. The O_2 faces less competition for axial ligation sites on the cobalt center within the anion-rejecting Nafion coatings, and this could conceivably result in more rapid reduction rates.

Relatively long integration times were required for reduction by $Ru(NH_3)_6^{2+}$ of the last 25-30% of the CoP incorporated in the Nafion coatings, indicating that some of the catalyst resides in portions of the coatings that are less accessible to the $Ru(NH_3)_6^{3+/2+}$ mediator couple than is the majority of the catalyst. Only the more accessible catalyst sites would contribute to the current responses observed for the reduction of O_2 at the effective reaction times at the rotating disk electrode ($< 1s$). Hence, the actual value of κk_1 within the Nafion coatings may be even larger than the values listed in Table 2.3.

It is also of interest to compare the catalytic behavior of the cobalt porphyrin catalyst immobilized in Nafion coatings with that resulting when it is bound directly to the electrode surface by irreversible adsorption. The latter was the procedure employed successfully in a previous study of the catalysis of O_2 reduction by a cobalt porphyrin that was insoluble in water (28). The water-soluble porphyrin investigated in the present study spontaneously adsorbs on pyrolytic graphite electrodes in amounts of a monolayer or two, but it begins to desorb from the surface within a few minutes after transfer to a pure supporting

electrolyte solution. The electrochemistry of the adsorbed and unadsorbed cobalt porphyrin will be discussed in more detail in Chapter III. Nevertheless, by working rapidly, it was possible to make rotating disk measurements of O_2 reduction at electrodes on which known quantities of the porphyrin were adsorbed. Linear Koutecky-Levich plots resulted with intercepts that yielded values of k_1 for the adsorbed porphyrin of ca. $10^5 M^{-1}s^{-1}$. This value is somewhat larger than the average value of κk_1 in Table 2.3, probably because all the adsorbed porphyrin participates in the catalysis while only a portion of that incorporated in Nafion is able to do so (vide supra). However, the Nafion coated electrodes can be adjusted to yield plateau currents no smaller than those obtained with the catalyst adsorbed on the surface in the same solutions, and the catalytic activity is much longer lived with the Nafion coatings. Thus, incorporation of the porphyrin catalyst within the Nafion coatings (along with the necessary mediator) is advantageous with respect to catalyst longevity. Of course, the O_2 reduction proceeds at the more negative potential determined by the formal potential of the mediator redox couple when the catalyst is immobilized within Nafion instead of adsorbed directly on the electrode but this drawback should be avoidable by designing rapidly reacting redox mediators with more positive formal potentials.

Optimization of the Catalyst-Mediator System. It is of general interest to consider how to utilize catalyst-mediator combinations incorporated in polymer coatings in order to obtain the best catalytic efficiencies, defined as the ratio of the measured plateau current, i_{lim}, to the corresponding Levich current, i_A. For a system such as the present one that operates on the right-hand side of the zone diagram in Figure 2.8 (*i.e.*, under conditions where the currents are independent of the concentration of $Ru(NH_3)_6^{3+}$ in the coating) the experimental variable that can be adjusted to alter the catalytic efficiency is the coating thickness, ϕ. (It is assumed that the concentration of catalyst within the

coating material is already at its highest practical value.) For sufficiently thin coatings ($i_s >> i_{k_1}$), eqn. 2.13 simplifies to eqn. 2.15,

$$\frac{1}{i_{lim}} = \frac{1}{i_A} + \frac{1}{i_{k_1}} \quad , \tag{2.15}$$

and the catalytic efficiency is given by eqn. 2.16,

$$CAT\ EFF = \frac{i_{k_1}}{i_{k_1} + i_A} \quad . \tag{2.16}$$

With electrode rotation rates great enough to avoid depletion of the substrate concentration at the coating/solution interface, $i_A >> i_{k_1}$ so that CAT EFF = i_{k_1}/i_A and, since $_{k_1}$ is proportional to Γ_{CoP} (eqn. 2.11), which increases linearly with the coating thickness, CAT EFF increases linearly with ϕ. However, i_s decreases as ϕ increases, and when i_s and i_{k_1} become comparable, the increase in CAT EFF with ϕ is smaller and CAT EFF ultimately becomes independent of ϕ when $i_{k_1} >> i_s$ (eqn. 2.13). The expected relationship between ϕ and CAT EFF is depicted in Figure 2.10. The portions of the curve corresponding to the relevant domains of the kinetic zone diagram of Figure 2.8 have been labeled in Figure 2.10. It is apparent from the figure that the optimum coating thickness, ϕ_{opt}, corresponds to the intersection of the two linear portions of the curve. With $\phi < \phi_{opt}$, higher currents can be obtained by increasing ϕ while with $\phi > \phi_{opt}$, the small additional increases in CAT EFF that can be realized require much larger increases in ϕ and, therefore, in consumption of the (often precious) catalyst. Figure 2.10 may be regarded as a plot of catalyst cost ($) vs. turnover rate (CAT EFF) and in these terms it seems clear that the point labeled ϕ_{opt} represents the optimum exploitation of the catalytic capabilities of the system. Even in cases where conservation of catalyst is less important than obtaining the maximum possible current densities (*i.e.*, maximum CAT EFF values), Figure 2.10 serves as a useful guide for choosing experimental operating

Figure 2.10. Relationship between catalytic efficiency, CAT EFF $\equiv i_{lim}/i_A$, and coating thickness for a catalyst-mediator combination incorporated in polymer coatings on electrodes. The diagram applies to the situation when the current is no longer affected by changes in the concentration of mediator in the coating. The labels on the three segments of the solid curve correspond to the zones in the diagram of Figure 2.8. The solid line was calculated from the following relevant equations: R1, eqn. 2.16 ($i_{k_1} << i_A$); R1 + S, eqn. 2.13; SR1, eqn. 2.13 ($i_s << i_{k_1}$). ϕ_{opt} and $(CAT\ EFF)_{opt}$ defined by eqns. 2.17 and 2.18 correspond to the coating thickness at which the catalyst is utilized most efficiently.

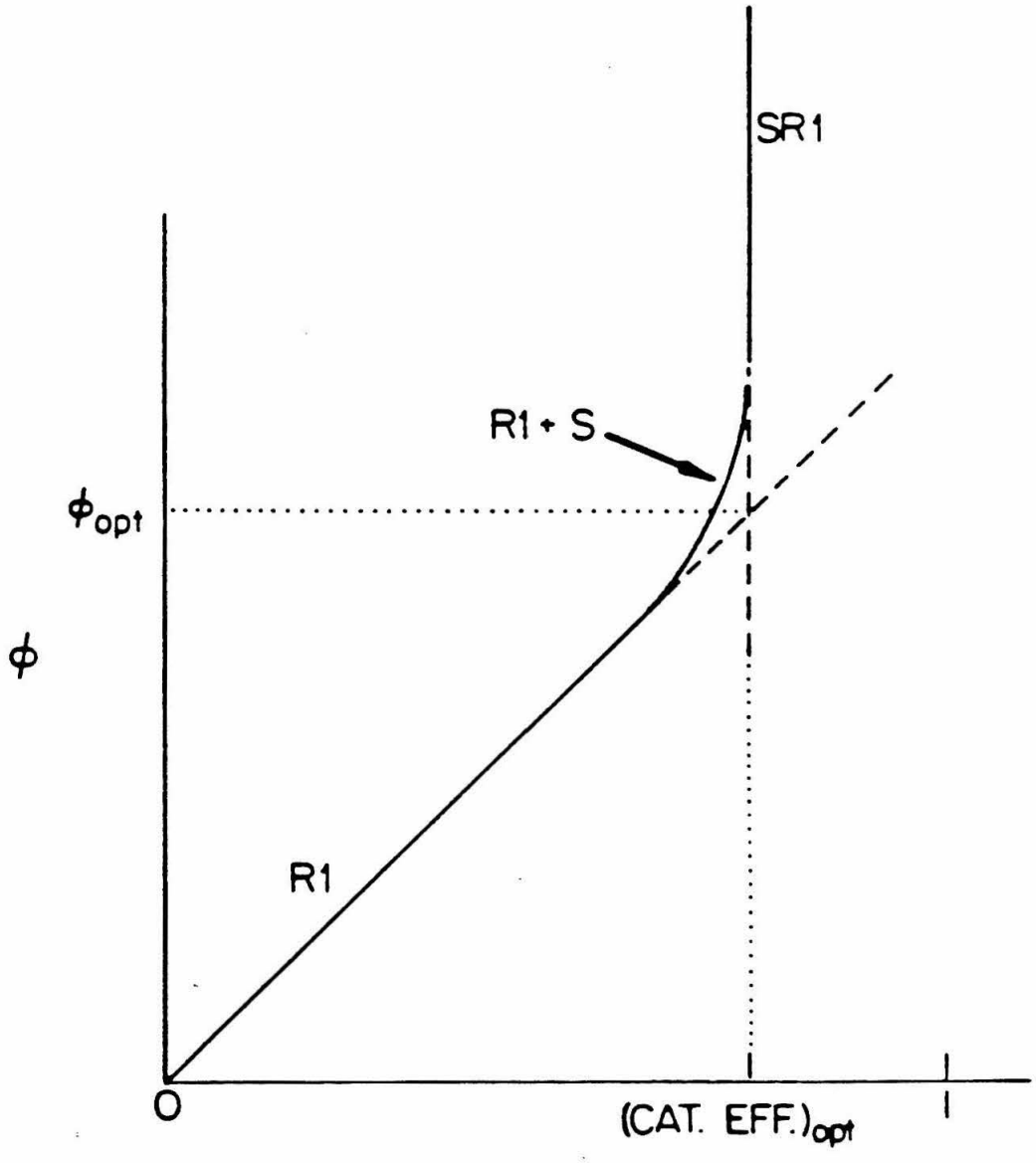
SR1
R1 + S
ϕ_{opt}
ϕ
R1
O
(CAT. EFF.)$_{opt}$
CAT. EFF.

conditions because the maximum possible value of CAT EFF, corresponding to the SR domain of the zone diagram, can be obtained with ϕ values only somewhat greater than ϕ_{opt}.

It can be derived from eqns. 2.8, 2.11 and 2.13 that

$$\phi_{opt} = \left(\frac{D_s}{k_1 [CoP]_p} \right)^{1/2} \tag{2.17}$$

where $[CoP]_p$ is the concentration of cobalt porphyrin in the coating. For the experimental conditions employed in most of the experiments summarized in Table 2.3, the coating thickness was rather close to the optimal value. For example, in experiment 1, ϕ_{opt} calculated from eqn. 2.17 is 1.6×10^{-5}cm, and the actual value of ϕ was $\sim 3 \times 10^{-5}$ cm. As expected from Figure 2.10, small decreases in ϕ produced essentially no changes in the plateau current under these conditions because we were operating on the steeply rising portion of the curve (i.e., in the R1+S and SR1 domains) in Figure 2.10.

The catalytic efficiency obtained when $\phi = \phi_{opt}$ is given by eqn. 2.18,

$$(CAT\ EFF)_{opt} = \frac{\kappa (D_s k_1 [CoP]_p)^{1/2}}{\frac{D_{O_2}}{\delta} + \kappa (D_s k_1 [CoP]_p)^{1/2}} \quad , \tag{2.18}$$

where D_{O_2} is the diffusion coefficient of O_2 in the bulk of the solution and δ, the thickness of the Levich layer (13,22) at the coating/solution interface, is determined by the electrode rotation rate. Equation 2.18 leads to the unsurprising conclusion that the largest values of $(CAT\ EFF)_{opt}$ will result when the coatings are loaded with as much catalyst as they can accommodate. However, increases in $[CoP]_p$ can result in the system's moving into a new domain of the zone diagram (Figure 2.8) unless i_s^* and i_E remain much larger than the increasing $i_{k_1}^*$. Thus, it is important to check that the system remains in one of the R1 + S zones (R, R1 +S, SR1) before utilizing eqn. 2.17 to calculate

the optimal coating thickness or eqn. 2.18 to calculate the corresponding optimal catalytic efficiency.

Concluding Remarks

The demonstration that functioning electrode coatings can be fashioned from premixed solutions of soluble Nafion and porphyrin catalysts is an encouraging result; the more so because the catalyst appears to lose none of its reactivity and is longer lived than when adsorbed directly on the electrode surface. This method also allows easy variations of the catalyst concentration in Nafion coatings, which is one of the important parameters in the kinetic analysis. That rapidly diffusing, cationic redox couples are readily incorporated by Nafion coatings adds to their appeal because it permits the use of catalysts that are essentially immobile in the coatings, *e.g.*, metalloporphyrins, metalloproteins, etc. The relatively low values of the diffusion coefficient of O_2 within Nafion coatings despite its small size suggests that alternative coating materials that are more highly swollen and may therefore yield larger substrate diffusion rates would be worth developing for use with catalyst-mediator combinations now that the factors which can be varied to obtain optimal catalytic efficiencies have been delineated.

References and Notes

1. a. Rubinstein, I.; Bard, A.J., J. Am. Chem. Soc., 102(1980)6641.
   b. Ibid., J. Am. Chem. Soc., 103(1981)5007.
   c. Henning, T. P.; White, H. S.; Bard, A.J., J. Am. Chem. Soc., 103(1981)3937.
   d. White, H.W.; Leddy, J.; Bard, A.J., J. Am. Chem. Soc., 104(1982)4811.
   e. Martin, C. R.; Rubinstein, I.; Bard, A.J., J. Am. Chem. Soc., 104(1981)4817.
   f. Krishnan, M.; Zhang, X.; Bard, A.J.,J. Am. Chem. Soc., 106(1984)7371.
2. a. Buttry, D.A.; Anson, F.C., J. Electroanal. Chem.,130(1981)333.
   b. Ibid., J. Am. Chem. Soc., 104(1982)4824.
   c. Ibid., J. Am. Chem. Soc., 105(1983)685.
   d. Ibid., J. Am. Chem. Soc., 106(1984)59.
   e. Tsou, Y. -M.; Anson, F. C., J. Electrochem, Soc., 131(1984)595.
   f. Buttry, D. A.; Saveant, J.-M.; Anson, F. C., J. Phys. Chem., 88(1984)3086.
3. a. Andrieux, C. P.; Dumas-Bouchiat, J. M.; Saveant, J.-M., J. Electroanal. Chem., 87(1978)39.
   b. Ibid., 87(1978)55.
   c. Ibid., 88(1978)43.
   b. Ibid., 113(1980)1.
   e. Ibid., 113(1980)19.
4. Pladziewicz, J. R.; Meyer, T. J.; Broomhead, J. A.; Taube, H., Inorg. Chem., 12(1973)639.
5. Hambright, P.; Fleischer, E. B., Inorg. Chem., 9(1970)1757.
6. Oyama, N.; Anson, F. C., Anal. Chem., 52(1980)1192.
7. Stanbury, D. M.; Haas, O.; Taube, H., Inorg. Chem., 19(1980)518.
8. "Solubilities of Inorganic and Metallorganic Compounds", Linke, W. F., vol. 11, 4th ed., American Chemical Society, Washington, D. C., 1965.

9. An alternative mechanism in which the porphyrin catalyst acts to stabilize O_2^- generated in an outer-sphere reaction between O_2 and $Ru(NH_3)_6^{2+}$ could be ruled out both by the lack of inhibition by $Ru(NH_3)_6^{3+}$ and the observation that the catalyzed reaction proceeded much more rapidly than the rate with which $Ru(NH_3)_6^{2+}$ reduces O_2 to O_2^- (7).
10. Kreyszig, E., "Advanced Engineering Mathematics", 4th ed., Wiley, New York, 1979, p. 787.
11. Rohrbach, D. F.; Deutsch, E.; Heineman, W. R.; Pasternak, R. F., Inorg. Chem., 16(1977)2650.
12. Andrieux, C. P.; Saveant, J.-M., J. Electroanal. Chem., 131(1982)1.
13. Levich, R. G., "Physicochemical Hydrodynamics", Prentice-Hall, Englewood Cliffs, N. J., 1962.
14. Saveant, J.-M.; Vianello, E., Electrochim. Acta, 8(1963)905.
15. Andrieux, C. P.; Merz, A.; Saveant, J.-M.; Tomahogh, R., J. Am. Chem. Soc., 106(1984)1957.
16. Andrieux, C. P.; Dumas-Bouchiat, J. M.; Saveant, J.-M., J. Electroanal. Chem., 169(1984)9.
17. Andrieux, C. P.; Saveant, J.-M.; J. Electroanal. Chem., 171(1984)65.
18. Andrieux, C. P.; Saveant, J.-M.; J. Electroanal. Chem., 134(1982)163.
19. Wan, G.-X.; Shigehara, K.; Tsuchida, E.; Anson, F. C., J. Electroanal. Chem., 179(1984)239.
20. Koutecky, J.; Levich, R. G., Zh. Fiz, Khim., 32(1957)1565.
21. Oyama, N.; Anson, F. C., J. Electrochem. Soc., 127(1980)640.
22. Bard, A. J.; Faulkner, L. R., "Electrochemical Methods", Wiley, New York, 1980, p. 288.
23. Anson, F. C.; Ohsaka, T.; Saveant, J.-M., J. Phys. Chem., 87(1983)640.
24. The first "master differential equation" on p. 69 of reference 17 was the equation employed in the numerical integration.

25. von Smoluchowski, M., Phys. Z. 17(1916)557, 585; Z. Phys. Chem., 92(1917)129.

26. Serratrice, G,; Delpuech, J.J.; Diguet, R., Nouv. J. Chem., 6(1982)489.

27. Sakai, T.; Takenaka, H.; Torikai, E., J. Electrochem. Soc., 133(1986)88.

28. Durand, R. R., Jr.; Anson, F. C., J. Electroanal. Chem., 134(1982)273.

CHAPTER III

RELATION BETWEEN THE REDUCTION POTENTIALS OF ADSORBED AND UNADSORBED COBALT(III) TETRAKIS (4-N-METHYLPYRIDYL)PORPHYRIN AND THOSE WHERE IT CATALYZES THE ELECTROREDUCTION OF DIOXYGEN

Introduction

Chapter II presented an example of a water-soluble cobalt porphyrin incorporated in Nafion coatings on graphite electrodes that is much more stable than when adsorbed directly on the electrode surface. Although the electrochemical response of the directly adsorbed cobalt tetrakis(4-N-methylpyridyl)porphyrin (CoTMPyP) on graphite electrodes exists only for a short period of time, it is still possible to observe the electrochemistry of this temporarily adsorbed molecule and to compare it with that of homogeneously distributed CoTMPyP in aqueous solutions. This chapter describes the adsorption behavior of CoTMPyP on graphite electrodes and its roles in the electrocatalysis of dioxygen reduction.

Most commonly, monomeric cobalt porphyrins, CoP, are irreversibly adsorbed on graphite or carbon electrodes and catalyze the electroreduction of O_2 to H_2O_2 at potentials significantly more negative than the formal potential of the $Co^{III/II}$ couple for the adsorbed porphyrin (1,2). This observation is most simply explained by a catalytic mechanism in which the reduction of the cobalt center of the porphyrin from Co(III) to Co(II) is not coupled to the catalytic cycle. The latter involves coordination of O_2 to the reduced cobalt center followed by the reduction of the adduct at potentials determined by its electrochemical properties rather than those of the original cobalt porphyrin (2). This mechanistic scheme has accomodated the results we have obtained with a series of monomeric cobalt porphyrins (1,2). However, the Co(III/II) formal potential for CoTMPyP evaluated recently by Rohrbach *et al.* (3) (0.175 volt vs. SCE) is more negative, instead of more positive, than the potential where this porphyrin catalyzes the reduction of O_2, (~0.25 volt). The origin of this apparently dissimilar behavior was traced to an unusually large change in the formal potential of the $Co^{III/II}$ couple upon the adsorption of the porphyrin on the graphite electrode surface. The purpose of this Chapter is to draw attention to the magnitude of the shifts in cobalt porphyrin formal potentials that their

adsorption on electrode surfaces can produce and to assess its significance on the mechanism of the catalyzed reduction of O_2.

Experimental

$[Co^{II}TMPyP](PF_6)_4$ was prepared as described by Hambright and Fleischer (4) and purified according to the procedure of Kobayashi *et al.* (5). $Co^{III}TMPyP$ was generated by controlled potential oxidation at 0.6 volt at a graphite-plate electrode.

The electrochemical apparatus, instrumentation, and procedures were similar to those described in references 6 and 7. The working electrodes were cylindrical pyrolytic graphite rods mounted to expose the edges of the graphite planes (Union Carbide Co., Chicago). They were polished with No. 600 SiC paper (3M Co., St. Paul, MN) and mounted as described in reference 2. Measurements were conducted at $22 \pm 2°C$ with solutions prepared from distilled water that had been passed through a purification train (Barnsted Nanopure + Organopure). Potentials are given with respect to a saturated calomel electrode, SCE.

Results and Discussion

Cyclic voltammograms recorded with an edge-plane pyrolytic graphite electrode in a 0.2 mM solution of $Co^{III}TMPyP$ are shown in Figure 3.1. There is a prominent response near 0.5 volt but little evidence of electroactivity in the vicinity of the reported formal potential for the $Co^{III/II}TMPy$ couple, 0.175 volt (3). The couple near 0.5 volt evidently arises from adsorbed reactant because i) the response persists when the electrode is transferred to a pure supporting electrolyte solution (cf. the first wave in Figure 3.4B), ii) the peak currents are linear functions of scan rate, and iii) the response is present when the potential of a rotating disk electrode is scanned at 100 mV s^{-1} (Figure 3.2A) but absent when the voltammogram is recorded at steady-state (Figure 3.2B). The peaked response at 0.5 volt in Figure 3.2A matches that obtained at the stationary electrode in Figure 3.1, as expected if both responses arise

Figure 3.1. Steady-state cyclic voltammetry of 0.2 mM CoTMPyP in 0.5 M CF_3COOH saturated with argon (dotted curve no COTMPyP present). Scan rates: dashed curve and dotted curve, 100 mV s^{-1}; solid curve, 200 mV s^{-1}.

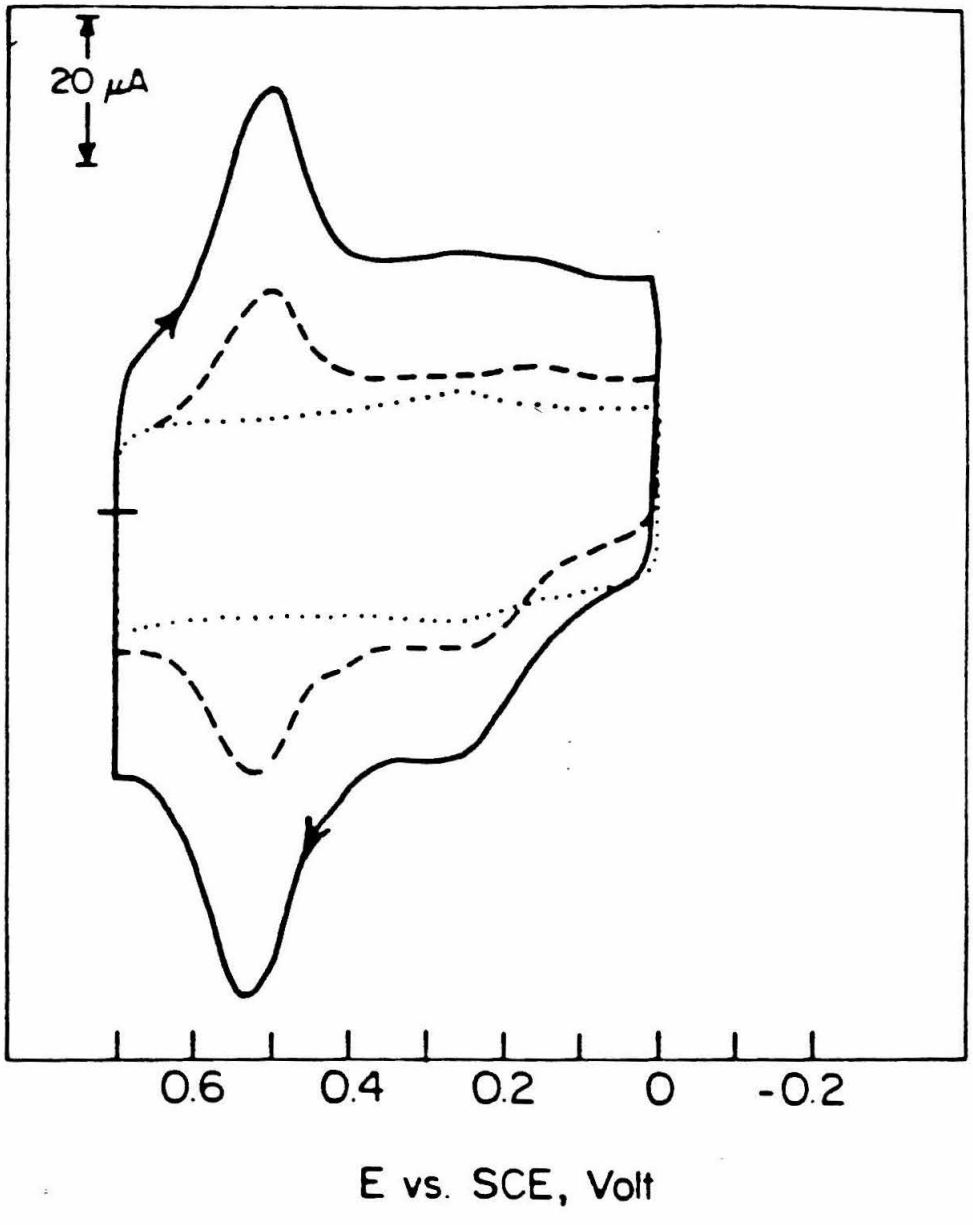
20 μA
0.6
0.4
0.2
0
-0.2
E vs. SCE, Volt

Figure 3.2.

(A) Non-steady-state current-potential response obtained with a rotated disk electrode in the solution used to record Figure 3.1 (rotation rate 400 rpm; potential scanned at 100 mv s^{-1}).

(B.) Repeat of part A under steady-state conditions. Potential scan rate = 0 mV s^{-1}.

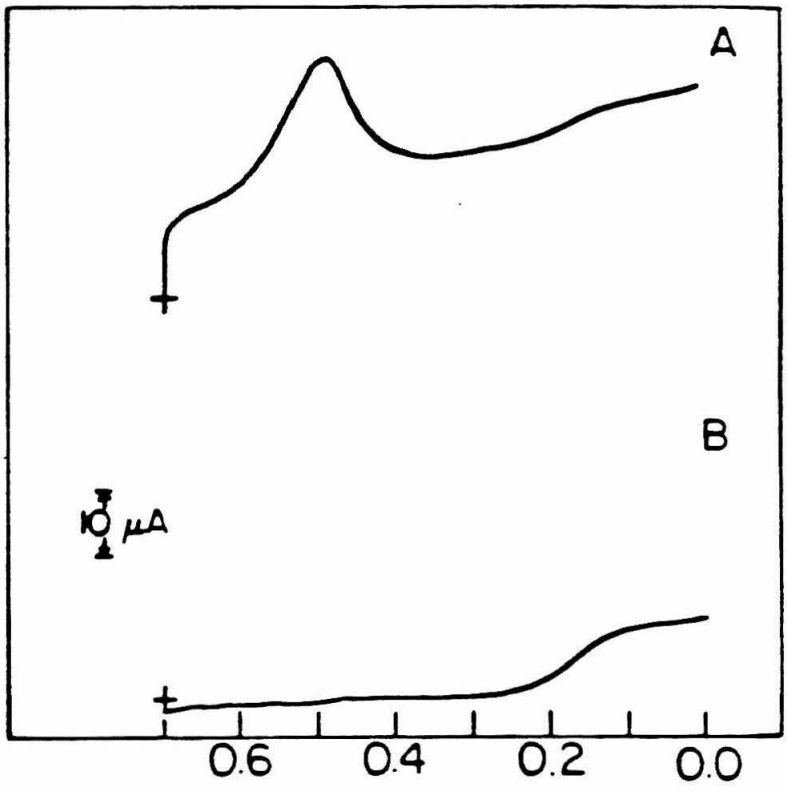
A
B
10 μA
0.6
0.4
0.2
0.0
E vs. SCE, Volt

from adsorbed reactant. The stable wave obtained in Figure 3.2B has a half-wave potential of 0.18 volt, very close to the solution formal potential of the $Co^{III/II}TMPyP$ couple measured by Rohrbach *et al.* (3). This wave is therefore assignable to the reduction of $Co^{III}TMPyP$ in solution. The steady-state limiting current measured on the plateau of the wave, $25\mu A\ cm^{-2}$, is smaller than the value calculated from the Levich equation (8), $36\mu A\ cm^{-2}$, using the reported diffusion coefficient for $Co^{III}TMPyP$ of $2.3 \times 10^{-6}\ cm^2\ s^{-1}$ (9). This may result from the adsorbed porphyrin's acting as a barrier to the diffusion of the dissolved porphyrin to the electrode surface. Penetration of the adsorbed layer by the dissolved porphyrin is probably required because the rate of electron self-exchange between the +3 and +2 oxidation states of CoTMPyP would not be expected to be high enough to provide an efficient pathway for transport of electrons from the electrode surface across the adsorbed layer to the dissolved reactant. The same effect is presumably responsible for the lack of a clear second peak in the voltammograms of Figure 3.1. Only by combining cyclic and rotating disk voltammetry were the two, well-separated responses for the adsorbed and unadsorbed porphyrin revealed clearly.

The adsorption of CoTMPyP is much weaker on gold than on graphite electrodes and the voltammetric response is correspondingly more normal. Figure 3.3 contains a cyclic voltammogram recorded at a 0.458 cm^2 gold electrode. The single wave obtained with $E^f = 0.18$ V has a peak current close to that calculated for a diffusion-controlled reduction and no response remains if the electrode is transferred to pure supporting electrolyte.

However, a recent study by Bedioui *et al.* (15) showed that CoTMPyP adsorbed strongly on their gold electrodes, and the Co(III/II) potentials were the same for the adsorbed and unadsorbed CoTMPyP, *i.e.*, 0.45V vs. SCE. Because the Bedioui *et al.* gold electrode has been subjected to an electrochemical cleaning treatment (potential cycling between -0.8 and +1.2V vs. SCE) before

Figure 3.3. Steady-state cyclic voltammogram for CoTMPyP at a stationary gold electrode (0.458 cm^2)(scan rate 100 mV s^{-1}). Other conditions as in Figure 3.1.

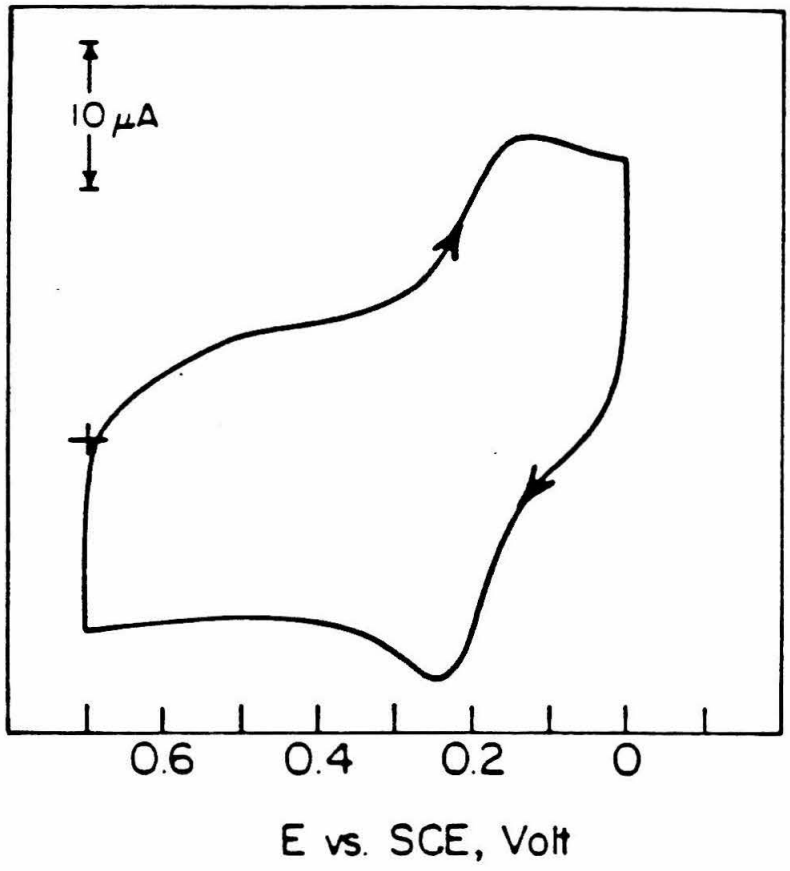
10 μA
0.6
0.4
0.2
0
E vs. SCE, Volt

each experiment, which allows the formation of a monolayer of oxide and its subsequent reduction, it is possible that this kind of surface treatment would alter the surface roughness of the gold electrode and subsequently affect the adsorption behavior of molecules on its surfaces. It is worthy of notice that the Co(III/II) formal potential of dissolved CoTMPyP reported by Bedioui *et al.* (0.45V vs. SCE) is very different from our results (0.18 V vs. SCE) and those of Rohrback *et al.* (0.175V vs. SCE), although Bedioui *et al.* claimed that their value was in accordance with that of Rohrback *et al.* (3). One possible explanation of this discrepancy is that the electrochemical response which Bedioui *et al.* observed for dissolved CoTMPyP may be mainly due to the inevitably adsorbed CoTMPyP on their gold electrodes, similar to our results shown in Figure 3.1. Simple experiments such as scan rate dependence of the peak currents (linear relationship for adsorbed species) or rotating disk voltammetry (as those shown in Figure 3.2) would be able to help resolve the question of why an incorrect numerical value was obtained with the Co(III/II) potential of dissolved CoTMPyP in the work reported by Bedioui *et al.* (15).

The result of repeating the 100 mV s^{-1} scan of Figure 3.1 at a graphite electrode in the presence of air is shown in Figure 3.4A. The large wave corresponding to the catalyzed reduction of O_2 is well-separated from the surface wave for the reduction of adsorbed $Co^{III}TMPyP$. Although the O_2 reduction wave appears in the same vicinity as the **solution** formal potential of the $Co^{III/II}$ couple, the dissolved porphyrin contributes little or nothing to the catalysis because the catalytic current is not diminished when the electrode is transferred to a solution containing no dissolved $Co^{III}TMPyP$ (Figure 3.4B). Thus, adsorbed CoTMPyP, with a formal potential near 0.5 volt, catalyzes the reduction of O_2 at potentials near 0.23 volt.

The greater visibility of the wave for the reduction of dissolved CoTMPyP in steady-state rotating disk current-potential curves (Figure 3.2B) than in

Figure 3.4. Reduction of O_2 as catalyzed by CoTMPyP at a stationary edge-plane pyrolytic graphite electrode (scan rate 100 mV s^{-1}).

(A) For 0.5 M CF_3COOH electrolyte + 0.2 mM CoTMPyP saturated with air.

(B) After electrode from A was transferred to 0.5 M CF_3COOH saturated with air.

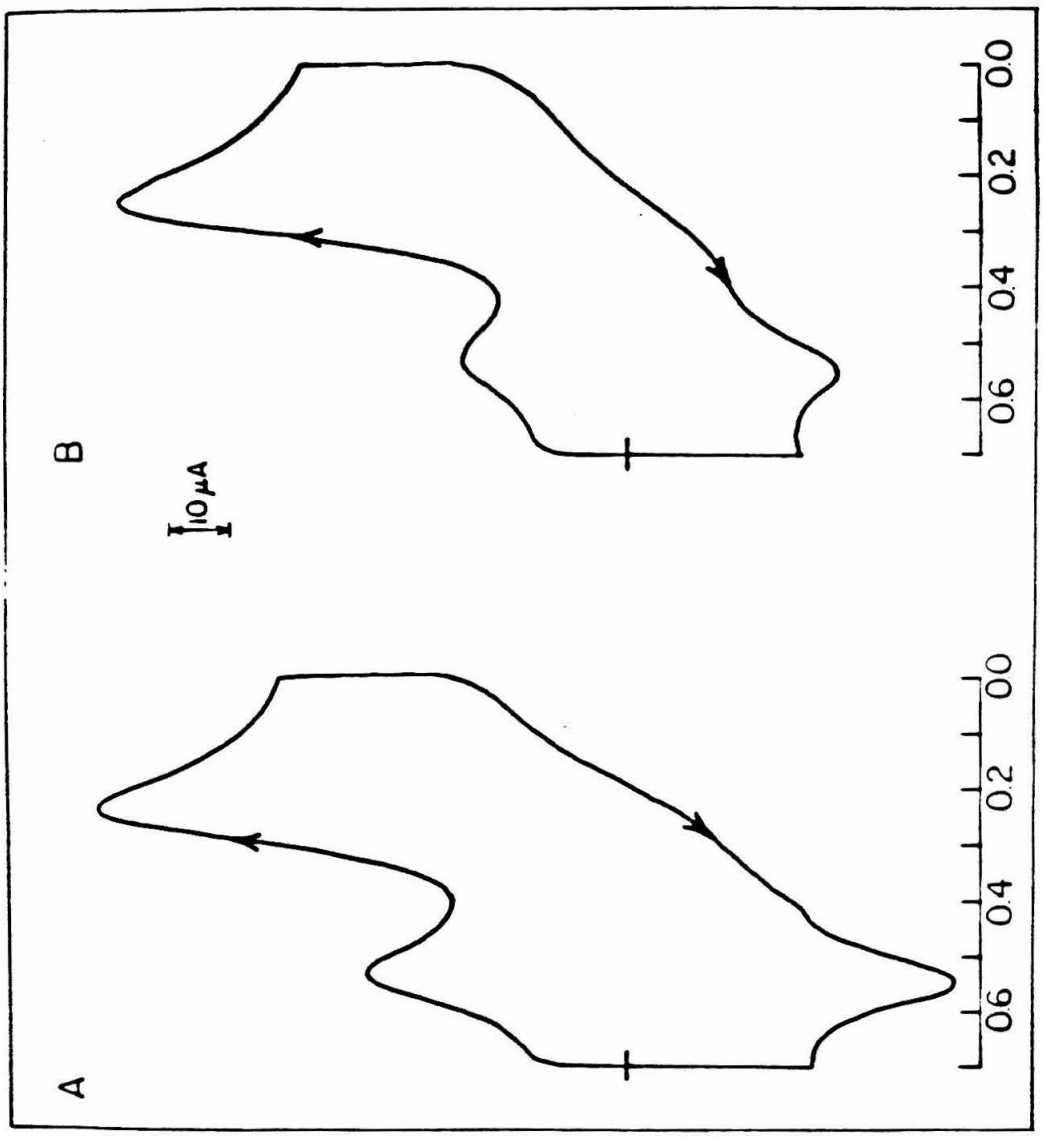
A
B
10 μA
0.6
0.4
0.2
0.0
E vs. SCE, Volt

cyclic voltammograms (Figure 3.1) is attributable, in part, to the relatively high background current that flows at edge-plane graphite electrodes when their potentials are scanned at the 100-200 mV s^{-1} rates that are typical of cyclic voltammetry.

The rate of oxidation of $Co^{II}TMPyP$ by O_2 was examined spectrophotometrically by mixing the two reactants and monitoring the spectra of the resulting solution in the region between 400 and 500 nm. In 0.1 M H_2SO_4 saturated with air, an electrolyte similar to that employed in some previous studies (5, 13, 14), the spectrum observed matched that reported for $Co^{II}TMPyP$ (3) for at least sixty seconds after mixing; even after one hour, the oxidation was less than 50% complete. Addition of a slight excess of Fe^{+3} produced an immediate conversion to the spectrum of $Co^{III}TMPyP$ (3). The oxidation of $Co^{II}TMPyP$ (5μM) by O_2 in 0.5 M trifluoroacetic acid, the electrolyte employed in this study, proceeds somewhat more rapidly but the half-life of $Co^{II}TMPyP$ is still over 5 minutes. Thus, $Co^{II}TMPyP$ and O_2 can coexist in solution for periods that are long compared to the time required for reactants to cross the diffusion layer in typical cyclic or rotating disk voltammetric experiments (0.1-1 s).

The large difference in the Co(III/II) formal potentials between adsorbed and unadsorbed CoTMPyP as measured with graphite electrodes indicates unusually favorable interactions between the cobalt center and the electrode surface when the cobalt is in the reduced state. It has been suggested in previous studies (10) that organic functional groups known to be present on the graphite surface may serve as ligands that stabilize Co(II) more than Co(III). Whatever the origin of the shift in formal potential, it is responsible for the separation between the potentials where the cobalt center exhibits its redox activity and the potentials where the porphyrin catalyzes the reduction of O_2. Because of the magnitude and direction of this separation, the mechanism of the catalysis is best regarded as "CE catalytic". That is, the O_2 substrate

undergoes a chemical reaction (C) with the (reduced) catalyst that precedes its electrochemical reduction (E). Since the reduced catalyst and substrate can co-exist in solution for periods long compared with the effective measurement times in electrochemical experiments, the "EC catalytic" mechanism (in which catalyst reduction triggers substrate reduction) that has been proposed for some porphyrin catalyzed electroreductions of O_2 (5, 13, 14) is clearly inapplicable to the present case (11). The fact that the catalyzed reduction of O_2 proceeds not far from the formal potential of the $Co^{III/II}$ couple for the unadsorbed porphyrin is coincidental and does *not* imply that outer-sphere electron transfer between O_2 and the reduced catalyst is the rate-limiting step.

The literature now contains reports on the catalysis of the electroreduction of O_2 by a variety of cobalt porphyrins that includes both water-soluble and water-insoluble examples. Table 3.1 is a summary of the reported formal redox potentials of the cobalt porphyrins and of the potentials where they exhibit catalytic activity toward the reduction of O_2. The pattern that emerges from the potentials listed in Table 3.1 is of catalysts that exhibit redox activity in the adsorbed state at potentials more positive than those where thay catalyze O_2 reduction and those where the dissolved porphyrin is electroactive. The redox activity of the dissolved coblat porphyrin catalysts appears at potentials on both sides of those where O_2 reduction proceeds as would be expected if the dominant catalytic pathway involved the (inevitably present) adsorbed catalyst.

Concluding Remarks

The rotating disk electrode technique proved very useful in the electrochemical study of dissolved CoTMPyP in the **presence** of adsorbed CoTMPyP. One of the primary conclusions resulting from this study is the unusual positive shift (+370mV) of the Co(III/II) potential upon the adsorption of the cobalt porphyrin (CoTMPyP) on the graphite electrode surfaces. Based upon the "CE catalytic" mechanism of the electrochemical reduction of O_2 by monomeric

Table 3.1

Formal Potentials ($Co^{III/II}$) and O_2 Reduction Potentials for Substituted Cobalt Porphyrins[a].

Entry	Porphyrin	E^f, V vs. SCE		E_{O_2}, V vs. SCE		Reference
		adsorbed	dissolved	$E_{1/2}^{b,d}$	$E_p^{c,d}$	
1.	tetraphenyl-	0.75	-	0.18	-	1
2.	octaethyl-	0.60	-	0.18	-	1
3.	tetra(p-methoxy)-phenyl-	0.64	-	0.15	-	1
4.	tetra(p-sulfonato)-phenyl-	0.50	-	0.20	-	1
5.	monomeric porphyrin I in reference (2)	0.52	-	0.20	-	2
6.	tetrapyridyl-	0.55	-	0.20	-	1
7.	tetra(4-N-methyl-pyridyl)-	0.52	0.18;0.175[e]	-	0.23	this work
8.	tetrapyridyl-	0.175	-0.095	-	0.105	13
9.	tetra-o-aminophenyl-	0.27[f]		-	0.05	12
10.	tetra(4-N-N'-N"-trimethylanilinium)-	0.12-0.16	0.14	-	0.08	14
11.	$\alpha,\beta,\gamma,\delta$-tetra[1-(2-hydroxyethyl)-pyridinium-4-yl)]-	-	-0.035	-	-0.07	5

a. Porphyrins 1-7: edge-plane graphite electrode; 0.5 M CF_3COOH supporting electrolyte. Porphyrins 8-11: glassy carbon electrode; 0.05 M H_2SO_4 supporting electrolyte.

b. Half-wave potential for reduction of O_2 at a rotating disk electrode.

c. Voltammetric peak potential for the reduction of O_2 at a stationary electrode.

d. The precise values of $E_{1/2}$ and E_p show weak dependences on electrode rotation rate, potential scan rate and catalyst concentration.

e. Reported in reference 3.

f. The origin of the single wave is unclear from the data presented.

cobalt porphyrins, the potentials where O_2 is reducible are restricted to the potential region close to or more negative than the Co(III/II) potential. Factors which cause such positive shift of Co(III/II) potentials may be important in the future design of efficient catalytic systems.

References and Notes

1. Durand, Jr., R.R.; Ph.D. Thesis, California Institute of Technology, 1984.
2. Durand, Jr., R.R.; Anson, F.C.; J. Electroanal. Chem., 134(1982)273.
3. Rohrbach, D.F.; Deutsch, E.; Heineman, W.R.; Pasternack, R.F., Inorg, Chem. , 16(1977)2650.
4. Hambright, P.; Fleischer, E.B., Inorg. Chem., 9(1970)1757.
5. Kobayashi, N.; Fujihira, M.; Osa, T.; Kuwana, T.,Bull. Chem. Soc. Jpn., 53(1980)2195.
6. Oyama,N.; Anson, F.C., Anal. Chem., 52(1980)1192.
7. Geiger, T.; Anson, F.C., Anal. Chem., 52(1980)2448.
8. Bard, A.J.; and Faulkner, L.R., "Electrochemical Methods", Wiley, New York, p. 522.
9. Forshey, P.A.; Kuwana, T.; Kobayashi, N.; Osa, T., Adv. Chem. Ser., 201(1982)601.
10. Bettelheim, A.; Chan, R.J.H.; Kuwana, T., J. Electroananl. Chem., 110(1980)93.
11. The possibility that the "EC catalytic" mechanism might not apply to the cobalt tetra-o-aminophenylporphyrin catalyzed reduction of O_2 has been mentioned in a previous preliminary report (12) but the consequences of the possibility were not elaborated.
12. Kobayashi, N.; Matsue, T.; Fujihira, M.; Osa, T., J. Electroanal. Chem., 103(1979)427.
13. Bettelheim, A.; Chan, R.J.H.; Kuwana, T., J. Electroanal. Chem., 99(1979)391.
14. Ozer, D.; Parash, R.; Broitman, F.; Mor, U.; Bettelheim, A., J. Chem. Soc., Faraday Trans. I, 80(1984)1139.
15. Bedioui, F.; Devynck, J.; Hinnen, C.; Rouseau, A.; Bied-Charreton, C.; Gaudemer, A., J. Electrochem. Soc., 132(1985)2120.

CHAPTER IV

BEHAVIOR OF FOUR ANTHRACENE-LINKED DIMERIC METALLOPORPHYRINS AS ELECTROCATALYSTS FOR THE REDUCTION OF DIOXYGEN

Introduction

Significant progress in the catalysis of the electroreduction of O_2 to H_2O by metalloporphyrins has been achieved in recent years (1-19). The best catalysts from this class have involved pairs of transition metal centers in dimeric porphyrins (1-3) but diporphyrins containing only one transition metal center (cobalt) have also shown high catalytic activity in the direct, four-electron reduction of O_2 (5). Diporphyrins in which the two porphyrin rings are linked by an anthracene molecule attached at the 1 and 8 position to *meso* sites on the porphyrin rings (Figure 4.1) have been the subject of recent studies in which very attractive catalytic activities were demonstrated (5, 6). The present work describes an investigation of the behavior of the four new metallodiporphyrins identified in Figure 4.1 in order to compare their catalytic behavior with that of the more extensively studied doubly-bridged cofacial porphyrins (1-3). The catalytic mechanisms employed by both types of diporphyrins are only partially understood and their unusual activities make a more complete elucidation of the mechanisms by which they operate an important objective in continuing efforts to improve their performance and stability.

Experimental

Materials. The synthesis of anthracene-linked dimeric metalloporphyrins (Figure 4.1) has been described (20, 21). Edge-plane graphite electrodes were prepared as described in Chapter III. They were polished with No. 600 silicon carbide paper (3M Co., St. Paul, MN) and mounted as previously described (22). The rotating graphite disk-platinum ring electrode (Pine Instrument Co.) was polished with 0.3 μm alumina on a microcloth (Buehler Ltd.) before each experiment. The polished platinum ring electrode was activated by cycling its potential several times between +1.2 and -0.3V in 0.1 M $HClO_4$-0.1M $NaClO_4$ while rotating the electrode at 3000 rpm. The theoretical collection efficiency of the electrode was 0.18, which matched the experimental value measured with

Figure 4.1. Structures of the four dimeric metalloporphyrins examined in this study.

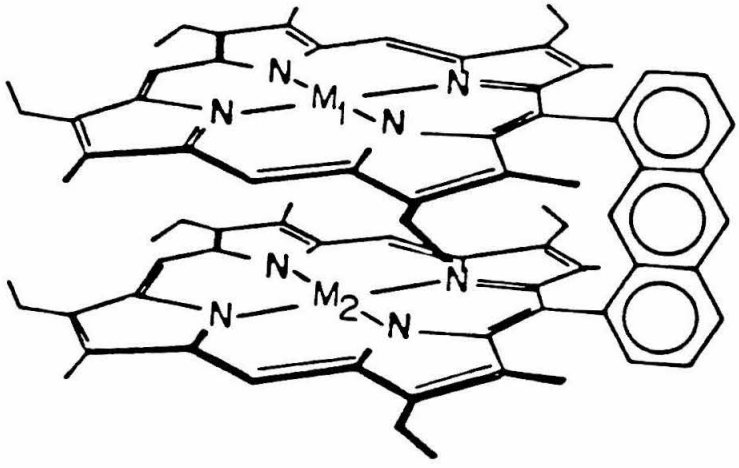

M_1	M_2
Co	Cu
Fe	H, H
Fe	Fe
Co	Fe

the $Fe(CN)_6^{3-/4-}$ couple. When the ring reaction was oxidation of H_2O_2, smaller experimental collection efficiencies of monomeric cobalt were typical (23). To establish an effective collection efficiency for H_2O_2 a monomeric cobalt porphyrin known to catalyze the quantitative reduction of O_2 to H_2O_2 (9) was adsorbed on the graphite disk electrode. The resulting electrode produced a reasonably reproducible collection efficiency of 0.11 that was used in subsequent calculations. Aqueous solutions were prepared from distilled water that had been passed through a purification train (Barnsted Nanopure + Organopure). Other chemicals were reagent grade and were used as received.

Procedures. The polished pyrolytic graphite electrodes were coated with porphyrin catalysts by transferring 30 μl aliquots of dichloromethane solutions (containing $6x10^{-10}$ mole of porphyrins) onto the electrode surface and allowing the solvent to evaporate. The electrochemical apparatus, instrumentation, and procedures were similar to those previously described (3). Potentials are quoted with respect to a saturated calomel electrode, SCE. Measurements were conducted at 22±2°C.

Results

Voltammetry of the Adsorbed Porphyrins in the Absence of O_2. All of the dimeric metalloporphyrins studied are insoluble in aqueous solutions. Deposition of layers of the porphyrins on pyrolytic graphite electrodes by evaporation of aliquots of nonaqueous solutions spread across the electrode surface produced coatings with cyclic voltammetric responses attributable to the oxidation and reduction of both the metal centers and the porphyrin rings. This study was restricted to the responses believed to originate in the metal centers. The prominence of the voltammetric waves depended upon the metal ions present in the porphyrin rings and varied considerably with the pH of the supporting electrolyte. For example, voltammograms obtained at pH 0 in the absence of O_2 with coatings of the four porphyrins are shown in the upper curves

in Figure 4.2. Multiple waves of varying magnitude are apparent in each case and the assignment of the waves to particular redox processes is not straightforward at this pH. Increases in pH produced changes in the shapes, peak potentials and relative prominence of the waves (Figure 4.3 and 4.4). By comparing the responses exhibited by the four porphyrins as a function of pH it was possible to identify with reasonable certainty peaks arising from the Fe(III/II) couples in the three iron-containing coatings and the Co(III/II) couple in the Co-Cu porphyrin. The assignments were further tested by comparing the pH dependences of the formal potentials of the waves for the coatings with the half-wave potentials for the reduction of O_2 at coated, rotating disk electrodes. Current-potential curves for the latter process are shown in the lower curves in Figures 4.2, 4.3, and 4.4. Prior work(11, 24) has established a pattern in which monomeric cobalt porphyrins catalyze the reduction of O_2 to H_2O_2 at potentials 100-300 mV more positive than do iron porphyrins. The latter are also active for the reduction of H_2O_2 to H_2O, usually at slightly more negative potentials than those where they catalyze the reduction of O_2 to H_2O_2 (11). These previously observed differences in the behavior of other metalloporphyrins proved helpful both in assigning the waves exhibited by the catalysts and in suggesting the possible positions of catalyst waves that were too ill-defined to be separated from background currents. Figure 4.5 summarizes the pH dependences observed for the surface waves that could be assigned and the pH dependences of the corresponding $E_{1/2}$ values for O_2 reduction at rotated electrodes.

Co-Cu Diporphyrin. For the Co-Cu porphyrin, a wave attributed to the Co(III/II) couple was identified at potentials similar to those observed previously for the corresponding Co-H_2 complex in which only one of the porphyrin rings was metallated (5). No wave for a Cu(II/I) couple was observable. The current-potential curves for O_2 reduction at coated, rotating disk electrodes consist of a single wave at all pH values (Figures 4.2-4.4). The catalyzed O_2 reductions occur

Figure 4.2. Electrochemical responses at pyrolytic graphite electrodes coated with the four porphyrins of Figure 4.1. Upper curves: Cyclic voltammetry; scan rate = 100 mV s^{-1}. The dashed curve is the voltammogram obtained at an uncoated electrode. Lower curves: Reduction of O_2 at coated rotating disk electrodes. Rotation rate = 400 rpm; scan rate = 5 mV s^{-1}. All electrodes were coated with 1.9 x 10^{-9} mole cm^{-2} of each porphyrin. Supporting electrolyte: 1 M CF_3COOH saturated with argon (upper curves) or air (lower curves). The current scales shown apply to all corresponding curves.

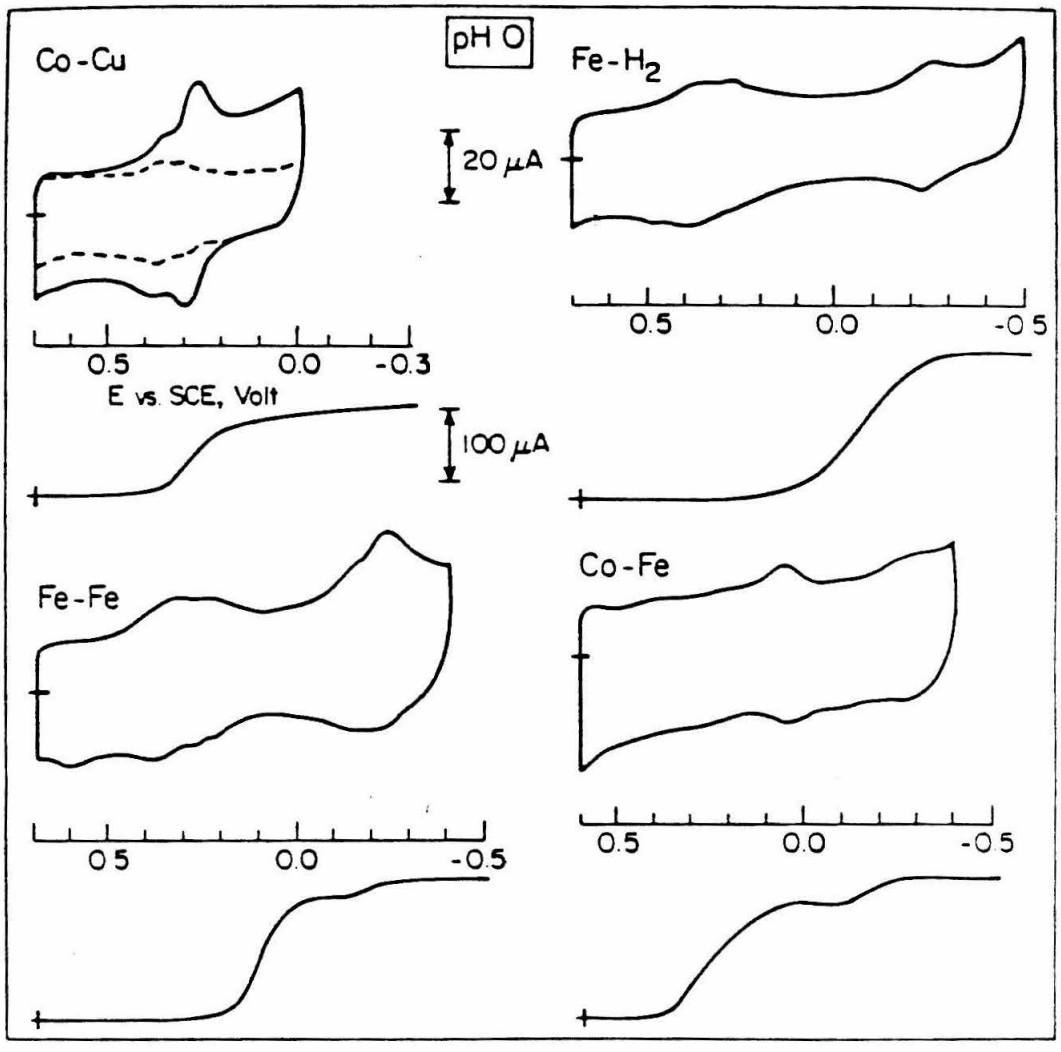
pH 0
Co-Cu
Fe-H2
20 μA
0.5
0.0
-0.3
E vs. SCE, Volt
100 μA
0.5
0.0
-0.5
Fe-Fe
Co-Fe
0.5
0.0
-0.5
0.5
0.0
-0.5

Figure 4.3. pH dependence of electrochemical responses for coated electrodes. The format and experimental conditions at each pH correspond to those in Figure 4.2. Ionic strength was maintained at 0.1 M by addition of CF_3COONa. Buffer concentrations were 10 mM except at pH 1.0 (0.1 M CF_3COOH). Acetate buffers were used at pH 3.5 and 4.7. The current and potential scales shown apply to all corresponding curves.

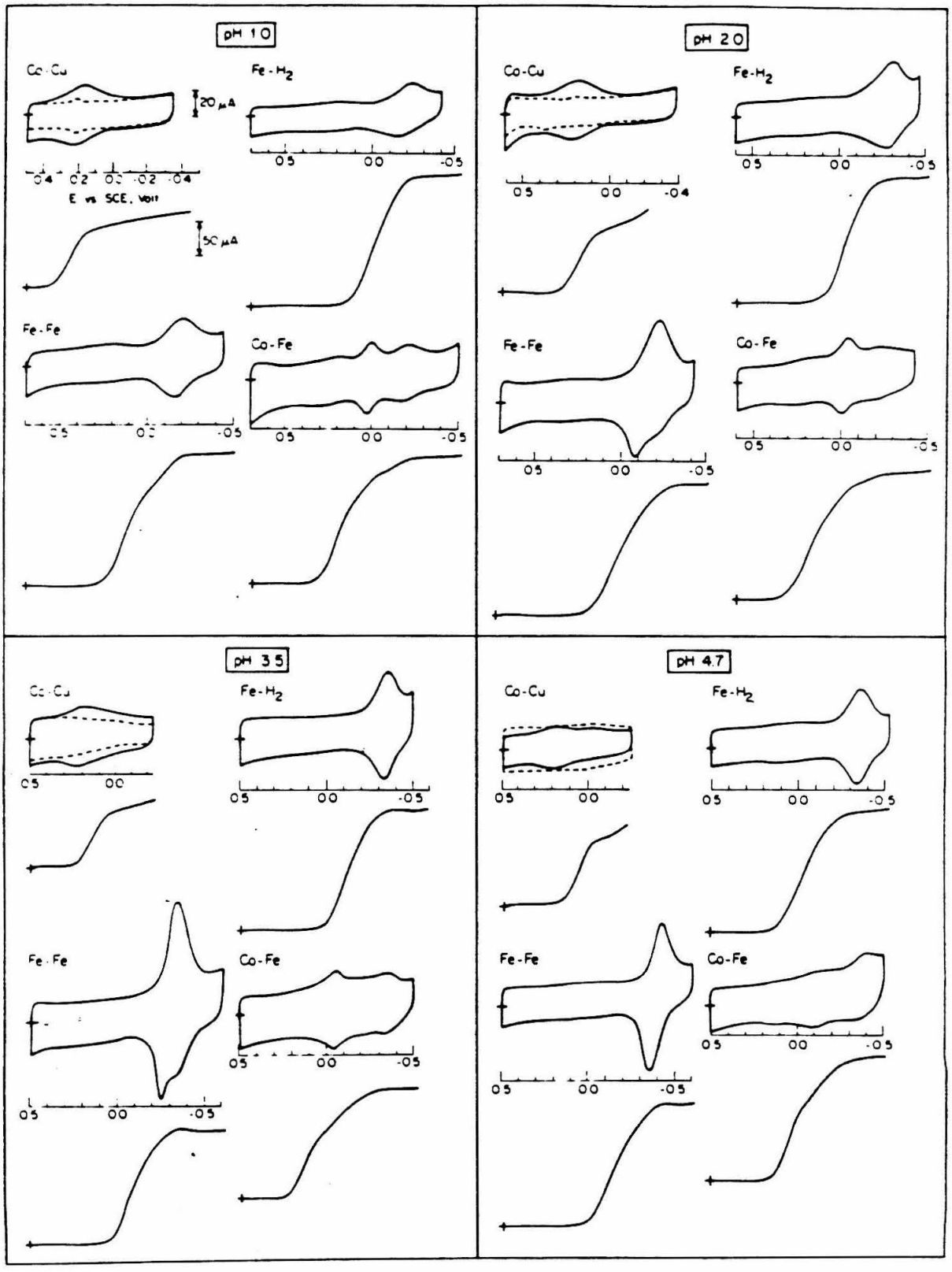
pH 1.0
Co-Cu
Fe-H2
20 μA
E vs SCE, Volt
50 μA
Fe-Fe
Co-Fe
pH 2.0
Co-Cu
Fe-H2
Fe-Fe
Co-Fe
pH 3.5
Co-Cu
Fe-H2
Fe-Fe
Co-Fe
pH 4.7
Co-Cu
Fe-H2
Fe-Fe
Co-Fe

Figure 4.4. An extension of Figure 4.3 to higher pH values. Buffers: pH 6.0, 8.0 - phosphate; pH 10 - carbonate. The current and potential scales shown apply to all corresponding curves.

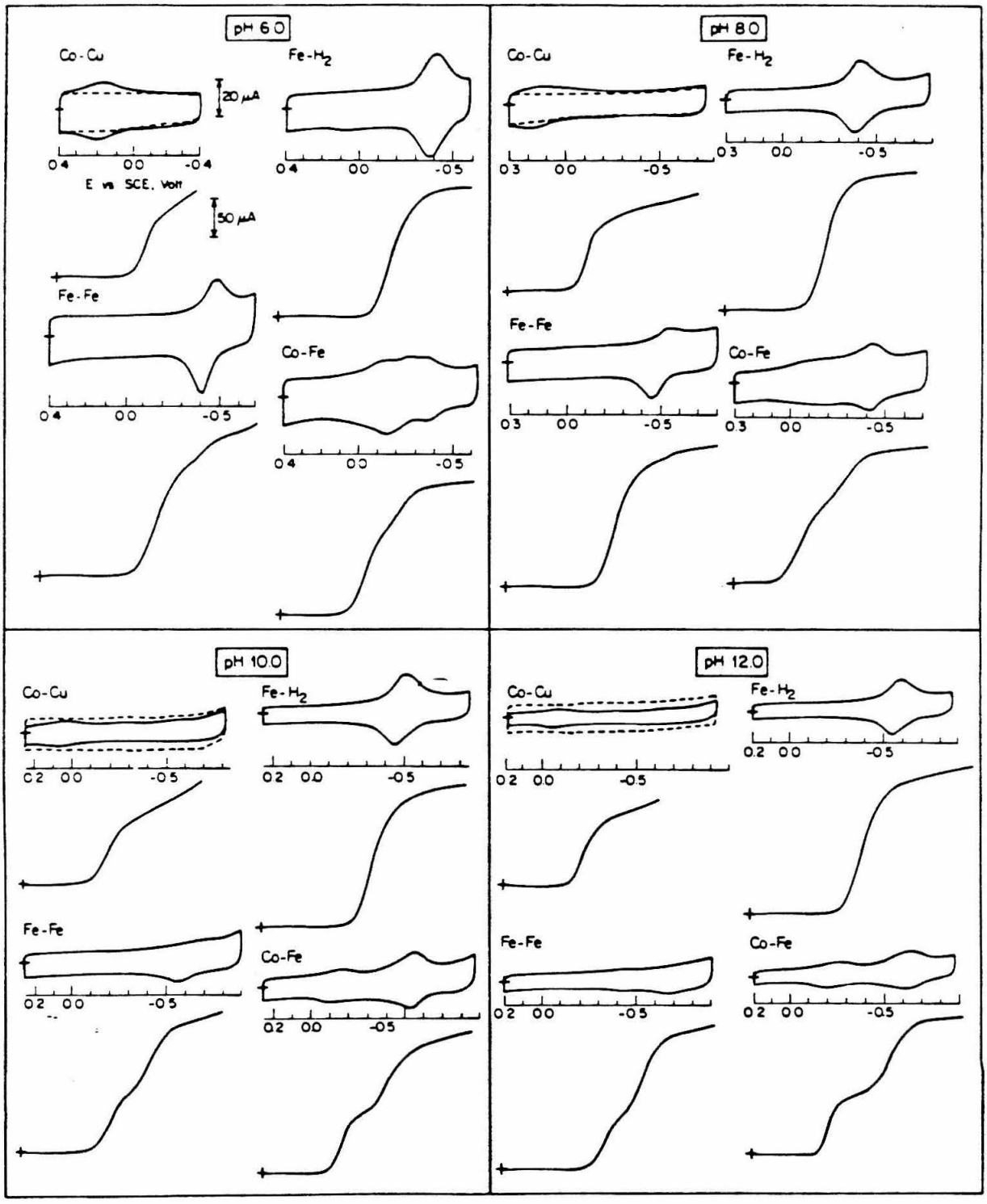
pH 6.0
Co-Cu
Fe-H2
20 μA
0.4 0.0 -0.4
E vs SCE, Volt
50 μA
Fe-Fe
Co-Fe
0.4 0.0 -0.5
pH 8.0
Co-Cu
Fe-H2
0.3 0.0 -0.5
Fe-Fe
Co-Fe
pH 10.0
Co-Cu
Fe-H2
0.2 0.0 -0.5
Fe-Fe
Co-Fe
pH 12.0
Co-Cu
Fe-H2
0.2 0.0 -0.5
Fe-Fe
Co-Fe

Figure 4.5. pH dependence of formal potentials of adsorbed porphyrins (•) and of half-wave potentials for O_2 reduction at porphyrin-coated rotating (400 rpm) disk electrodes (▪). Ionic strength maintained at 0.1 M except for the open points (1 M CF_3COOH).

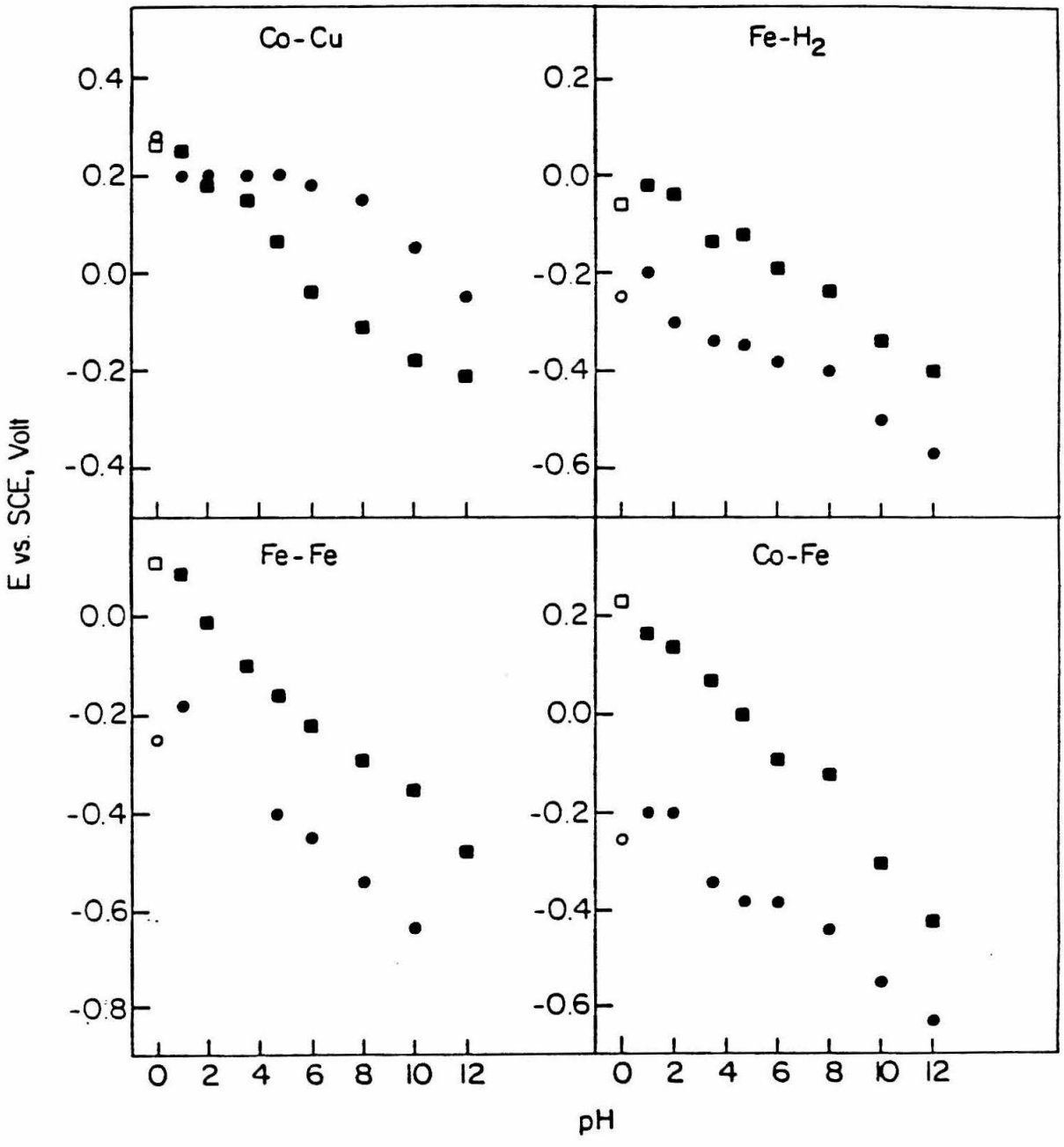
Co-Cu
Fe-H2
Fe-Fe
Co-Fe
E vs. SCE, Volt
pH
0.4
0.2
0.0
-0.2
-0.4
-0.6
-0.8
0
2
4
6
8
10
12

at potentials near (low pH), or more negative than (intermediate and high pH) that for the Co(III/II) couple. Rotating ring-disk measurements showed that the reduction produced H_2O_2 essentially quantitatively (Figure 4.6). Thus, the binuclear Co-Cu porphyrin exhibited catalytic behavior very similar to that of most monomeric cobalt porphyrins (24-26).

Fe – H_2 Diporphyrin. Incorporation of iron(III) in one of the two rings of the dimeric porphyrin produced a catalyst that was effective at potentials positive of those where the well-formed waves for the Fe(III/II) couple appeared at all pH values. Both the formal potential of the Fe(III/II) couple and the $E_{1/2}$ values for O_2 reduction decrease as the pH is increased but the changes do not occur in parallel (Figure 4.5).

Disk current-potential curves for O_2 reduction at rotating ring-disk electrodes exhibit only a single wave (Figure 4.6) but the corresponding ring currents pass through a maximum, showing that the primary reduction product changes from H_2O_2 to H_2O as the disk potential becomes more negative. The magnitude of the disk plateau current at low rotation rates is close to that expected for the four-electron reduction of O_2 to H_2O.

Monomeric iron porphyrins often catalyze the reduction of O_2 in two closely-spaced steps corresponding to a first reduction to H_2O_2 and a subsequent reduction to H_2O(11). The two steps are merged into a single wave in the case of iron protoporphyrin IX but the presence of the two step reduction is evident from the maximum in the anodic ring current that is measured with rotating ring-disk electrodes(11). Thus, the Fe-H_2 dimeric porphyrin appears to behave similarly to iron protoporphyrin IX and other conventional monomeric iron porphyrins.

Fe-Fe Diporphyrin. Voltammograms for coatings of the Fe-Fe diporphyrin exhibit only one clear peak that shifts to more negative potentials with increasing pH between pH 1 and 8 (Figures 4.2-4.4). The wave becomes in-

Figure 4.6. Reduction of O_2 at porphyrin-coated rotating graphite disk-platinum ring electrodes. Supporting electrolyte: 1 M CF_3COOH saturated with air. Ring potential = 1.0 volt. Rotation rate: 100 rpm. Disk potential scanned at 5 mV s^{-1}. The current scales shown apply to all corresponding curves.

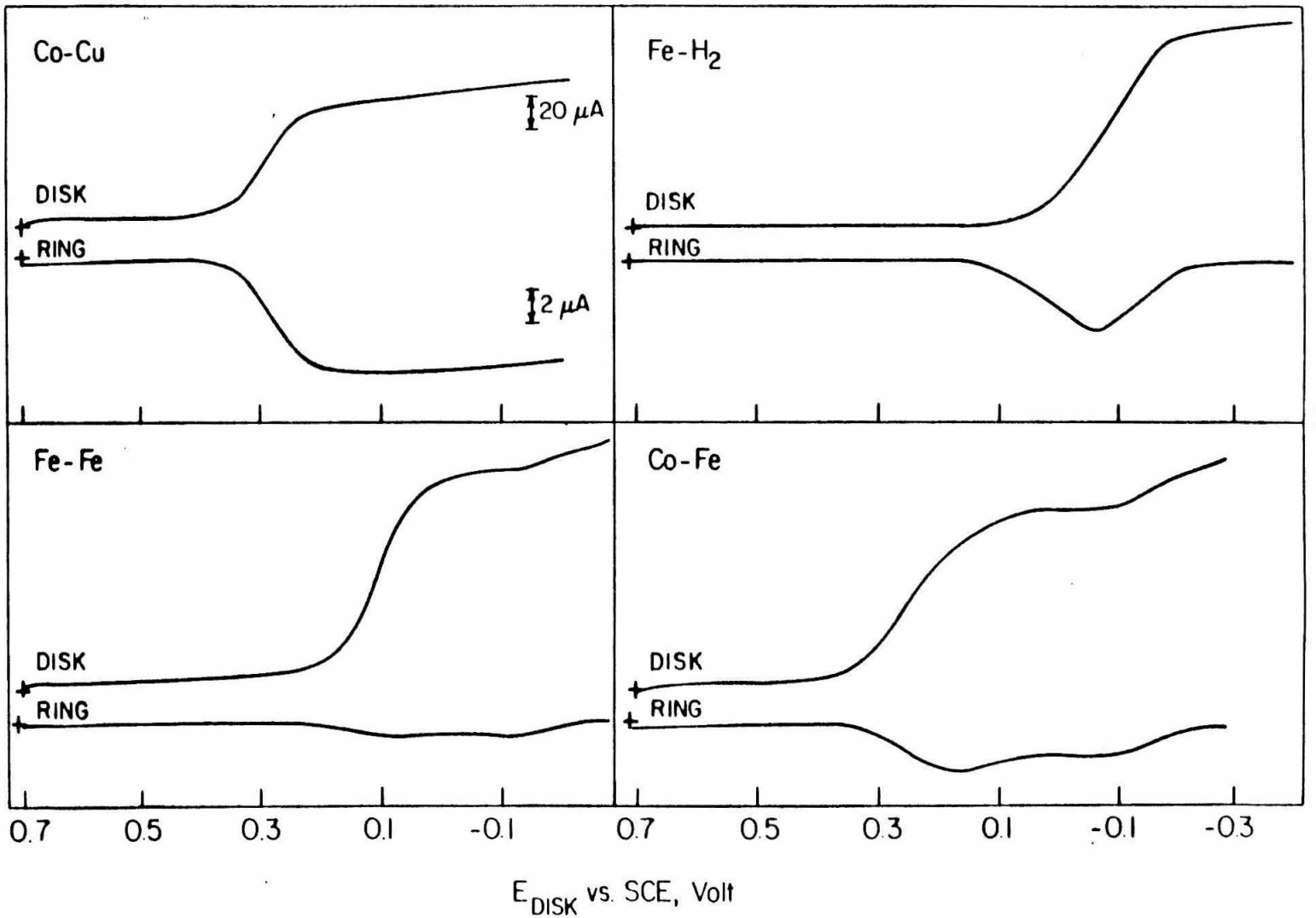
Co-Cu
20 μA
DISK
RING
2 μA
Fe-H2
DISK
RING
Fe-Fe
DISK
RING
Co-Fe
DISK
RING
0.7
0.5
0.3
0.1
-0.1
0.7
0.5
0.3
0.1
-0.1
-0.3
E DISK vs. SCE, Volt

distinct at pH 10 and disappears into the background at pH 12. The Fe-Fe diporphyrin contains a μ-oxo bridge between the Fe(III) ions (27) that is almost certainly absent when they are reduced to Fe(II). This may account for the persistence of the pH dependence of the formal potential at low pH values where typical monomeric iron porphyrins yield pH-independent formal potentials (11, 12). However, the peculiar pH dependence of the apparent formal potential of the adsorbed Fe-H_2 diporphyrin (Figure 4.5) casts some uncertainty on this interpretation. The magnitudes of the peak currents and the widths of the waves vary considerably as the pH is changed (Figure 4.2-4.4). The catalyzed reduction of O_2 at electrodes coated with the Fe-Fe diporphyrin occurs in two steps that are just observable in disk current-potential curves at most pH values but are very clear from the corresponding ring current-potential curves (Figure 4.6). At pH 0, where a clear plateau is evident for the first reduction step (Figure 4.6), the plateau current is much larger than that corresponding to the two-electron reduction of O_2, and the corresponding ring current is quite small. The reduction of O_2 also begins at more positive potentials than it does in the case of Fe-H_2 diporphyrin coatings. The introduction of the second Fe(III) into the Fe-H_2 diporphyrin produces a Fe-Fe catalyst with significantly different behavior towards O_2 reduction. However, at potentials of -0.2 volt or less, both the Fe-H_2 and Fe-Fe diporphyrin coatings catalyze the reduction of O_2 primarily to H_2O. Differences in the behavior of the Fe-H_2 and Fe-Fe diporphyrins on the rising portions of the O_2 reduction waves are evident in the ratio of ring to disk currents as a function of disk potential (Figure 4.6). The smaller this ratio, the smaller the quantity of O_2 that is reduced to H_2O_2 instead of H_2O. As can be seen from Figure 4.6, the ratio is smaller for the Fe-Fe than the Fe-H_2 diporphyrin, which indicates that the presence of the second iron center facilitates the four-electron reduction of O_2.

Co-Fe Diporphyrin. The behavior of the Co-Fe diporphyrin was more

complex than that of the other three porphyrins examined. The number and prominence of peaks in voltammograms of coatings of the diporphyrin in the absence of O_2 varied with pH (Figures 4.2-4.4). No well-defined wave attributable to the Co(III/II) couple was obtained. Even at pH values where two waves were clearly evident (pH 1, 3.5, 6, 12 in Figures 4.3 and 4.4) their peak potentials were too negative to correspond to the Co(III/II) porphyrin couple that was observed, for example, with the Co-Cu and Co-H_2 (5) diporphyrins. Voltammetric peaks assignable to the Fe(III/II) porphyrin couple were present at most pH values and formal potentials estimated from the voltammograms are included in Figure 4.5. The origin of the additional peaks present in the voltammograms of the Co-Fe diporphyrin remains obscure.

Coatings of the Co-Fe diporphyrin catalyze the reduction of O_2 at more positive potentials than do the Fe-Fe or Fe-H_2 diporphyrins. At pH 0, current-potential curves for O_2 reduction at coated rotating-disk electrodes consist of two distinct waves, the first of which appears to be made of two closely-spaced components (Figure 4.2). The plateau current for the first wave corresponds to more than two electrons per O_2 molecule and the total current on the second plateau is not far from that expected for a four-electron reduction. The position of the first wave is consistent with a cobalt-catalyzed reduction based on previous experiments with other cobalt porphyrins(24). However, the magnitude of the plateau current is larger than that obtained with monomeric cobalt porphyrins and the Co-Cu diporphyrin (Figure 4.2) that catalyze the two-electron reduction of O_2. Experiments with the rotating ring-disk electrode (Figure 4.6) showed that H_2O_2 is produced in greater quantity during the first half of the rising portion of the first O_2 reduction wave. On the second half of the wave less H_2O_2 is detected at the ring as expected from the larger magnitude of the disk current. It seems clear that the iron ion present in the Co-Fe diporphyrin facilitates the reduction of O_2 beyond H_2O_2, and it does so at potentials where

the iron is present as Fe(III). The second wave for O_2 reduction in the current-potential curves (well separated at low and high pH values) corresponds to those expected for iron porphyrin-catalyzed reductions.

The two O_2 reduction waves are less well separated at intermediate pH values (Figure 4.3) but they become distinct again in alkaline supporting electrolytes (Figure 4.4, pH 10 and 12). However, the magnitude of the first plateau current decreases substantially with pH until, at pH 12, it corresponds closely to the two-electron reduction of O_2. The ability of the Fe(III) center to facilitate the reduction beyond the H_2O_2 stage is apparently lost in alkaline solutions.

Kinetic Analysis of Rotating Disk Plateau Currents. The plateau currents obtained at rotating graphite disk electrodes coated with the porphyrin catalysts did not increase linearly with (rotation rate)$^{1/2}$ indicating that the rate of supply of O_2 to the electrode surface was not the only current-limiting process. The rate of reaction (*e.g.*, coordination) of O_2 with the metal centers in the catalyst coatings has been identified as the current-limiting step in previous related studies (3,5). Koutecky-Levich (K-L) plots (28) of (plateau current)$^{-1}$ vs. (rotation rate)$^{-1/2}$ were used to measure the relative rates of the current-limiting processes for the four catalysts and to assess the average number of electrons involved in the catalyzed reduction of O_2. In Figure 4.7 the K-L plot for the Co-Cu diporphyrin is shown along with theoretical plots for the diffusion-convection limited reduction of O_2 to H_2O_2 or H_2O. The experimental points lie on a line almost parallel to the theoretical line for the two-electron reduction of O_2 as expected if the product of the diporphyrin-catalyzed reduction were exclusively H_2O_2. Essentially similar behavior is obtained with coatings of most monomeric cobalt porphyrins (24, 25). The reciprocal intercept of the K-L plot corresponds to a kinetic current that measures the rate of the current-limiting reaction between O_2 and the Co-Cu diporphyrin in the coating. In

favorable cases such kinetic currents can be analyzed to obtain second-order rate constants for the current-limiting reaction. This analysis was not attempted in the present instance because of uncertainties in determining the quantities of the initially deposited catalyst that remained in the coatings during the rotating disk experiments.

Koutecky-Levich plots for the reduction of O_2 catalyzed by coatings of the Fe-H_2 and Fe-Fe diporphyrins are shown in Figure 4.7. Rotating ring-disk measurements (Figure 4.6) show that the mononuclear catalyst yields mainly H_2O_2 on the lower half of the rising portion of the O_2 reduction wave. However, the primary reduction product shifts to H_2O on the upper half of the wave and on the current plateau. The slope of the K-L plot for this catalyst is close to that expected for the four-electron reduction of O_2 and the rotating ring-disk results confirm that little or no H_2O_2 is formed at potentials on the plateau of the wave. (The ability of this and the other catalysts to serve as catalysts for the reduction of H_2O_2 is described in a succeeding section.) The good linearity of the K-L plot indicates that the electrode process leading to H_2O_2 and the one leading to H_2O are both first-order with respect to O_2.

The positive intercept of the K-L plot for the plateau currents corresponds to a kinetic current proportional to the rate of the current-limiting reaction. The kinetic current is also proportional to the number of electrons involved in the electrode reaction so that the approximately two-fold larger kinetic current obtained with the four-electron Fe-H_2 diporphyrin compared with the two-electron Co-Cu diporphyrin is a reflection of the stoichiometric difference and does not indicate a significant difference in the reactivity of the two species in the current-limiting reaction that is presumed to be the formation of an O_2-diporphyrin complex.

The Fe-Fe diporphyrin that catalyzes the reduction of O_2 in two steps yields a mixture of H_2O_2 and H_2O on the plateau of the first wave but only H_2O on

Figure 4.7. Koutecky-Levich plots for O_2 reduction in 1 M CF_3COOH at diporphyrin-coated rotating graphite disk electrodes. For the Fe-Fe and Co-Fe catalysts the upper and lower solid lines correspond to the first and second plateau currents, respectively. Dashed lines are calculated for the diffusion-convection limited two- or four-electron reduction of O_2. Other conditions as in Figure 4.2.

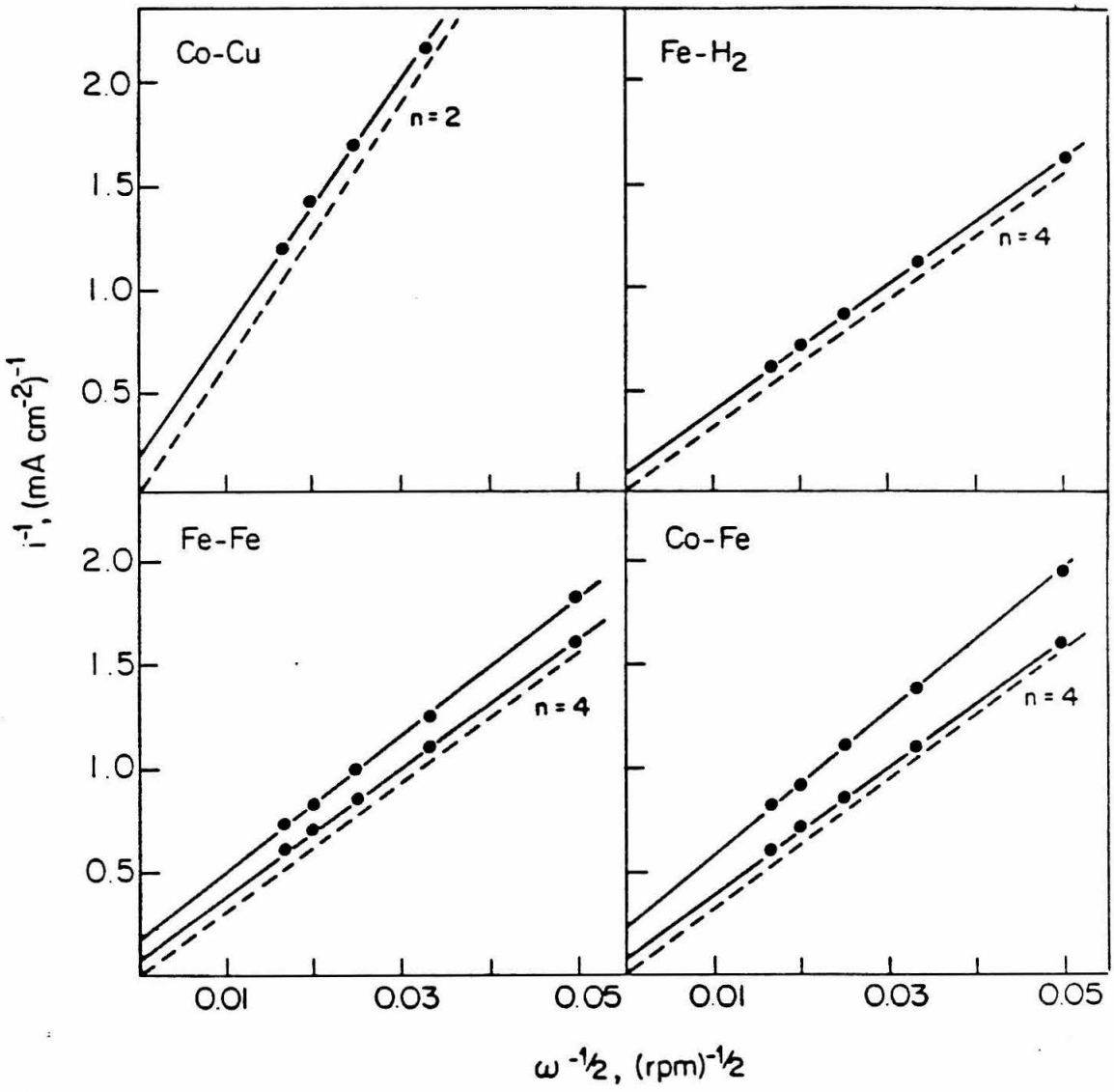
Co-Cu
n = 2
Fe-H2
n = 4
Fe-Fe
n = 4
Co-Fe
n = 4
2.0
1.5
1.0
0.5
0.01
0.03
0.05
i-1, (mA cm-2)-1
ω -1/2, (rpm)-1/2

the plateau of the second wave as judged from the results of rotating ring-disk experiments (Figure 4.6). For a simple case in which O_2 is reduced to H_2O_2 or H_2O by non-interacting pathways, the reciprocal slope of K-L plots should correspond to apparent n values of (4-2α) where α is the fraction of O_2 reduced to H_2O_2. The ratio of the disk to ring current for the first wave in Figure 4.6 yields α = 0.11 (using 0.11 as the collection efficiency for H_2O_2 at the ring). Thus, a K-L plot with a slope corresponding to 3.78 electrons per O_2 molecule is expected. The observed value is 3.8±0.1, suggesting that the reaction pathways leading to H_2O_2 and to H_2O are independent of each other.

The Co-Fe diporphyrin also catalyzes the reduction of O_2 in separated steps. Rotated ring-disk electrode measurements (Figure 4.6) indicate that ca. 25% of the O_2 is reduced to H_2O_2 on the first plateau and > 95% is reduced to H_2O on the second plateau. The reciprocal slopes of the corresponding K-L plots correspond to apparent n values of 3.6± 0.1 and 4.1±0.1 respectively, compared with the values of 3.5 and 4.0 calculated from the ring-disk results. Despite the relatively modest change in the reaction stoichiometry between the first and second plateaus, the increase in the kinetic currents derived from the reciprocal intercepts of the two K-L plots points to a two- to three-fold increase in catalyst reactivity between the two plateaus. The most likely difference in the state of the catalyst on the second current plateau is its reduction from $Co^{II} - Fe^{III}$ to $Co^{II} - Fe^{II}$. Reduction of the iron center in the diporphyrin to Fe(II) should increase its affinity for O_2 and could also increase the rate of intercavity binding of O_2 by providing a second receptive site for the initial binding step.

Catalyzed Reduction of H_2O_2. The three diporphyrins containing iron ions exhibited substantial activity as catalysts for the reduction of H_2O_2(Figure 4.8). This was not surprising in the light of previous studies (11, 12). The Co-Cu diporphyrin exhibited a smaller, multiple-wave response towards H_2O_2. This evidence for a slow catalytic pathway that is potential-dependent in the

Figure 4.8. Current-potential curves for the reduction of 1 mM H_2O_2 at rotating graphite disk electrodes coated with diporphyrins. Supporting electrolyte: 1 M CF_3COOH saturated with argon. Rotation rate: 400 rpm. Scan rate: 5 mV s^{-1}. The dashed line shows the response at an uncoated electrode.

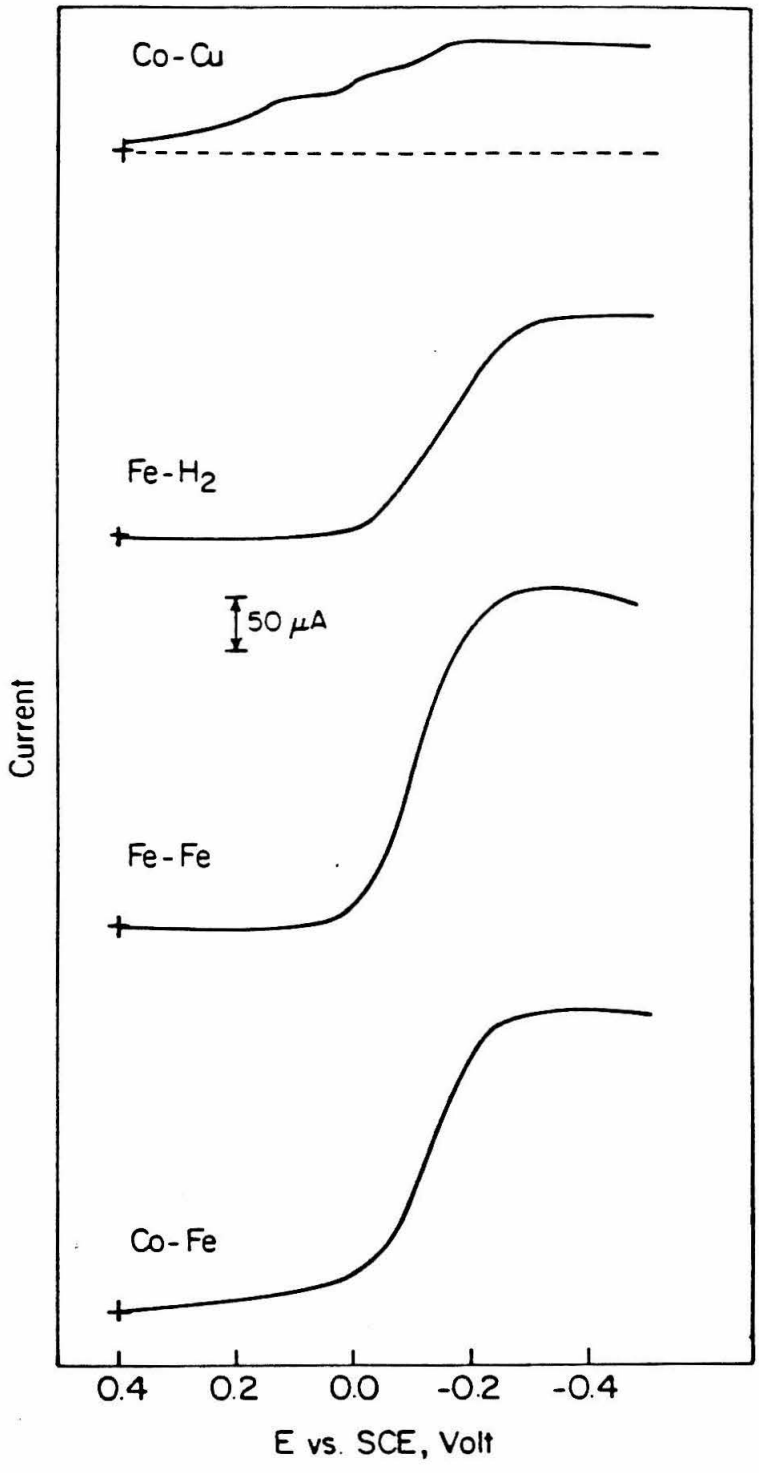
Co-Cu
Fe-H2
50 μA
Fe-Fe
Co-Fe
Current
0.4
0.2
0.0
-0.2
-0.4
E vs. SCE, Volt

range where the same catalyst sustains a rapid reduction of O_2 to H_2O_2 (Figure 4.2) helps to explain the more inclined plateau currents uniformly observed in current-potential curves for O_2 reduction at rotating disks coated with the Co-Cu diporphyrin (Figures 4.2-4.4). The small increases in current could result from the slow reduction of the H_2O_2 present at the electrode surface during the more facile reduction of O_2.

The catalysis by the iron-containing diporphyrins of the reduction of H_2O_2 seems not to begin with its disproportionation. This was demonstrated, as in a previous study (11), by employing a rotating graphite disk-carbon paste ring electrode. The disk was coated with the catalysts and the ring with a cobalt porphyrin that is a good catalyst for the electro-reduction of O_2 at the potential (-0.1 volt) where the ring electrode was held. Rotation of the coated disk at open circuit in deoxygenated solutions of H_2O_2 produced no cathodic ring current, showing that the H_2O_2 did not undergo catalytic disproportionation by contact with the coated disk.

The potentials where the catalyzed reduction of H_2O_2 proceeds in Figure 4.8 are rather close to the peak potentials of the waves assigned to the reduction of the Fe(III) centers (Figure 4.5), suggesting a simple outer-sphere reduction of O_2 by the Fe(II) form of the diporphyrins, as proposed previously for monomeric iron porphyrin catalysts (11).

Discussion

There are both similarities and differences in the behavior of the four diporphyrins examined here that, taken together, are helpful in trying to understand the mechanisms through which they, and related complexes investigated earlier (5), function as O_2 reduction catalysts.

Co-Cu Diporphyrin. Most macrocyclic complexes of Cu(II) are rather poor catalysts for the electro-reduction of O_2 (29) so that it was not surprising to find that the Co-Cu diporphyrin behaves similarly to monomeric cobalt

porphyrins (24) except for a somewhat greater activity towards the reduction of H_2O_2. However, it should not be overlooked that the corresponding Co-H_2 diporphyrin in which the second ring contains two protons in place of the Cu(II) ion has been shown to be an effective catalyst for the four-electron reduction of O_2 by a mechanism that does not involve the generation and subsequent reduction of H_2O_2 (5). The apparent absence of such a catalytic pathway in the Co-Cu diporphyrin strongly suggests that the protons in the second ring of the Co-H_2 analogue play an important role in guiding the reaction along a four-electron reduction pathway, possibly by helping to stabilize the partially reduced dioxygen species that is believed to be coordinated to the cobalt(II) center in the transition state.

Fe-H_2 and Fe-Fe Diporphyrins. The two iron-containing diporphyrins share the common ability of iron porphyrins to catalyze the reduction of O_2 at potentials significantly positive of the formal potential of the Fe(III)/Fe(II) couple (Figure 4.5). Since the diporphyrin is not expected to be reactive toward O_2 in its Fe(III) state, one interpretation of the positive potentials at which O_2 reduction commences is that the small quantities of Fe(II) diporphyrin that are formed at these positive potentials react very rapidly with O_2 to yield an adduct that is immediately reduced. A difficulty with this explanation is the large magnitudes of the rate constants for both the binding of O_2 to the Fe diporphyrin reaction and for the electron transfer between the adsorbed adduct and the electrode that are required to accommodate the difference between the Fe(III)/Fe(II) formal potential and that where O_2 is reduced. For example, the difference of 370 mV shown in Figure 4.5 for the Fe-Fe diporphyrin at pH 0 leads to a calculated rate constant of 6×10^9 $M^{-1}s^{-1}$ for the O_2-Fe diporphyrin binding reaction, which seems unrealistically large.

An alternative reaction scheme might involve the reduction of O_2 to O_2^- which rapidly binds to the Fe(III)-diporphyrin and subsequently disproportion-

ates or is further reduced. However, the formal potential of the O_2/O_2^- couple (-0.57 V vs. SEC (30)) is too negative to contemplate the production of O_2^- at potentials as positive as 0.12 V where the catalyzed reduction of O_2 proceeds (Figure 4.2), because the affinity of O_2^- for Fe(III) porphyrins is known to be relatively low (31).

It is conceivable that adsorption of the porphyrins produces an array of effective formal potentials for the Fe(III/II) centers that spans several hundred millivolts. The (small) portion of such adsorbed porphyrins that are reduced to Fe(II) at potentials well ahead of the primary peak might constitute the active catalyst that is responsible for the appearance of reduction current at potentials where most of the adsorbed porphyrin remains oxidized and unreactive. However, the shape of the voltammetric waves in Figure 4.2 do not suggest that much of the catalyst is reducible at potentials where the O_2 reduction is observed. It seems accurate to conclude that an entirely satisfactory catalytic mechanism to account for the potentials where adsorbed iron porphyrins and diporphyrins exhibit their activity toward O_2 in aqueous acid has yet to be proposed.

Co-Fe Diporphyrin. In a previous study of the catalytic behavior of a mixed cobalt-iron cofacial porphyrin (3) the two metal centers appeared to act independently: A first wave corresponding to the cobalt porphyrin-catalyzed two-electron reduction of O_2 to H_2O_2 was followed by a wave at the more negative potentials expected for the iron porphyrin-catalyzed reduction of H_2O_2 to H_2O (11, 12). The Co-Fe diporphyrin examined in this study exhibits contrasting behavior because the height of the first (composite) wave (Figure 4.2) signals that more than two electrons are involved, yet the potentials where the wave appears (0.3 - 0.1 V) are too positive for the iron-porphyrin catalyzed reduction of H_2O_2 to proceed (compare with Figure 4.8). Simultaneous participation of both metal centers to provide a parallel four-electron pathway seems likely and

one possibility is depicted in Figure 4.9. In this scheme the acidic protons of the water molecule presumed to be axially coordinated to the Fe(III) center interact with the peroxide molecule coordinated to the cobalt(II) center (within the cavity of the diporphyrin) to render it reducible to two water molecules before it can escape from the cavity in the form of unreducible H_2O_2. Proceeding in parallel with this four-electron pathway would be a two-electron pathway in which the O_2 is coordinated to the cobalt center outside of the cavity so that interaction with the iron center is absent and H_2O_2 is the final reduction product. The relative rates of two such pathways would determine the height of the first reduction wave in Figure 4.2. The inability of the Co-Cu diporphyrin to catalyze the reduction of O_2 beyond the H_2O_2 stage is compatible with the suggestion that acidic protons on a water molecule coordinated to the iron are important in the four-electron pathway available with the Co-Fe catalyst. The copper(II) center in the Co-Cu diporphyrin probably lacks an axial water ligand which, in any case, would be much less acidic than the water coordinated to an iron (III) center.

At pH values above 8 the first O_2 reduction wave becomes smaller (Figure 4.4) and at pH 12 its height indicates that the reduction does not proceed beyond II_2O_2. This behavior is consistent with the mechanistic scheme depicted in Figure 4.9 because the hydroxide ion is very likely to replace the water molecule inside the cavity that is coordinated to the Fe(III) center at this pH. The hydroxide proton is much less likely to participate in interactions with peroxide species so that further reduction is not facilitated and H_2O_2 becomes the final reduction product on the plateau of the first wave.

The difference in the behavior of the present anthracene-linked Co-Fe diporphyrin (13) and the previous doubly bridged Co-Fe cofacial diporphyrin may be largely steric in that the structure of the present porphyrin might more easily accommodate the types of interactions between O_2 and the two metal

Figure 4.9. A mechanistic scheme showing two independent catalytic pathways for reduction of O_2 at electrodes coated with the Co-Fe diporphyrin. The electrode potential is maintained at a value where the cobalt and iron centers are in their +2 and +3 oxidation states, respectively. Only the coordinated water molecules inside the diporphyrin cavity are shown.

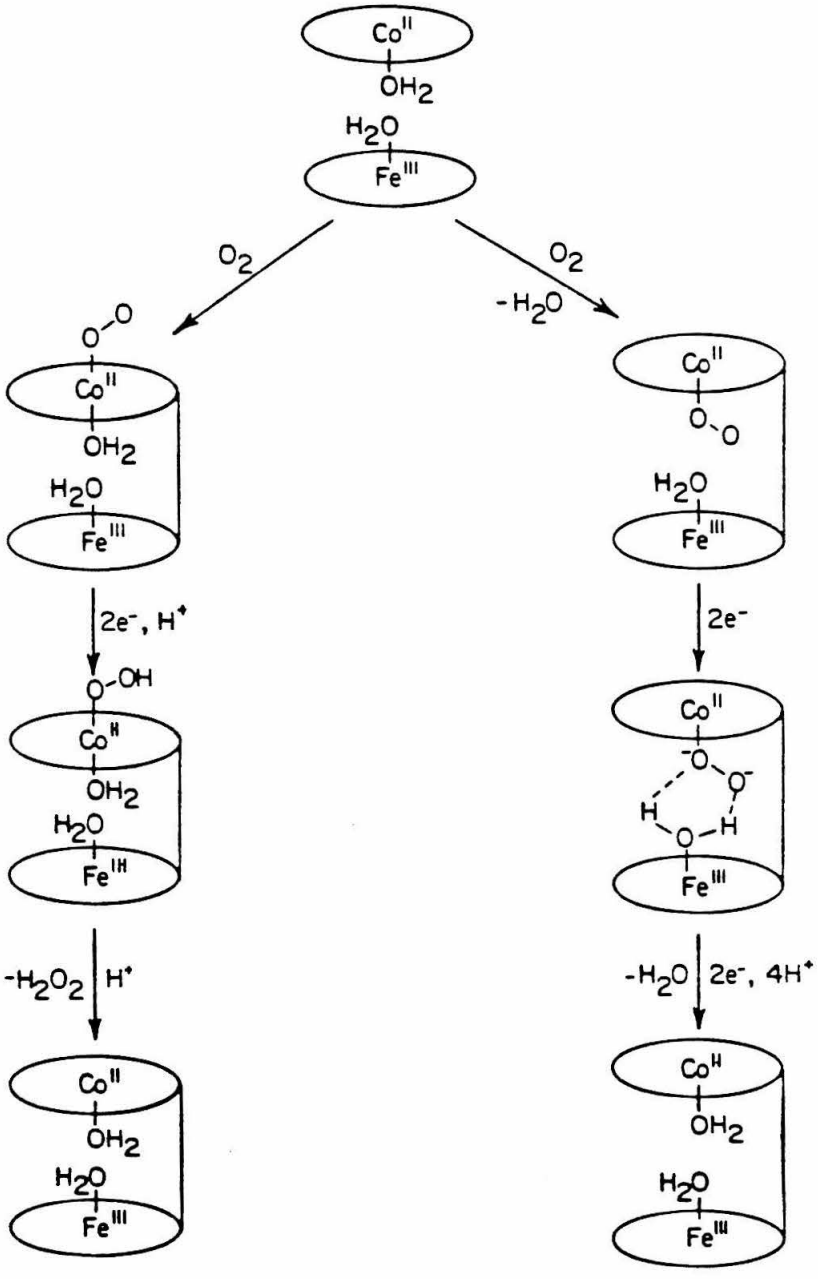
Co II
OH2
H2O
Fe III
O2
O2
-H2O
O-O
Co II
OH2
H2O
Fe III
Co II
O-O
H2O
Fe III
2e-, H+
2e-
O-OH
Co II
OH2
H2O
Fe III
Co II
H
H
Fe III
-H2O2
H+
-H2O
2e-, 4H+
Co II
OH2
H2O
Fe III
Co II
OH2
H2O
Fe III

centers depicted in Figure 4.9.

The suggestion inherent in the mechanistic scheme depicted in Figure 4.9 is that properly positioned proton sources within the catalyst molecules may allow the four-electron reduction of O_2 to be favored. To explore this idea, two additional monomeric cobalt porphyrin molecules were synthesized in the laboratory of Professor C. K. Chang (32). Their structures are shown in Figure 4.10. Porphyrin A has a carboxyl group positioned above the porphyrin ring while porphyrin B has three basic nitrogen atoms that would be protonated in acidic environments just as is the second porphyrin ring in the Co-H_2 catalyst.

Rotating ring-disk measurements of the reduction of O_2 were carried out with electrodes coated with these two porphyrins. The results showed that hydrogen peroxide is the predominant reduction product and the slopes of K-L plots corresponded to reductions involving 2.2 to 2.3 electrons. Thus, it appears that merely attaching acidic groups near the cobalt porphyrin center in catalysts of this type is not enough to provide good activity in the catalysis of four-electron reductions. The acidity of the proton-bearing groups in porphyrins A and B (Figure 4.10) is not likely to differ substantially from that in the Co-H_2 complex that catalyzes the four-electron reduction of O_2. The exact positioning of the proton sources may be the crucial requirement that is met with the Co-H_2 and Co-Fe catalysts but not with porphyrins A or B. Further testing of these speculations will require the preparation of a greater variety of derivatives analogous to those in Figure 4.10.

Concluding Remarks

The electrocatalytic behavior of four new dimeric porphyrins toward the reduction of O_2 at graphite electrodes has been examined for the following combinations: Co-Cu, Co-Fe, Fe-Fe, Fe-H_2. The Co-Cu diporphyrin catalyzes the reduction of O_2 to H_2O_2, but no further. The other three catalysts all exhibit mixed, but non-interacting pathways leading to both H_2O_2 and H_2O.

Figure 4.10. Structures of monomeric cobalt porphyrins with potentially acidic sites introduced close to the porphyrin ring.

A

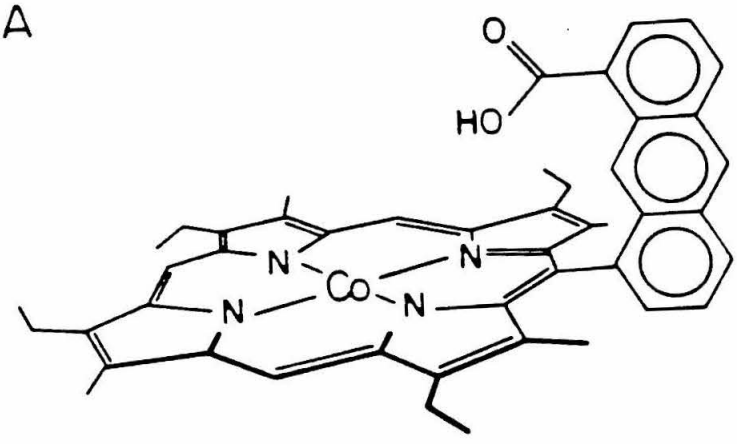

B

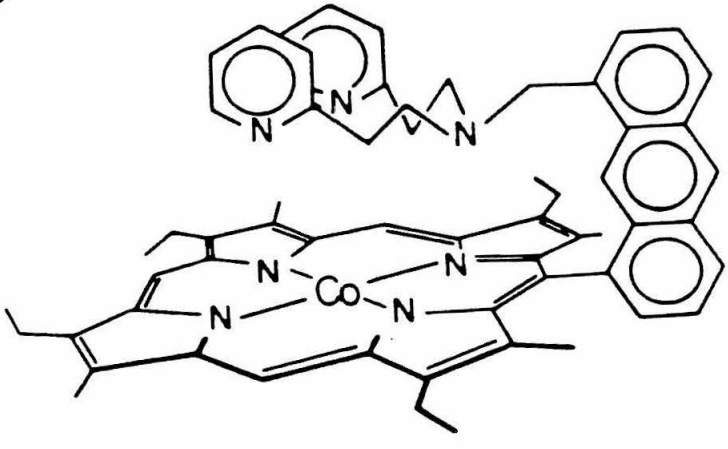

The rotaing ring-disk results suggest that the pathways that lead to H_2O do not involve H_2O_2 as an intermediate.

Perhaps one of the most important results presented in this Chapter is that in acidic media the Co-Fe diporphyrin catalyzes the electroreduction of O_2 to H_2O at potentials where H_2O_2 is not reducible. It is proposed that the acidic protons of the water molecule coordinated to the Fe(III) center interact with the peroxide molecule coordinated to the cobalt (II) center to render it reducible to two H_2O. This proposed mechanism has lead to the investigation of the catalytic behaviors of two porphyrins with acidic groups attached near the cobalt center. Although they catalyzed only the two-electron reduction of O_2, it will be very interesting to test other molecules with acidic protons attached in approximately the same positions to the cobalt center as in Co-Fe or Co-H_2 diporphyrins.

References and Notes

1. Collman, J.P.; Marrocco, M.; Denisevich, P.; Koval, C.; Anson, F.C., J. Electroanal. Chem., 101(1979)117.
2. Collman, J.P.; Denisevich, P.; Konai, Y.; Koval, C.; Anson, F.C., J. Am. Chem. Soc., 102(1980), 6027.
3. Durand, Jr., R.R.; Bencosme, C.S.; Collman, J.P.; Anson, F.C., J. Am. Chem. Soc., 105(1983), 2710.
4. Liu, H.-Y.; Weaver, M.J.; Wang, C.B.; Chang, C.K., J.Electroanal. Chem., 145(1983)439.
5. Liu, H.-Y.; Abdulmuhdi, I.; Chang, C.K.; Anson, F.C., J. Phys. Chem., 89(1985)665.
6. Eaton, S. S.; Eaton, G. R.; Chang, C. K., J. Am. Chem. Soc., 107(1985)3177.
7. Behret, H.; Clauberg, W.; Sandstede, G., Ber. Bunsenges, Phys, Chem., 83(1979)139.
8. Tarasevich, M.R.; Radyushkina, K.A., Russ. Chem. Rev., 49(1980)718.
9. van Veen, J.A.R.; van Baar, J.F.; Kroese, C.J.; Coolegem, J. G. F.; deWit, N.; Colijn, H. A., Ber. Bunsenges. Phys. Chem., 85(1981)700.
10. Bettelheim, A.; Parash, R.; Oxer, D., J. Electrochem. Soc., 129(1982)2247.
11. Shigehara, K.; Anson, F.C., J. Phys. Chem., 86(1982)2776.
12. Forshey, P.A.; Kuwana, T.; Kobayashi, N.; Osa, T., Adv. Chem. Ser., 201(1982)601.
13. Forshey, P.A.; Kuwana, T., Inorg. Chem., 22(1083)699.
14. Kobayashi, N.; Osa, T., J. Electroanal. Chem., 157(1983)269.
15. Ozer, D.; Parash, R.; Broitman, F.; Mor, U.; Bettelhem, A., J. Chem. Soc., Faraday Trans. I, 80(1984)1139.
16. Ikeda, O.; Fukuda, H.; Tamura, H., J. Chem. Soc., Chem. Commun., (1982)567.
17. Kobayashi, N.; Nishiyama, Y., J. Electroanal. Chem., 1181(1984)107.

18. Ikeda, O.; Okabayahsi, K.; Yoshida, N.; Tamura, H., J. Electroanal. Chem., 191(1985)157.
19. Ikeda, O.; Kojima, T.; Tamura, H., J. Electroanal. Chem.,200(1986)323.
20. Chang, C. K.; Abdulmuhdi, I.; J. Org. Chem., 48(1983)5388.
21. Chang, C.K.; DiNello, R.K.; Dolphin, D., Inorg. Synth., 20(1980)147.
22. Oyama, N.; Anson, F. C., Anal. Chem. 52(1980)1192.
23. Geiger, T.; Anson, F. C., J. Am. Chem. Soc., 103(1982)7489.
24. Durand, Jr., R. R.; Anson, F. C., J. Electroanal. Chem., 134(1982)273.
25. Chan, R. J.; Su, Y. O.; Kuwanna, T., Inorg. Chem., 24(1985)3777.
26. Ni., C.-L.; Anson, F. C., Inorg. Chem., 24(1985)4754 and references therein.
27. Chang, C. K.; Liu, H.-Y.; Abdulmuhdi, I., J. Am. Chem. Soc., 106(1984)2725.
28. Koutechy, J.; Levich, V. G., Zh. Fiz. Khim., 32(1956)1565.
29. Savy, M.; Andro, P.; Bernard, C.; Manger, G., Electrochim. Acta, 18(1973)191.
30. Ilan, Y. A.; Zapski, G.; Meisel, D., Biochem. Biophys. Acta, 420(1976)209.
31. Paternack, R. F.; Halliwell, B., J. Am. Chem. Soc., 101(1979)1026.
32. The procedures employed in the synthesis of the porphyrins in Figure 4.10 will be described in a forthcoming publication.

APPENDIX I

A COMPUTER PROGRAM FOR SOLVING NUMERICALLY THE MASTER DIFFERENTIAL EQUATION WHICH GOVERNS THE KINETICS OF REDOX POLYMER ELECTRODES AS DESCRIBED IN CHAPTER II

Introduction

A computer program to solve numerically the "master differential equation" (eqn. 5.1) as described in Chapter II and ref. 1 is presented here.

$$\frac{d^2a^*}{dy^2} - \frac{i^*_{k_1}\sigma a^*\left\{1+\frac{i^*_s}{i_E}[a^*-a^*_0-y(\frac{da^*}{dy})_1]\right\}}{1+\sigma\left\{1+\frac{i^*_s}{i_E}[a^*-a^*_0-y(\frac{da^*}{dy})_1]\right\}} = 0 \quad , \tag{5.1}$$

with y=0: $\frac{da^*}{dy} = 0$; y=1:a^*=1,i = $i^*_s(\frac{da^*}{dy})_1$; $i = i^*_s(\frac{da}{dy})_1$. This program is written in FORTRAN and calls a subroutine (DVERK) from the IMSL Library(2) to solve first-order differential equations by using the Runge-Kutta method (3).

A sample calculation is listed below:

Input parameters: i_E = 1.5 mA cm^{-2}, i_s = 1.1 mA cm^{-2}, i_{k_1} = 3.6 mA cm^{-2}, i_A = 0.32 mA cm^{-2}, and σ = 1020. Output: i_{lim} = 0.27 mA cm^{-2}.

Saveant and coworkers have developed theories (1, 4-7) which describe the kinetics of redox polymer films on electrodes in the context of rotating disk electrode techniques. In analyzing the interplay of the various transport and kinetic processes that determine the measured plateau currents at electrodes, it is instructive to utilize kinetic zone diagrams such as Figure 2.7 in Chapter II. In the kinetic cases labeled "General Case", it is necessary to solve numerically the "master differential equation" (11) in the same (1) or similar (4-7) form as eqn. 5.1 to calculate the desired rate constant. The applicability of Saveant's treatment has already been demonstrated in several cases (1, 8-9) so that the computer program listed here may be of some interest to those who are interested in applying Saveant's theories to their systems.

```
      PROGRAM TPRV
C THIS PROGRAM SOLVES THE TWO POINT BOUNDARY VALUE PROBLEM
C AUG 24 1984
      EXTERNAL DERIV      ! state equations
      PARAMETER N=1000    ! number of integration steps
      PARAMETER M=100     ! absolute maximum number of iterations
      DIMENSION Y(N),A(N)
      DIMENSION XOUT1(M),XOUT2(M),AO(M),A1(M),ADOTO(M),ADOT1(M)
      DIMENSION XX(2,2),XXI(2,2),DX1(M),DX2(M)
      DIMENSION X(2),XDOT(2),C(24),W(2,9)     ! variables used in integration
      COMMON/C/SIGMA,XA,XE,XK,XS,XSSTAR,AAO,AADOT1

C INITIALIZE EVERYTHING ************************************************
      WRITE(6,601)
  601 FORMAT('$SIGMA = ')
      READ(5,4)SIGMA
      WRITE(6,602)
  602 FORMAT('$IA    = ')
      READ(5,4)XA
      WRITE(6,603)
  603 FORMAT('$IE    = ')
      READ(5,4)XE
      WRITE(6,604)
  604 FORMAT('$IK    = ')
      READ(5,4)XK
      WRITE(6,605)
  605 FORMAT('$IS    = ')
      READ(5,4)XS
      TX1 = 0.00001          ! tolerance in the value of AO
      TX2 = 0.000001         ! tolerance in the value of ADOT1
      WRITE(6,1)
    1 FORMAT('$MAXIMUM NUMBER OF ITERATIONS = ')
      READ(5,2)NM
    2 FORMAT(I4)
      WRITE(6,8)
    8 FORMAT('$THE 1ST GUESS OF ADOT1       = ')
      READ(5,4)ADOT1(1)
    4 FORMAT(F20.13)
      WRITE(6,9)
    9 FORMAT('$THE 2ND GUESS OF ADOT1       = ')
      READ(5,4)ADOT1(2)
      WRITE(6,6)
    6 FORMAT('$THE GUESS OF AO = ')
      READ(5,4)AO(1)
```

```
C ASSIGN Y ***********************************************************
      TINCRM = 1./FLOAT(N)                          ! increment of integration
      DO 50 I=1,N
50      Y(I) = 1.-FLOAT(I)*TINCRM

C MINIMIZATION WITH RESPECT TO ADOT(1) *** USE ADOT(0)=0. AS CRITERIA **
C INTEGRATE & CALCULATE THE FUNCTION OF A(Y) ***************************
      DO 155 J1=1,NM
      WRITE(6,10)
   10 FORMAT(/,'       A(0)        ADOT(1)       A(0)        ADOT(0)')
      F? = 1.0                                  ! step size factor
      AAO = AO(J1)                              ! used in common statement
      DO 150 J=1,NM
        TOL = 0.00001                           ! tolerance of integration routine
        AADOT1 = ADOT1(J)                       ! used in common statement
        XSSTAR = XS*XA/(XA+XS*AADOT1)
        K=1                                     ! initialize integration
        X(1)=1.0                                ! assign initial value for integration
        X(?)=AADOT1                             ! assign initial value for integration
        DO 100 I=1,N
          TIMEND = 1.-FLOAT(I)*TINCRM           ! start & end of integration step
          TIME = 1.-FLOAT(I-1)*TINCRM
          CALL DVERK(2,DERIV,TIME,X,TIMEND,TOL,K,C,?,W,IER)
          A(I) = X(1)
C         CHECK FOR INTEGRATION ERRORS
          IF(K.GE.0 .AND. IER.LE.0) GO TO 100
          WRITE(6,99) TIMEND, K, IER, (JJ,C(JJ),JJ=1,?4)
   99     FORMAT(' ERROR IN DERIV AT T= ',F8.2,/,' K(IND) = ',
     *       I4/,' IER    = ',I4//,24(' C(',I2,') = ',F12.5/))
          TOL = TOL*1.1
          WRITE(6,182) TOL
  182     FORMAT(' TOL = ',F8.4)
  100   CONTINUE
        XOUT1(J1)= X(1)                         ! output of the effect of input
        XOUT2(J) = X(2)                         ! output of the effect of input
  140   WRITE(6,22)AO(J1),ADOT1(J),XOUT1(J1),XOUT2(J)
   22   FORMAT(4E13.5)                                                  .....

C CHECK TO SEE IF THE ORIGINAL ASSUMPTIONS ON ADOT1 ARE CORRECT ********
      DX?(J) = XOUT2(J) - 0.0
```

```
      IF(ABS(DX2(J)).LE.TX2)GOTO 151
C DETERMINE THE NEXT VALUE OF ADOT1 ************************************
      IF(J .EQ. 1)GO TO 150
C     CALCULATE THE MATRIX RELATING OUTPUT TO INPUT ********************
      XXI(2,2)=(ADOT1(J)-ADOT1(J-1))/(XOUT2(J)-XOUT2(J-1))
C     CALCULATE THE STEP SIZE FACTOR E2 ********************************
      E2 = 1./(1.+ABS(XOUT2(J)/XOUT2(J-1)))
C     CALCULATE THE NEXT VALUES OF ADOT1 TO TRY ************************
      ADOT1(J+1) = ADOT1(J) - E2*XXI(2,2)*DX2(J)
  150 CONTINUE

C MINIMIZATION WITH RESPECT TO A(0) ************************************
C CHECK TO SEE IF THE ORIGINAL ASSUMPTIONS ON AO ARE CORRECT ************
  151 DX1(J1) = XOUT1(J1) - AO(J1)
      IF(ABS(DX1(J1)).LE.TX1)GOTO 600
      WRITE(6,7)
    7 FORMAT(/,'$HIT RETURN TO CONTINUE, 1 TO QUIT')
      READ(5,2)IQUIT
      IF(IQUIT .NE. 0)GOTO 600
      AO(J1+1)=XOUT1(J1)          ! use the last value as the start of a new iteration
      ADOT1(1)=ADOT1(J-1)
      ADOT1(2)=ADOT1(J)
  155 CONTINUE

C WRITE Y, A ***********************************************************
600   open(unit=11,file='A',status='new')
      WRITE(11,21) ((Y(I),A(I)),I=1,N)
   21 FORMAT(2E13.5)
      CLOSE(UNIT=11)
      WRITE(6,23)AADOT1*XSSTAR
   23 FORMAT(' I = ',E13.5)
      STOP
      END


      SUBROUTINE DERIV(N,TIME,X,XDOT)
C FIND THE DERIVATIVES OF THE STATE EQUATIONS.
      DIMENSION X(N),XDOT(N)
      COMMON/C/SIGMA,XA,XE,XK,XS,XSSTAR,AAO,AADOT1
      TEMP = 1 + XSSTAR/XE*(X(1)-AAO-TIME*AADOT1)
      XDOT(1) = X(2)
      XDOT(2) = XK/XS*SIGMA*X(1)*TEMP/(1.+SIGMA*TEMP)
      RETURN
      END
```

References and Notes

1. Andrieux, C.P.; Saveant, J.-M., J. Electroanal. Chem., 171(1984)65.
2. IMSL Library contains a set of computational subroutines provided by the International Mathematical and Statistical Library, Inc.
3. Gerald, C.F.; Wheatley, P.O., "Applied Numerical Analysis" 3rd ed.; Addison-wesley; 1984; p306.
4. Andrieux, C.P.; dumas-Bouchiat, J.-M.; Saveant, J.-M., J. Electroanal. Chem., 131(1982)1.
5. Andrieux, C.P.; Saveant, J.-M., J. Electroanal. Chem., 134(1982)163.
6. Andrieux, C.P.; Saveant, J.-M., J. Electroanal. Chem., 142(1982)1.
7. Andrieux, C.P.; dumas-Bouchiat, J.-M.; Saveant, J.-M., J. Electroanal. Chem., 169(1984)9.
8. Andrieux, C.P.; Saveant, J.-M.; Shigehara, K., J. Electroanal. Chem., 145(1983)423.
9. Andrieux, C.P.; Saveant, J.-M.; Ohsaka, T., J. Electroanal. Chem., 105(1983)4883.
10. Krishnon, M.; Zhang, X.; Bard, A.J., J. Am. Chem. Soc. 106(1984)7371.
11. The "master differential equation" describes the kinetics under the General Case and other cases (such as R+S, E, R, etc). To obtain kinetic information under kinetic cases other than the General Case, one can use either the given analytical solutions or the numerical solution to the "master differential equation".

APPENDIX II

A PULSE POLAROGRAPHIC MEASUREMENT OF THE KINETICS OF DISSOCIATION OF THE $[Ru^{III}(edta)]_2$ DIMER

Introduction

An interesting dimeric ethylenediaminetetraacetato (edta) complex containing two ruthenium ions with an average oxidation state of $III\frac{1}{2}$ has been described in two recent studies (1, 2). The $[Ru^{III1/2}(edta)]_2$ dimer is reasonably stable but upon reduction by one electron the resulting $[Ru^{III}(edta)]_2$ complex decomposes in acidic solution to yield the well-known monomeric $Ru^{III}(edta)OH_2$ complex (3). A preliminary estimate of the rate of the monomerization reaction was given by Ikeda *et al.* (1) at a single pH but no systematic kinetic study of the reaction has been reported. The study reported in this Appendix was undertaken because of a continuing interest in the electrochemistry of transition metal edta complexes (4-8) and with the hope that the pH dependence of the kinetics of the monomerization reaction could provide insight into the still uncertain nature of the metal-bridging ligand(s) that connect and bind the two ruthenium centers in the dimer together (2, 9).

The half-life of the $[Ru^{III}(edta)]_2$ complex varies from ca. 1 to a few seconds over the pH range from 3 to 6 so that reverse pulse polarography with a dropping mercury electrode (10) provided a convenient method for examining the kinetics of the monomerization reaction.

Experimental

Materials. $H[Ru(edta)(OH_2)]$ was prepared according to previously described procedures (2, 3a). Since solid samples of the dimeric complex containing $Ru(III\frac{1}{2})$ undergo slow decomposition(2), solutions of the dimer were freshly prepared from the stable $Ru^{III}(edta)OH_2$ complex according to the following procedure: 2 mg of $H[Ru^{III}(edta)OH_2]$ were dissolved in 10 ml of acetate buffer solution (pH 4.8) and the stoichiometric quantity of H_2O_2 needed to oxidize all of the Ru(III) to $Ru(III\frac{1}{2})$ was added from a freshly standardized solution of H_2O_2. Our observations confirmed the previous report (2) that the oxidation

proceeds quantitatively to yield the dimeric complex (2). The resulting solution was adjusted to the desired pH and used immediately for the electrochemical measurements.

Apparatus and Procedures. Cyclic voltammetry was carried out with conventional, commercially available instrumentation and a Metrohm hanging mercury drop electrode (Brinkmann Instruments). A drop area of 0.023 cm^2 was employed. Pulse polarography was conducted with a PAR Model 174 instrument (E G & G Instruments, Inc.) that had been modified to allow variable pulse widths (11). A conventional dropping mercury electrode, with a flow rate of 1.54 mg s^{-1}, a PAR Model 172A drop timer, a Houston Instruments X-Y recorder and a saturated calomel reference electrode were also employed. Spectra were obtained with a Hewlett-Packard Model 8450A spectrophotometer. Solutions were prepared from distilled water that was further purified by passage through a purification train (Barnsted Nanopure-Organopure). Measurements were carried out at the ambient laboratory temperature, 22 ± 2^0 C.

Results and Discussion

As shown in the cyclic voltammograms in Figure 6.1, the peak current for the reduction of the $[Ru^{III\frac{1}{2}}(edta)]_2$ dimer exceeds the corresponding anodic peak current, and increasingly so as the scan rate is decreased. The behavior is qualitatively in accord with that expected when the initial product of an electro-reduction reaction (*e.g.*, the dimer of Ru^{III}(edta) decomposes into a species (*e.g.*, the Ru^{III}(edta) monomer)) that is not oxidizable at the potential where the intial product is oxidized. The ratio of the anodic to the cathodic peak current of the cyclic voltammograms can be used to estimate the rate of the decomposition reaction (12) but we elected to utilize another technique to avoid the inaccuracies inherent in measuring the magnitude of anodic peak currents for voltammograms such as those in Figure 6.1.

Normal and reverse pulse polarography were well suited for our purposes

Figure 6.1. Cyclic voltammograms for 0.25 mM $[Ru^{III1/2}(edta)]_2$ recorded at a hanging mercury drop electrode with scan rates of 10, 50 and 100 mV s^{-1}. Supporting electrolyte: 50 mM acetate buffer (pH = 4.8). Ionic strength was adjusted to 0.2 M with CF_3COONa.

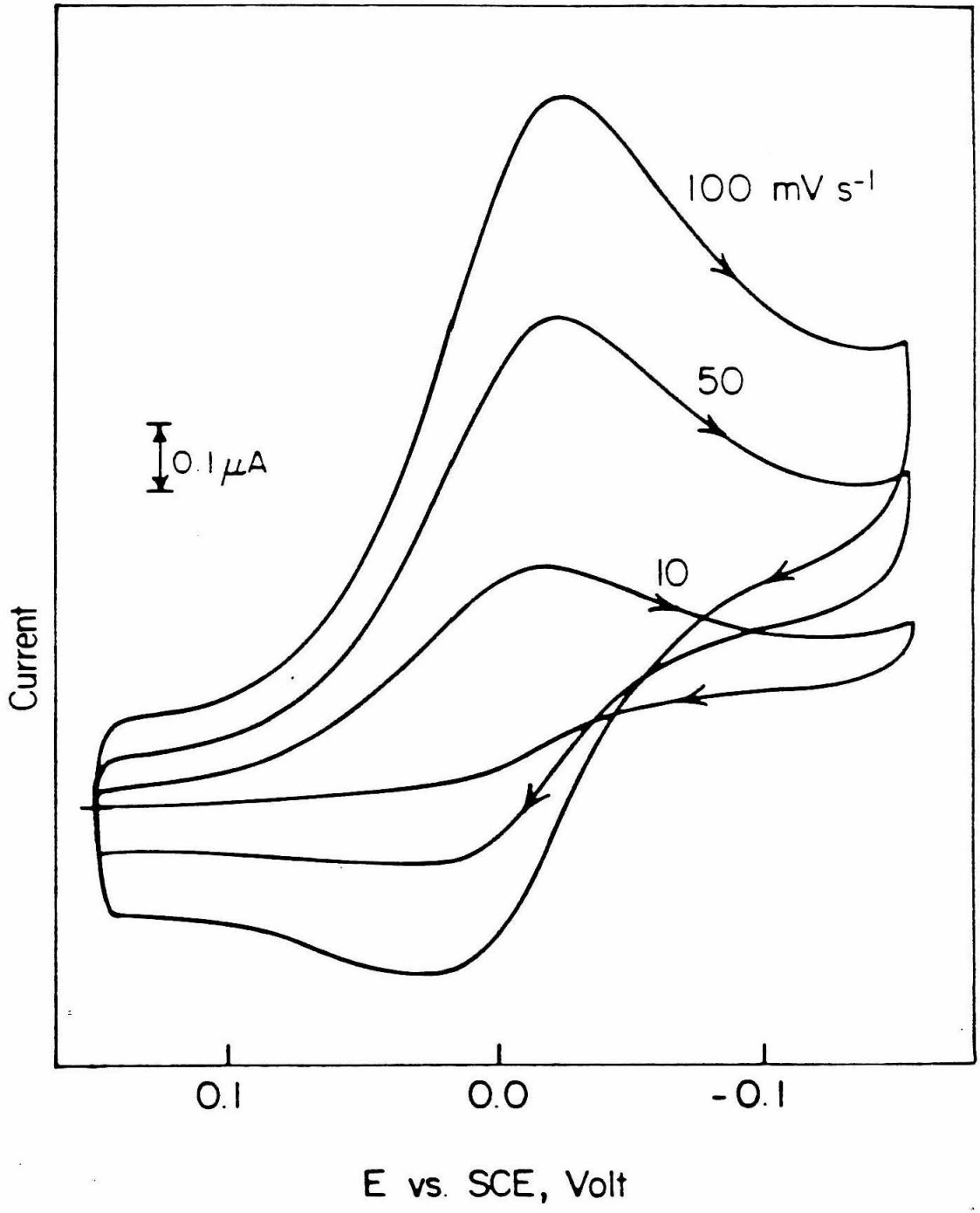
100 mV s-1
50
10
0.1 μA
Current
0.1
0.0
-0.1
E vs. SCE, Volt

(10, 13) and we applied these techniques to estimate the forward rate of reaction 6.1 under conditions where it was irreversible.

$$[Ru^{III}(edta)]_2 \underset{k_{-1}}{\overset{k_1}{<\!\!=\!\!>}} 2Ru^{III}(edta)OH_2 \qquad (6.1)$$

Representative polarograms recorded at different pulse widths are shown in Figure 6.2. The half-wave potentials are essentially independent of the pulse width between 2 and 90 ms, indicating that the electron-transfer reaction is reasonably rapid. The forward rate constant for reaction 6.1 is related to the ratio of the limiting currents of the reverse to the normal pulse polarograms, i_R/i_N, according to a rather complex relationship derived by Schwarz and Shain(14). Using the definitions of experimental times depicted in Figure 6.3 for the normal and reverse pulse experiments, the equations of Schwarz and Shain (14) can be simplified by restricting measurement times so that $k_1(t_e - t_p) < 2$ and $t_p/(t_e - t_p) < 1$. The resulting simplified expression is

$$-\frac{i_R}{i_N} = exp\left[\frac{-k_1(t_e - t_p)}{2}\right] I_0\left[\frac{k_1(t_e - t_p)}{2}\right]$$

$$+2exp\left[\frac{-k_1(t_e - t_p)}{2}\right] I_1\left[\frac{k_1(t_e - t_p)}{2}\right]\left[\frac{exp(-k_1t_p)[(k_1t_p - 1)exp(k_1t_p) + 1]}{k_1t_p}\right]$$

$$-\left[\frac{t_p}{t_e - tp}\right]^{1/2}\left[1 + \frac{t_p}{t_e - t_p}\right]^{-1/2}, \qquad (6.2)$$

where $I_0(x)$ and $I_1(x)$ are modified Bessel functions of orders 0 and 1, respectively (15).

Equation 6.2 was derived for the case of a planar electrode of constant area. The dropping mercury electrode could be regarded as essentially planar for the short pulse widths, t_p, employed in our experiments but its area was, of course, not constant. We corrected approximately for the effect of the increase in drop area by using the factor of 3/7 introduced by Ilkovic (16) to account for the

Figure 6.2. Normal and reverse pulse polarograms for a 0.25 mM solution of $[Ru^{III1/2}(edta)]_2$ at pH 4.8. $t_e = 2$ s; t_p = (A) 10.4; (B)39.7; (C) 90 ms. Other conditions as in Figure 6.1.

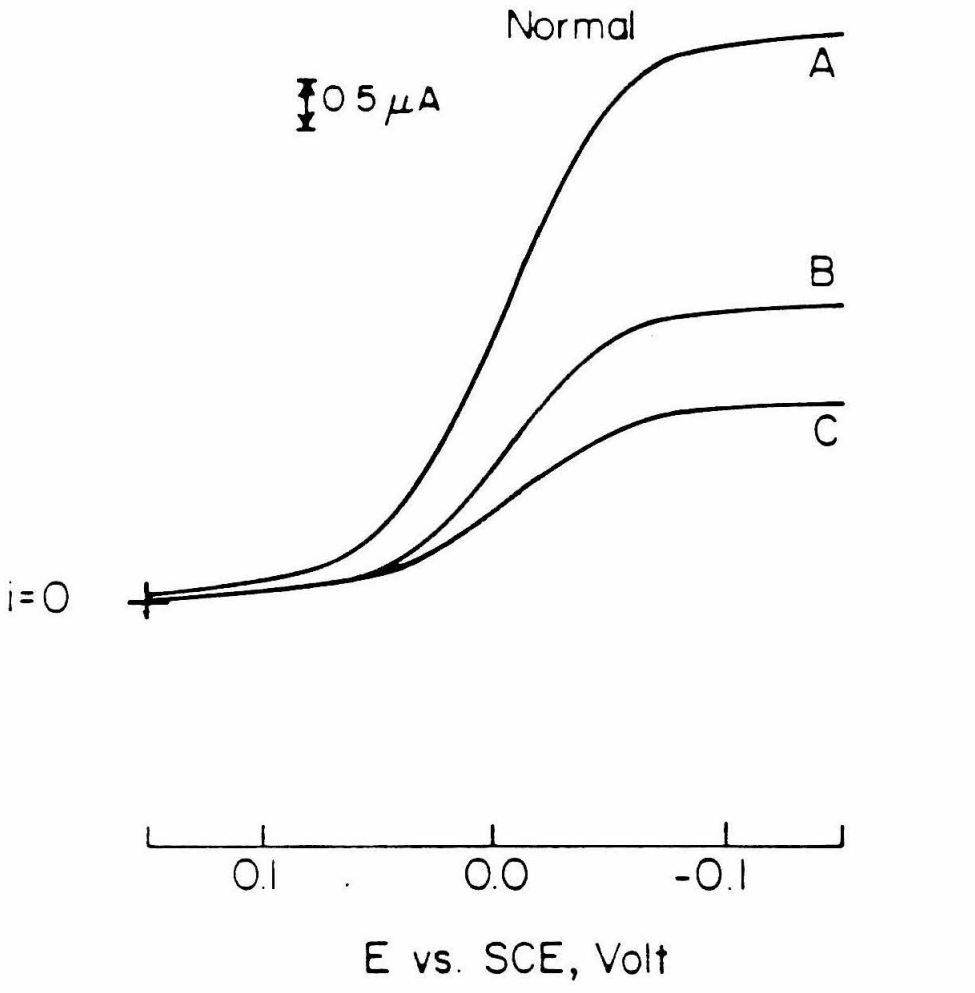
Normal
0.5 μA
A
B
C
i=0
0.1
0.0
-0.1
E vs. SCE, Volt

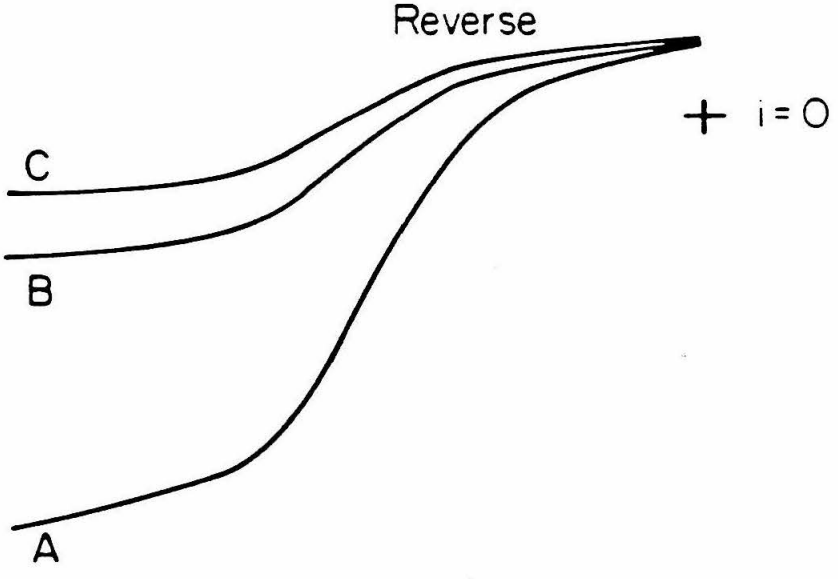
Reverse
i=0
C
B
A

Figure 6.3. Definitions of relevant times and limiting currents in normal and reverse pulse polarography. Currents are measured before the end of each pulse at time (t_e-0.08 ms).

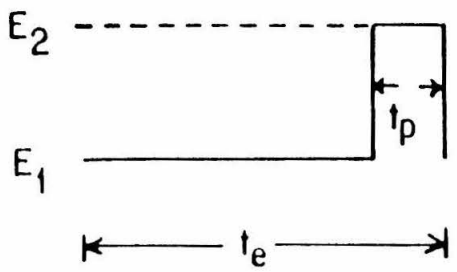

NORMAL

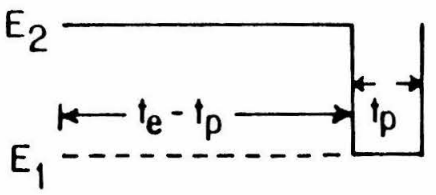

REVERSE

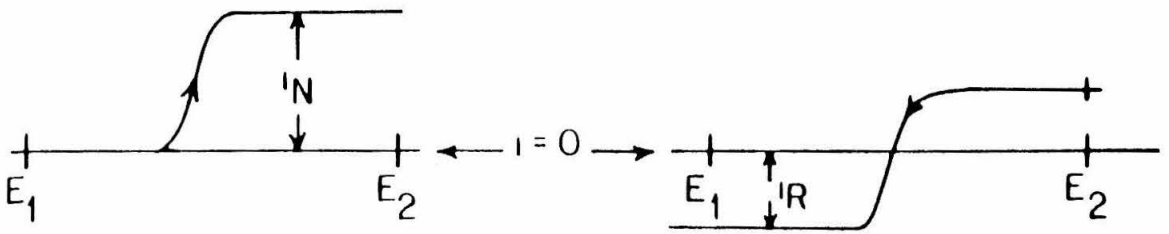

thinning of the diffusion layer produced by the expansion of the electrode. This approximation results in the substitution of $(3/7)(t_e - t_p)$ for $(t_e - t_p)$ in eqn. 6.2.

Representative working curves relating the limiting current ratio to the rate constant as calculated for the values of t_e and t_p employed in the experiments are shown in Figure 6.4. Table 6.1 summarizes the values of k_1 obtained from such curves at three pH values. The values of k_1 obtained were independent of the intitial concentration of $[Ru^{III1/2}(edta)]_2$ as expected for a first-order decomposition of $[Ru^{III}(edta)]_2$ (reaction 6.1). The average of k_1 at pH 4.8, 0.7 s^{-1}, compares favorably with the value estimated by Ikeda *et al.* from cyclic voltammetric observations at pH 4.7 (1).

Evidence of weak adsorption of $[Ru^{III1/2}(edta)]_2$ at mercury was obtained chronocoulometrically (17) and $Ru^{III}(edta)OH_2$ is also known to be weakly adsorbed (7). Since reactant and product adsorption can lead to depressed or enhanced limiting currents in pulse polarography (18) we checked to be sure that the adsorption was not extensive enough to produce such effects under our experimental conditions. Limiting currents that were linear functions of $t_p^{-1/2}$ for t_p values between 10 and 90 milliseconds were taken as good evidence that adsorption produced negligible effects on the measured limiting currents.

Effect of pH on Reaction 6.1. As shown in Table 6.1, the forward rate constant governing reaction 6.1 exhibits a mild decrease as the pH increases. At a fixed pH the current ratio is unaffected by a ten-fold increase in the buffer concentration so there is apparently no general acid catalysis of the monomerization of $[Ru^{III}(edta)]_2$. The dependence of the observed rate constant on the proton concentration is distinctly less than first-order between pH 3.5 and 6. Lower pH values could not be examined because $[Ru^{III1/2}(edta)]_2$ oxidizes the mercury electrode in more acidic solutions. At pH values between 7 and ca. 9 it was not possible to avoid the formation of (re-oxidizable Ru(II)) during the

Figure 6.4. Working curves calculated from equation 6.2 for t_e= 2 s and t_p= (A) 10.4; (B) 39.7; (C) 90 ms.

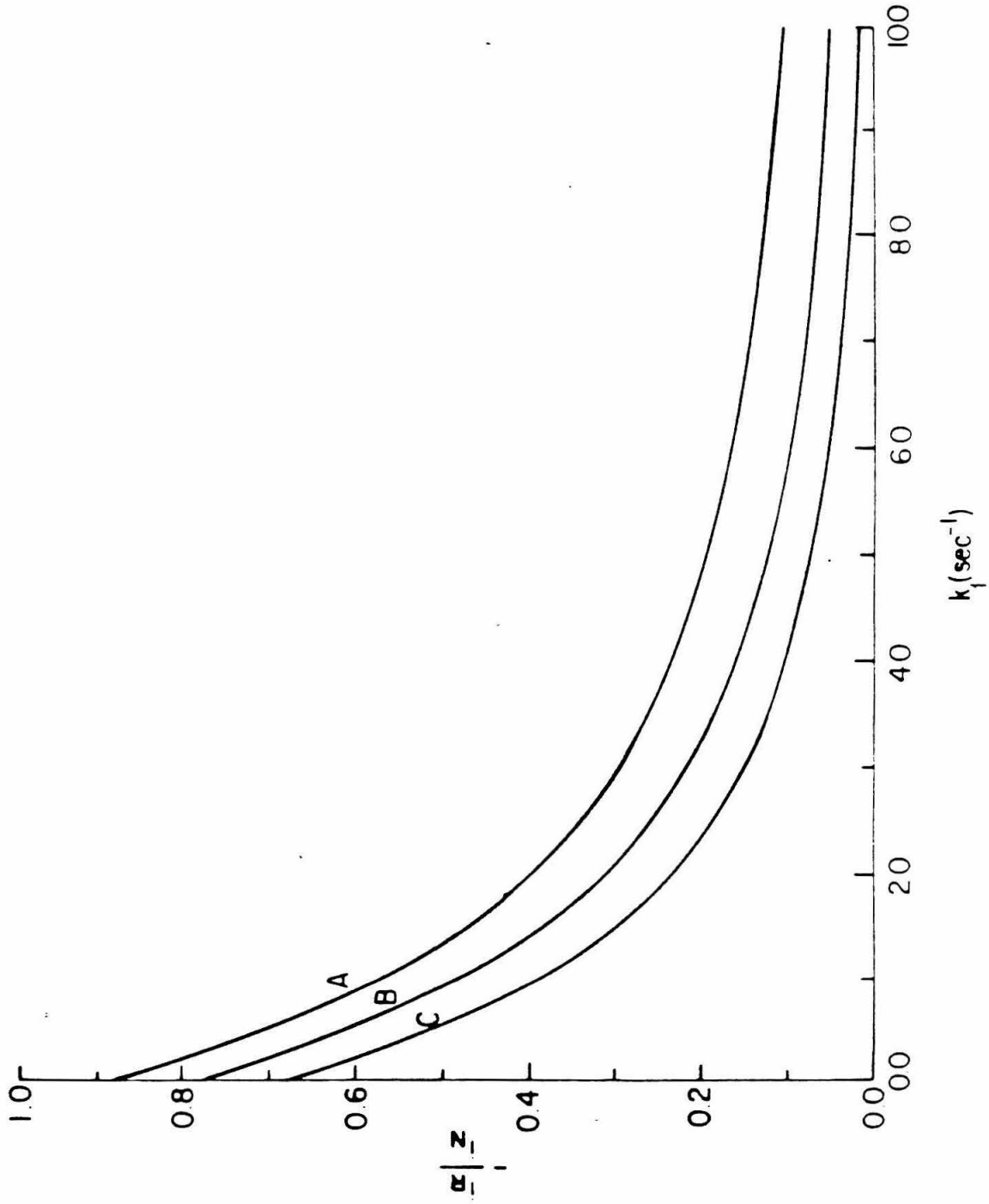
1.0
0.8
0.6
0.4
0.2
0.0
00
20
40
60
80
100
A
B
C
$\frac{a}{a} - \frac{z}{z}$
$k_1(sec^{-1})$

Table 6.1

Forward rate constants for reaction 6.1

		k_1, s^{-1} [a]		
t_e, [b]	t_p, [c]	pH = 3.5	pH = 4.8	pH = 6.0
s	ms			
1	90	1.1(0.89)[d]	0.7(0.44)	–[e]
1	39.7	1.2(0.48)	0.7(0.57)	–[e]
1	10.4	1.2(0.62)	0.6(0.72)	–[e]
2	90	1.6(0.27)	0.8(0.43)	0.4(0.52)
2	39.7	1.4(0.38)	0.8(0.52)	0.1(0.69)
2	10.4	1.3(0.5)	0.5(0.72)	0.3(0.77)
	Avg:	1.3	0.7	0.3

a. Obtained from working curves such as those in Figure 6.2.

b. Drop time of the dropping mercury electrode (c.f. Figure 6.3).

c. Pulse width (c.f. Figure 6.3).

d. The numbers in parentheses are the measured ratios of pulse polarographic limiting currens, $-i_R/i_N$.

e. i_R/i_N was too close to the value corresponding to $k_1 = 0$ for reliable estimates of k_1 to be obtained.

generation of the $[Ru^{III}(edta)]_2$ complex at the electrode surface because the formal potentials of the $Ru_2(III1/2)/Ru_2(III)$ and Ru(III)/Ru(II) couples are relatively close together in this pH range (2).

The analogous $Fe^{III}(edta)$ dimer, known to be an oxo-bridged complex, $[Fe(edta)]_2O$ (5), exhibits a pH dependence of its rate of decomposition that is consistent with protonation of the single bridging oxo ligand in the rate-determining step (5). The much weaker and non-linear dependence of the forward rate of reaction 6.1 on the proton concentration indicates that the $[Ru^{III}(edta)]_2$ dimer decomposes by a mechanistically more complex pathway than that followed by $[Fe^{III}(edta)]_2O$. One possibility is that the uncoordinated acetate groups present in the Ru(III) dimer participate in the decomposition mechanism in a pH dependent manner somewhat similar to that proposed by Matsubara and Creutz to account for the remarkable lability of the aquo ligand present in the $Ru^{III}(edta)OH_2$ complex (19).

At pH 11.3, the $[Ru^{III}(edta)]_2$ dimer is much more stable and yields ratios of i_R/i_N corresponding to negligible dissociation on the time scale of the pulse polarographic experiment, 2 s. Controlled potential reductions of $[Ru^{III1/2}(edta)]_2$ at pH 11.3 with a platinum gauze electrode can be carried out at -0.3 V without interference from subsequent reduction of $Ru^{III}(edta)$ that is formed slowly during the electrolysis. Solutions produced in this way show an absorption band at 568 nm that is not present in the spectrum of monomeric $Ru^{III}(edta)OH_2$ or the original $[Ru^{III1/2}(edta)]_2$ (Fig. 6.5). After completion of the electrolysis the absorption gradually decreases until a stable spectrum is obtained ($\sim$ 4h.)

The same stable spectrum (shown in Fig 6.5) could be obtained by equilibrating the $Ru^{III}(edta)$ monomer with the 0.1 M phosphate buffer at pH 11.3 under argon. The rate with which final equilibrium spectra were obtained was strongly dependent on the concentration of $Ru^{III}(edta)$. Dissolution of solid

Figure 6.5. Absorption spectra of solutions of Ru^{III}(edta).

(A) Solution containing 2.38 mM total Ru^{III}(edta) equilibrated at pH 11.3 (0.1 M phosphate) under argon until a stable spectrum was obtained. The calculated concentrations of Ru^{III}(edta)OH and $[Ru(edta)]_2$ are 2.1 mM and 0.14 mM, respectively (see text).

(B) Spectrum for 2.1 mM Ru^{III}(edta)OH at pH 9.3 (0.1 M phosphate) recorded immediately after preparation before any dimer had been formed.

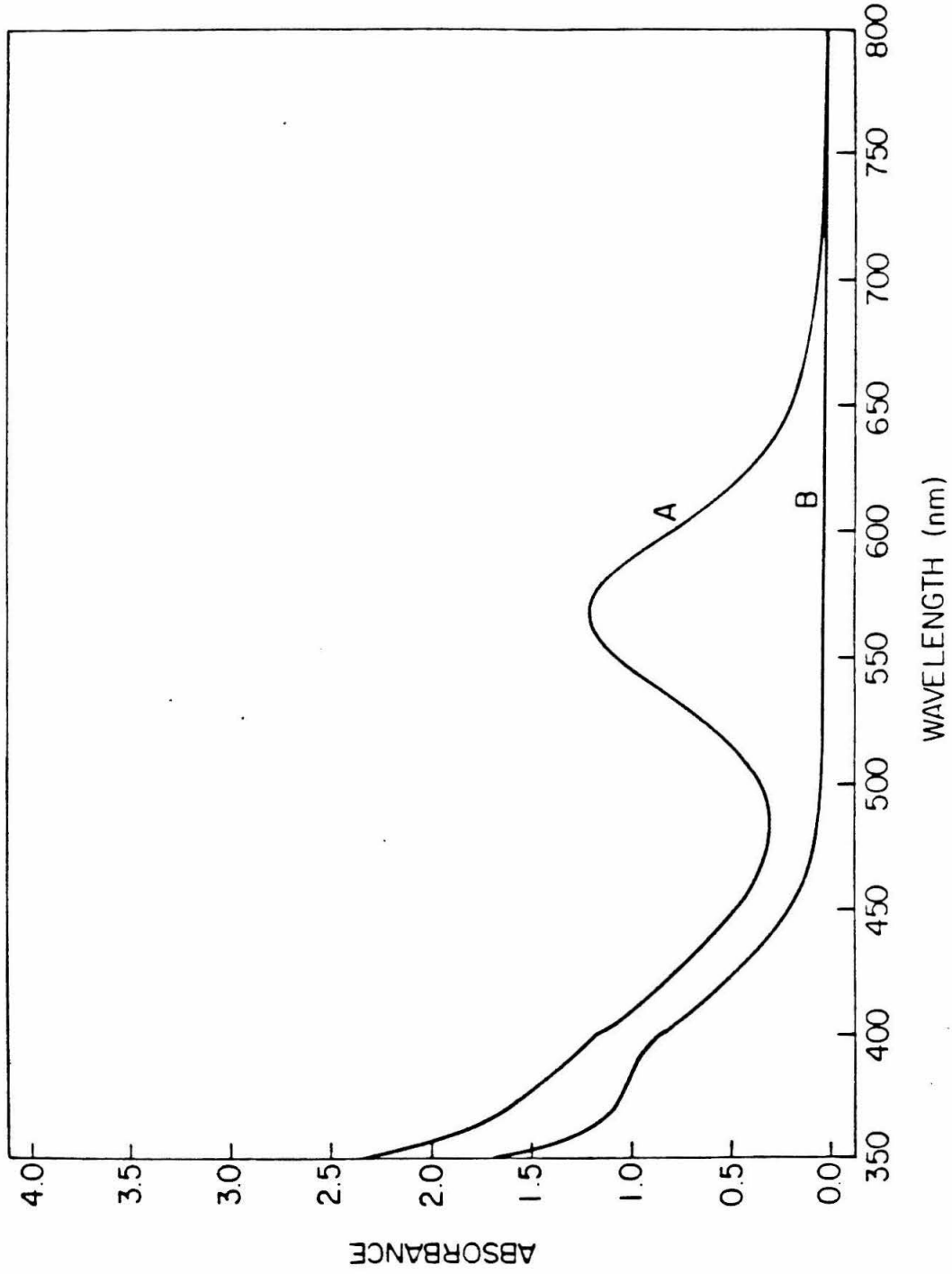
ABSORBANCE
4.0
3.5
3.0
2.5
2.0
1.5
1.0
0.5
0.0
350
400
450
500
550
600
650
700
750
800
WAVELENGTH (nm)
A
B

samples of the monomer in a minimum volume ($\leq$ 1 ml) of buffer and allowing the resulting solution to stand for several minutes before dilution to the final concentration proved effective in obtaining stable spectra. With lower monomer concentrations, *e.g.*, 0.1-1 mM, several hours are required for the band at 568 nm to become evident. This is the reason that the slow spontaneous dimerization was not detected in a previous study (2) and that the erroneous conclusion was reached that the dimerization was not thermodynamically favored, even at high pH. Thus, the band at 568 nm in the spectrum of Fig. 6.5 may be assigned to the $[Ru^{III}(edta)]_2$ dimer. The absorbance of the band is not proportional to the total concentration of $Ru^{III}(edta)$ over the concentration range 0.5-4 mN. The concentration dependence of the absorbance at 568 nm could be accounted for quantitatively by assuming a monomer-dimer equilibrium with a dimerization constant of 33 M^{-1}. The spectrum did not change between pH 11.3 and 11.9 but at lower pH values, *e.g.*, 8.3, where the dimer persisted for periods long enough for its spectrum to be monitored, the intensity of the band decreased and its maximum shifted to shorter wave lengths. The changes in the spectral features are not the result of acid-base reactions involving $Ru^{III}(edta)OH_2$ because the pK_a of this complex is 7.3 (2). The changes are also not explicable in terms of the simple dimerization reaction that has been shown to occur in the case of analogous $Fe^{III}(edta)$ complex (5), namely

$$2Fe^{III}(edta)OH_2 \rightleftharpoons [Fe^{III}edta]_2O + 2H^+ + H_2O \quad . \tag{6.3}$$

The expected effect on the spectrum of $[Ru^{III}edta]_2$ of an equilibrium such as reaction 6.3 is a calculable decrease in the intensity but not the position of the band arising from the dimer as the pH is decreased. This is not the result observed.

It is possible that the shifted, less intense band corresponds to a form of the dimer in which a bridging ligand (*e.g.*, an oxo ligand (2)) is protonated. Such

a species could be an intermediate in the slow dissociation of the dimer but we were unable to verify this speculation.

Thus, while we were able to determine a conditional equilibrium constant for the dimerization reaction in the pH range 11.3-11.9, the reasons for the increase in k_1 and changes in the dimer spectrum at lower pH values could not be specified. Note that at the concentration of Ru(III) used to record the spectrum in Fig. 6.5A only ca. 12% of the complex was present as the dimer. The molar absorbance of the dimeric complex is therefore rather larger, $\epsilon_{568} \simeq$ 8.6 x $10^3 M^{-1}cm^{-1}$ (pH 11.3, 0.1 M phosphate buffer).

CONCLUDING REMARKS

The combination of normal and reverse pulse polarography proved quite convenient for monitoring the kinetics of decomposition of the $[Ru^{III}(edta)]_2$ dimer at pH values between 3.5 and 6. The forward rate constant evaluated for reaction 6.1 was in agreement with the earlier estimate of Ikeda *et al.* (1). Although a pH-dependent conditional equilibrium constant for reaction 6.1 was evaluated at pH 11.3 and the absorption spectrum of the $[Ru^{III}(edta)]_2$ complex at this pH was presented, the identity of the ligands that bridge the two ruthenium centers in $[Ru^{III1/2}(edta)]_2$ and $[Ru^{III}(edta)]_2$ remains to be established.

References and Notes

1. Ikeda, M.; Shimizu, K.; Sato, G.P., Bull. Chem. Soc. Japan, 55(1982)797.
2. Baar, R.B.; Anson, F.C., J. Electroanal. Chem., 187(1985)265.
3. (a) Mukaida, M.; Okuno, H.; Ishimore, T., Nippon Kagaku Sasski, 86(1965)589.
   (b) Ezerskaya, N.A.; Solovykh, T.P.; Russ. J. Inorg. Chem. (Engl. Transl.), 11(1966)991, 1168, 1379.
   (c) ibid., 12(1967)1547.
   (d) ibid., 13(1968)96.
   (e) Scherzer, J.; Clapp, L.B., J. Inorg. Nucl. Chem., 30(1968)1107.
4. (a) Anson, F.C., Anal. Chem., 36(1964)520, 932.
   (b) Hubbard, A.T.;Anson, F.C., Anal. Chem., 38(1966)1601.
5. Schugar, H.; Hubbard, A.T.; Anson, F.C.; Gray, H.B., J.Am. Chem. Soc., 91(1969)71.
7. Gonzalez, S.; Anson, F.C., J. Electroanal. Chem., 129(1981)243.
8. Tang, T.-W.; Anson, F.C., J. Electroanal. Chem., 177(1984)183.
9. Baar, R.B., Ph.D. Thesis, Calif. Inst. of Technology, 1985.
10. Osteryoung, J.; Kirowa-Eisner, E., Anal. Chem., 52(1980)62.
11. Abel, R.H.; Christie, H.J.; Jackson, L.L.; Osteryoung, J.; Osteryoung, R.A., Chem. Instr., 7(1976)123.
12. Nicholson, R.S.; Shain, I., Anal. Chem., 36(1964)706.
13. Osteryoung, J.; Talmor, D.; Hermoling, J.; Kirowa-Eisner, E., J.Phys. Chem., 85(1981)285.
14. Schwarz W.M.; Shain, I., J. Phys. Chem., 69(1965)30.
15. These functions may be calculated from the polynominal approximations given in "Handbook of Mathematical Functions". Abramowitz, M.; Stegun, I., eds., NBS Applied Mathematics Series, 55(1964)378.
16. Ilkovic, D., Collec. Czech. Chem. Comm. 6(1934)498.
17. Anson, F.C.; Osteryoung, R.A., J. Chem. Ed., 60(1983)293.

18. Flanagan, J.B.; Takahashi, K.; Anson, F.C., J. Electroanal. Chem., 85(1977)257.

19. Matsubara, T.; Creutz, C., Inorg. Chem., 18(1979)1956.